

ADVANCES IN ELECTROMETALLURGY

No. 1 Volume 10 2012

ELECTROSLAG TECHNOLOGY

- A.D. Ryabtsev, A.A. Troyanskii, S.I. Davydov, V.V. Pashinskii, O.A. Snizhko, S.N. Ratiev and F.L. Leokha, **Producing commercial purity titanium by chamber electroslag remelting** 5
I.V. Protokovilov
Degassing of the electrode pressed from titanium sponge in the evacuation of the chamber electroslag remelting furnace 11
A.V. Gnatushenko, F.K. Biktagirov and A.P. Ignatov
Electroslag melting of chromium bronze BrKh 16
A.A. Polishko, L.B. Medovar, V.Ya. Saenko, A.Yu. Tunik and S.N. Stepanyuk
Distribution of non-metallic inclusions in the cast metal of 316 type steel after circumferential electroslag surfacing with liquid metal 20

ELECTRON BEAM PROCESSES

- V.F. Topol'skii, S.V. Akhonin, G.M. Grigorenko and I.K. Petrichenko
Development of new titanium biocompatible alloys for medical applications 24
V.I. Kostenko, M.P. Kruglenko, A.N. Kalinyuk and P.A. Pap
Production by electron beam remelting of defect-free titanium ingots with controlled oxygen content 29
A.I. Ustinov, Yu.V. Fal'chenko, T.V. Mel'nichenko, G.K. Kharchenko, L.V. Petrushinets and E.A. Shishkin
Multilayer Ti/Al foils: methods of production, properties and application in pressure welding 33
V.O. Mushegyan
Structure of molybdenum ingots modified with dispersed particles of a second phase 43

PLASMA ARC TECHNOLOGY

- V.N. Koleda, V.A. Shapovalov, F.K. Biktagirov, V.R. Burnashev and V.V. Yakusha
Plasma-arc melting on a dispersed substrate in a moving horizontal solidification mould 47

GENERAL PROBLEMS OF METALLURGY

- G.M. Grigorenko, S.V. Akhonin, T.G. Taranova, S.G. Grigorenko and O.M. Zadorozhnyuk
Dispersion-hardened titanium alloys of the Ti-Si-X system 52
A.L. Borisova, L.I. Adeeva, A.Yu. Tunik, M.V. Karpets, S.N. Stepanyuk and L.K. Doroshenko
Structural and phase transformations in the $Ti_{60}Cr_{32}Si_8$ phase, containing an approximant phase 62

ELECTROMETALLURGY OF STEEL AND FERROALLOYS

- R.V. Sinyakov
Aspects of using liquid cast iron in arc steel melting furnaces 68

Advances in Electrometallurgy is a cover-to-cover English translation of *Sovremennaya Elektrometallurgiya*, published four times a year by International Association 'Welding' at the E.O. Paton Electric Welding Institute, National Academy of Sciences of Ukraine, 11 Bozhenko Street, 03680 Kyiv, Ukraine

Editor-in-Chief

B.E. Paton

Editorial Board

D. Ablitzer (France)

D.M. Dyachenko, Executive secretary (Ukraine)

J. Foct (France)

T. El Gammal (Germany)

M.I. Gasik (Ukraine)

G.M. Grigorenko, Deputy Chief editor (Ukraine)

B. Koroushich (Slovenia)

V.I. Lakomsky (Ukraine)

V. Lebedev (Ukraine)

S.F. Medina (Spain)

L.B. Medovar (Ukraine)

A. Mitchell (Canada)

B.A. Movchan (Ukraine)

A.N. Petrunko (Ukraine)

Ts.V. Rashev (Bulgaria)

N.P. Trigub (Ukraine)

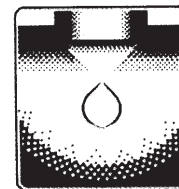
A.A. Troyansky (Ukraine)

M.L. Zhadkevich (Ukraine)

All rights reserved. This publication and each of the articles contained here are protected by copyright. Permission to reproduce materials from this journal must be obtained in writing from the Publisher

Published by

Cambridge International Science Publishing Ltd
7 Meadow Walk, Great Abington, Cambridge CB21 6AZ, England
Tel: +44 (0) 1223 893295; Fax: +44 (0) 1223 894539
email: cisp@cisp-publishing.com; <http://www.cisp-publishing.com>



ELECTROSLAG TECHNOLOGY

Producing commercial purity titanium by chamber electroslag remelting

**A.D. Ryabtsev, A.A. Troyanskii, S.I. Davydov, V.V. Pashinskii,
O.A. Snizko, S.N. Ratiev and F.L. Leokha**

Donetsk National Technical University; ZMTK Company, Donetsk

The capability of producing ingots of commercially pure titanium by recycling of titanium sponge and waste of titanium production (chips, cuts of reaction mass from covers of reaction retorts, tube waste) using the method of chamber electroslag remelting is shown. The results of titanium alloying by oxygen from a special master alloy, gas phase and micro- or nanopowders of titanium oxide in the process of titanium sponge remelting are given.

At present, in addition to β - and $\alpha+\beta$ -titanium alloys, the industry also used extensively α -alloys which include the so-called commercial purity titanium (CPT). The typical representatives of the CPT are the domestic alloys VT1-0, VT1-00 and foreign alloys Grade 1, Grade 2, Grade 3 and Grade 4. As a result of their properties, in particular, the high values of corrosion resistance and low density, these alloys represent structural materials for many components in petrochemical industry, engineering and constructional engineering. The strength of CPT is ensured mainly as a result of the higher oxygen content [1]. For example, the tensile strength of Grade 4 alloy (oxygen content 0.40 wt.%) is 550 N/mm², and yield limit 480 N/mm², which is respectively to and four times higher than these values for iodised titanium. The mechanical properties of titanium can be controlled by varying the

oxygen content.

The industrial technology of production of the titanium ingots consists of two stages: the first stage – production of titanium sponge, second stage – remelting of the sponge into ingots. Titanium can be alloyed in oxygen in any of these two stages. The most developed technology used in the industry is the technology of alloying titanium with oxygen in the stage of remelting the sponge into ingots [2]. In this case, the source of oxygen is the titanium scrap, various oxygen-containing master alloys and titanium oxide. One of the main problems in this case is the non-uniform distribution of oxygen along the height and cross-section of the melted ingot and also the problems in ensuring the required concentration. Therefore, the technology of production of ingots is usually based on a number of stages which

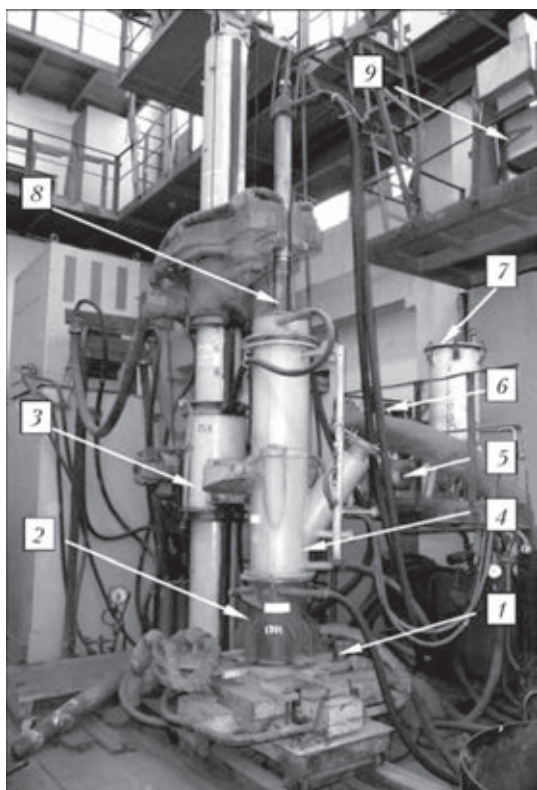


Fig. 1. General view of the chamber furnace for ESR based on equipment U-578: 1) the baseplate, 2) solidification mould; 3) the column with carriages; 4) protective jackets; 5) vacuum pump; 6) gas sampling device for gas cleaning; 7) filter; 8) electrode holder; 9) the dosing device.

are relatively complicated and requires high expenditure and resources.

This problem can be solved either by developing a new technology which will make it possible to produce the uniform distribution of oxygen in melting of titanium ingots, or the application of initial sponge with the initially high and uniform oxygen content. As regards the production of the sponge with higher oxygen content, this is possible by using methods such as the application of oxygen-containing compounds of oxytrichloride of vanadium [3] or titanium acid [4] in the production of titanium tetrachloride, and also a more promising method of adding oxygen to the titanium sponge by using an argon–oxygen mixture supplied into a retort directly in the process of magnesium thermal reduction of titanium [5, 6].

Table 1. The content of impurities in titanium produced by different methods

Titanium	O,w t.%	N,w t.%
VT1-00 – VAM	0.10	0.04
VT1-0 – VAM	0.20	0.04
Grade 1 – VAM	0.18	0.03
Grade 2 – VAM	0.25	0.03
Grade 3 – VAM	0.35	0.05
Grade 4 – VAM	0.40	0.05
CESR Ti from sponge	0.04-0.10	0.015-0.020
CESR Ti from pipe cut-offs	0.15-0.18	0.02-0.03
CESR Ti from shavings	0.40-0.50	0.025-0.035
CESR Ti alloyed with oxygen from master alloy	0.10-0.40	0.033-0.110
CESR Ti alloyed with oxygen from gas phase	0.075-0.27	0.020-0.030
CESR Ti alloyed with oxygen from titanium oxide micropowder	0.35-0.57	0.025
CESR Ti alloyed with oxygen from titanium oxide nanopowder	0.18-0.73	0.03

However, the sponge is only the semi-finished product and must be remelted into ingots. At the present time, the main processes for the melting and alloying the titanium sponge are vacuum-arc and electron beam remelting processes.

The possibilities of remelting processes can be greatly expanded and supplemented by electroslag technology – chamber electroslag remelting (CESR), especially in the area of introduction of oxygen into metal and ensuring the uniform distribution of oxygen along the height and in the cross-section of the ingots. CESR makes it possible to ensure a high level of purity, structural and chemical homogenising of the material as a result of the uniform melting of the consumable electrode and simultaneous solidification of the ingot which take place in the conditions of chemical vacuum, as a result of the presence of active components in the flux (in particular, metallic calcium) [7–9].

CESR is based on the ‘classic’ electroslag remelting, including the main equipment, baseplate, the solidification mould to which the chamber, protecting the melting space

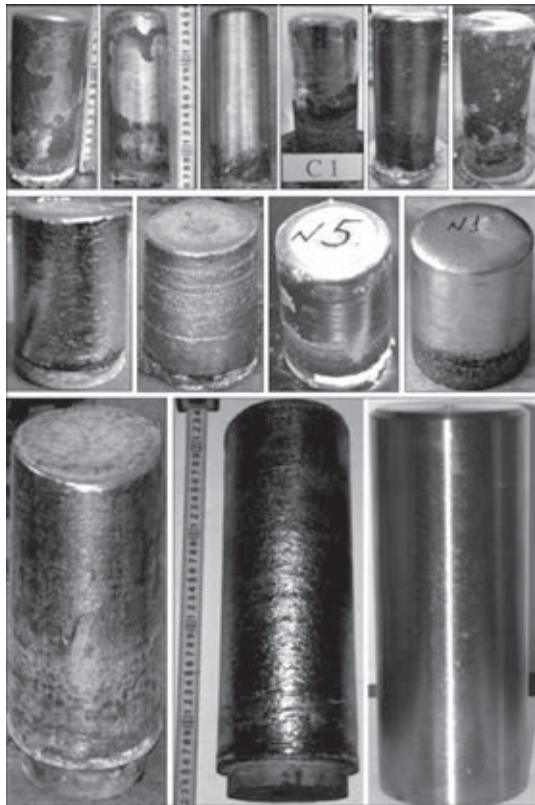


Fig. 2. Titanium ingots produced by CESR.

is added (as in the method of vacuum arc remelting), and the appropriate peripheral devices: vacuum system, filters, gas cleaning system, dosing device and cylinders with the gas, etc (Fig. 1). Therefore, the CESR method

is characterised by all advantages of ‘classic’ electroslag remelting, and the presence of the furnace chamber makes it is also possible to produce almost any controlled atmosphere in the melting space, including vacuum, and carry out the remelting of high-reactivity metals and alloys, including titanium alloys. In addition to this, the addition of metallic calcium with the slag results in the low values of partial pressure of oxygen, and also nitrogen and also in the gas phase thus creating the suitable conditions for refining and alloying the metals and alloys.

In the Donetsk State Technical University, investigations of CESR and application of calcium-containing fluxes have been carried out for more than 30 years. In this period, the theoretical fundamentals of the process were developed, the main relationships of the process were investigated, and the technologies of producing ingots from different metals and alloys were developed and applied [7–11]. In particular, the experimental results have made it possible to develop a technology for melting, refining and alloying of titanium, using for this purpose as the initial material various types of starting materials (sponge, shavings and waste) [7, 9, 12–15].

Table 1 gives the content of the harmful impurities in titanium produced by different methods. CESR can be used not only for melting

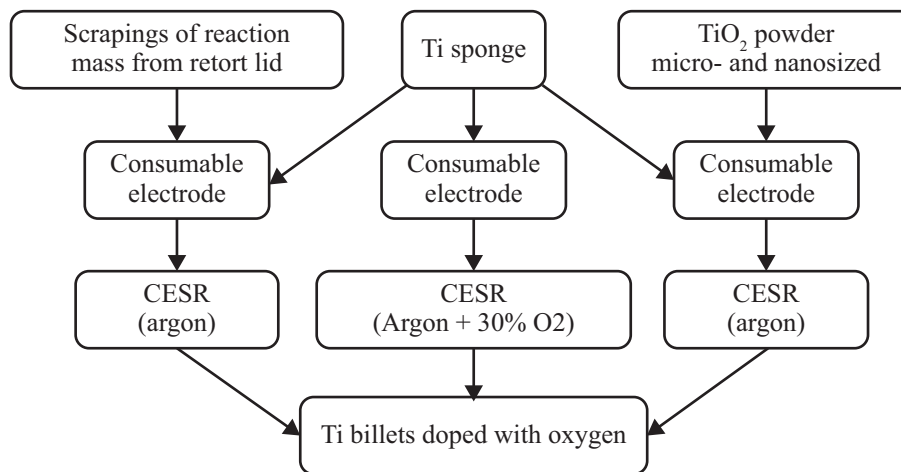


Fig. 3. The diagrams of alloying of titanium with oxygen applied in CESR.

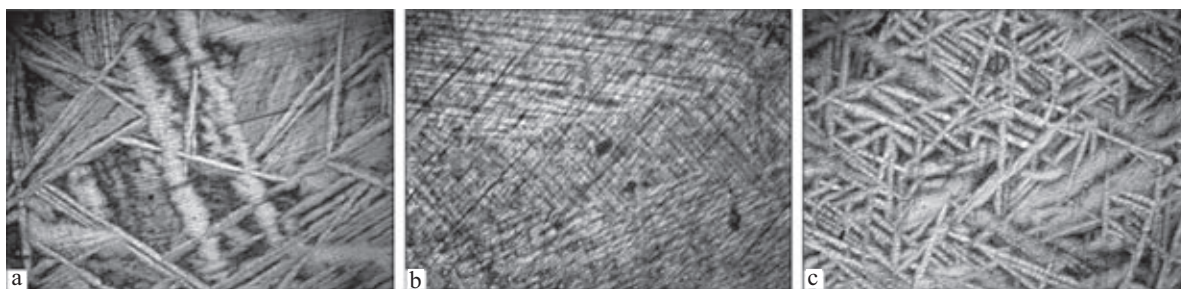


Fig. 4. Structures of titanium with the addition of titanium oxide micro-powder (a); without addition of the titanium oxide micro-powder (b); with the addition of titanium oxide nanopowders (c), $\times 100$.

high-purity titanium ingots from titanium sponge (Fig. 2) but also for utilising the waste of titanium production, producing the alloys of the type VT1-0 and VT1-00.

The new possibilities are offered by CESR in the alloying of titanium with oxygen using different technologies (Fig. 3) [13–15].

The experiments and production of pilot planned melts were carried out using, as the source of oxygen for alloying titanium, the oxygen-containing master alloy in the form of scrapings from the covers of equipment for reduction of titanium sponge, gas oxygen from commercial argon or especially prepared argon–oxygen mixture ($O_2 = 30\%$), micro- and nanopowders of titanium oxide.

When using the scrapings, ingots of titanium with 0.044–0.40% oxygen were produced [13]. This amount of oxygen greatly influences the hardness and strength of titanium and also its structure. Experimental metal was characterised by a single-phase structure, characteristic of commercial titanium, which acquired the typical needle appearance with the increase of the oxygen content to 0.4% so that it was classified as the α' -phase.

Should be mentioned that when carrying out the mechanical tests, the specimens produced from the ingots melted from 100% reaction mass ($[O] = 0.40$ wt.%), failed without elongation, and the specimens of metal produced by remelting the electrode including 50% each of titanium sponge and reaction mass ($[O] = 0.30$ wt.%) was also characterised by low values of the relative elongation (11% in comparison with the required value of

20% for the VT1-00 industrial alloy). This is associated with the fact that the reaction mass, as a result of its production technology, contains a higher (in comparison with titanium sponge) amount of impurities. For example, the nitrogen content is up to 10 times higher (0.011% in the initial titanium sponge and 0.11% in the reaction mass), and the iron content is almost twice as high (in the sponge 0.06 and 0.09% in the reaction mass), with the carbon content being four times higher (0.004 and 0.16%). Thus, it may be assumed that this type of master alloy can be used efficiently for the production of commercial purity titanium with a relatively low (up to 0.25%) oxygen content, for example, the alloys Grade 1 and Grade 2.

Another interesting application, including from the economy viewpoint, is the application of gaseous oxygen for alloying titanium. This can be realised more sufficiently in CESR. Alloying of titanium with oxygen from the gas phase in the process of vacuum arc and electron beam remelting is very difficult because of the presence of vacuum in the melting space.

Experimental verification of the method of alloying with oxygen was carried out in CESR of electrodes produced by pressing from titanium sponge with different initial oxygen content (0.035 and 0.11%), in argon and in a specially prepared argon–oxygen mixture ($O_2 = 30\%$) [14, 15]. This produced titanium with the mass fraction of oxygen in the range from 0.053 to 0.270 with different structures. For example, for the metal with the

oxygen content in the range 0.053–0.110% examination shows the characteristic coarse dendritic structure in which the differences between the individual sections were detected already at a low magnification.

In some cases, the dendrite areas contained a plate-shaped substructure characteristic of commercial purity titanium in the cast condition. With a further increase of the oxygen containing titanium to 0.22 wt.% the microstructure acquired the typical needle appearance. The needles of the α' -phase were long, 200–400 μm . This is associated with the fact that during the $\beta \rightarrow \alpha$ -transformation by the shear mechanism, the crystals of the α' -phase grow within the limits of the initial large dendrites of the β -phase.

The formation of this structure is accompanied by the rapid increase of hardness to 225 *HB*, the increase of strength and a small reduction of plasticity. However, on the whole, the resultant parameters of the mechanical properties of titanium, alloyed with oxygen from the gas phase, are within the range of the values for commercial titanium so that we can evaluate the possibilities of producing alloys of this type by the CESR method.

Another variant of alloying titanium with oxygen is the method of adding the TiO_2 powder into a consumable electrode from titanium sponge, which has been extensively tested in vacuum arc melting (VAM). Unfortunately, this method does not ensure the sufficiently high uniformity of the distribution of the powder in the electrode and, consequently, oxygen in the vacuum arc melted ingots. We tested the method of adding the TiO_2 powder to the compacted consumable electrode for CESR in which the titanium dioxide is not mixed into the sponge and is pressed into special orifices in the electrode. In the experiments, alloying was carried out using the TiO_2 powder of different fraction composition – micro- and nanosized. The CESR process is carried out in the neutral atmosphere. Experimental ingots with the oxygen content of 0.35–0.57% using the micro-powder, and

0.18–0.73% using the nanopowders of titanium oxide, were produced.

Investigations of the produced ingots showed that the addition of titanium oxide as the oxygen carrier refines the grains of the metal and leads to the formation of the structure of the ‘basket weaving’ type (Fig. 4a). The produced structure greatly differs from the structure of pure titanium in which it is equiaxed and coarse-grained (Fig. 4b).

The application of oxygen of the titanium oxide nanopowders as the carrier results in the formation of an even more developed and dispersed structure (Fig. 4c).

The variation of the structure of cast titanium as a result of alloying with oxygen increases the hardness. For example, if in the case of pure titanium the hardness was 121 *HB*, after adding the titanium oxide micro-powders the hardness reached 210 *HB* and 274 *HB* when using the nanopowders as the oxygen carrier.

Thus, the experimental results obtained for the produced metal show that it is possible to greatly define the macro- and microstructure of titanium as a result of adding the nanoparticles of TiO_2 during remelting. The experimental results also show that the addition of such particles results in the fragmentation of the dendrite in the macrolevel and supports the formation of the developed structure formed by the crystals of the needle shaped on the microlevel.

Conclusions

1. It is shown possible to produce titanium ingots of commercial purity by the method of chamber electroslag remelting of titanium sponge and waste of titanium production.
2. The metallurgical process of chamber electroslag remelting efficiently alloys titanium with oxygen from 0.035 to 0.73% by the application of the oxygen-containing master alloy, and also from the gas phase and titanium oxide.
3. The results of investigation of the struc-

ture and hardness measurements show that chamber electroslag remelting ensures satisfactory chemical and structural homogeneity of the titanium ingots.

References

1. Donachie, M.J., Titanium: a technical guide, Materials Park, Ohio, 2000.
2. Sergeev, V.V. (editor), Metallurgy of titanium, Metallurgiya, Moscow, 1971.
3. Patent number 2106418, Russian Federation.
4. Patent 8335 9093 US,
5. Yatsenko, A.P. in: Ti-2009 in CIS, Proceedings of the international conference, Odessa, May 17–20, 2009.
6. Davydov, S.I., et al., in: Ti-2007 in CIS, Yalta, 15-18.4. 2007, 65–73.
7. Troyanskii, A.A. and Ryabtsev, A.D., Titan, 2007, No. 1, 28–31.
8. Ryabtsev, A.D. and Troyanskii, A.A., Elektrometallurgiya, 2005, No. 4, 25–30.
9. Ryabtsev, A.D., et al., Refining of titanium and its alloys from nitrogen-rich inclusions in electroslag remelting, Tekhnopark, DonNTU UNITEX, 2011.
10. Active slag – ESR refining of titanium alloys for dissolution of nitrogen-rich inclusions, in: Proceedings of the Ninth world conference on titanium, St Peterburg, 1990.
11. Ryabtsev, A.D. and Troyanskii, A.A., Proc. of the 2005 Int. Symp. on Liquid Metal Proc. and Casting, LPMC 2005, Santa Fe, USA, September 2005, 227–232.
12. Ryabtsev, A.D., et al., Sovremennaya Elektrometallurgiya, 2009, No. 4, 1–3.
13. Ryabtsev, A.D., et al., Sovremennaya Elektrometallurgiya, 2007, No. 3, 3–6.
14. Ratiev, S.N., et al., Sovremennaya Elektrometallurgiya, 2010, No. 2, 8–12.
15. Ryabtsev, A.D., et al., Proceedings of the 2011 Intentional Symposium on Liquid metal processing and casting, LPMC 2011, Nancy, France, 2011, 39–42.

Submitted 16.1.2012

Degassing of the electrode pressed from titanium sponge in the evacuation of the chamber electroslag remelting furnace

I.V. Protokovilov

EO .P aton Electric Welding Institute, Kiev

The method of removal of adsorbed gases and moisture from the consumable electrode, pressed from titanium sponge, by heating with the electrical current in the process of evacuation of the chamber electroslag furnace is described.

The initial material for the production of titanium ingots and slabs is the titanium sponge [1]. The sponges used to produce (mostly by pressing) consumable electrode (Fig. 1) which are subsequently remelted into ingots by vacuum arc, electroslag remelting, magnetically controlled electroslag melting (MCESM), etc [1–4]. Electron beam melting is carried out using blanks pressed from titanium sponge or blocks of titanium sponge [5].

Titanium sponge is produced by magnesium thermal reduction of titanium tetrachloride [1, 6]. Subsequently, the porous titanium mass is purified to remove the magnesium vapours and chloride salts by long-term vacuum separation at temperatures of 850–1020°C [6]. Consequently, the titanium sponge contains the minimum content of harmful impurities (atmospheric gases) [7].

However, in the process of subsequent operations of crushing the sponge, transport, production of considerable electrodes, in long-term storage (especially if the appropriate rules are not adhered to), etc, the developed surface of titanium sponge and remnants of the chloride salts can absorb atmospheric gases (moisture).

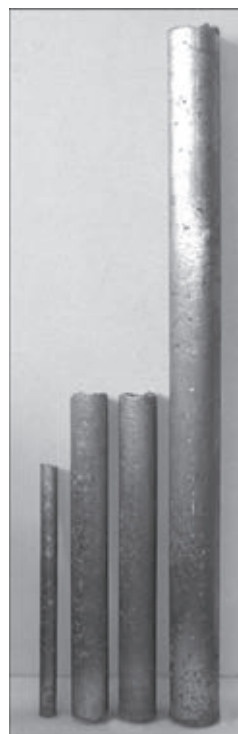


Fig. 1. Electrode with a diameter of 35, 75 and 100 mm, used in magnetically controlled electroslag melting, compacted from titanium sponge.

In subsequent metallurgical processing in the conditions of high values of temperature

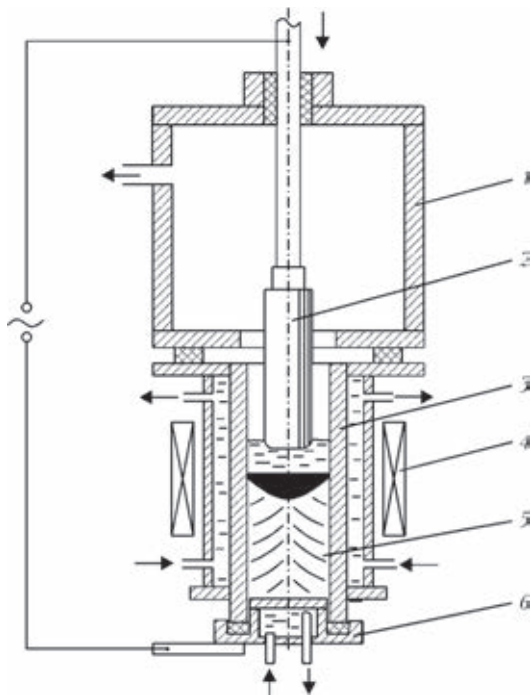


Fig. 2. Diagram of the process of magnetically controlled electroslag melting: 1) chamber; 2) consumable electrode; 3) solidification mould; 4) electromagnetic system; 5) the ingot; 6) the baseplate.

in vacuum, these impurities are sublimated and removed by the vacuum system. However, in remelting in the still atmosphere of the inert gas, these impurities can become the reason for the higher content of hydrogen, oxygen and nitrogen in the metal.

It should be mentioned that the atmospheric gases, adsorbed by the surface of the sponge (compacted electrode) are not dissolved in titanium and they can be removed by vacuum separation. However, this operation requires special equipment and greatly complicates and increases the cost of the technological cycle of melting ingots.

The aim of the present work is the evaluation of the possibility of degassing the consumable electrode, compacted from titanium sponge, directly in the furnace chamber prior to remelting by the MCESM method.

In the proposed method (Fig. 2), the consumable electrode, compacted from the titanium sponge, is assembled in the furnace

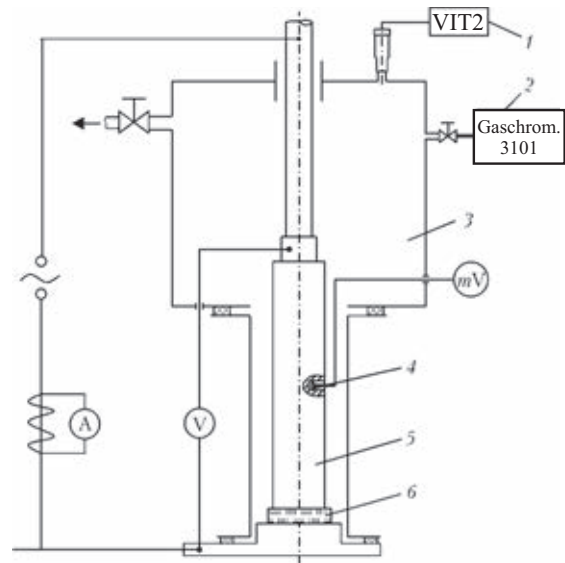


Fig. 3. Experimental setup: 1) the vacuum gauge; 2) the chromatograph; 3) the furnace chamber; 4) the thermocouple; 5) consumable electrode; 6) current-conducting seed.

ensuring electrical contact with the baseplate and, subsequently, the flux is charged into the melting zone and this is followed by sealing and evacuation of the furnace. When the required pressure is reached, the vacuum system is switched off and the melting space is filled with the inert gas. Subsequently, electrical voltage is applied to the electrodes and the base plate ensuring the formation of the slag pool and remelting of the electrode.

It has been proposed to carry out degassing of the consumable electrode, compacted from the titanium sponge, in the stage of evacuation of the melting space by heating with the electric current, supplied by a standard furnace transformer. To prevent melting of the flux and of the electrodes, the electrical voltage in the electrode should not exceed the value determined by the specific resistivity of the compacted mass and the geometrical dimensions of the electrode.

The main advantage of the proposed system for degassing the electrode is that it does not require additional equipment and the duration of the technological cycle of melting of the ingots is not increased.

To evaluate the efficiency and develop



Fig. 4. The electrode with a diameter of 75 mm, compacted from titanium sponge.

conditions for the degassing electrodes, a series of experiments was carried out (Fig. 3). The experiments were carried out using electrodes compacted from TG-130 titanium sponge, with a diameter of 75 mm and 600 mm long, which were stored for a long period of time (more than five years) in the open atmosphere (in an open container) (Fig. 4). The electrode was heated by electric current supplied from a TShP10000-1 furnace transformer, fitted with a unit for smooth regulation of the voltage. The actual conditions of current supply in magnetically controlled electroslog melting were simulated. The electrode temperature was controlled using a chromel–alumel thermocouple, fixed to the body of the electrode 25 mm from its surface. The pressure in the chamber was measured with a VIT-2 vacuum gauge. The hydrogen content of the furnace atmosphere was analysed using a Gazokhrom 3101 chromatograph. The main parameters of the process were recorded using a LabView program software.

To determine the heating conditions of the electrode, the dependence of the electrode temperature on the intensity of the electric

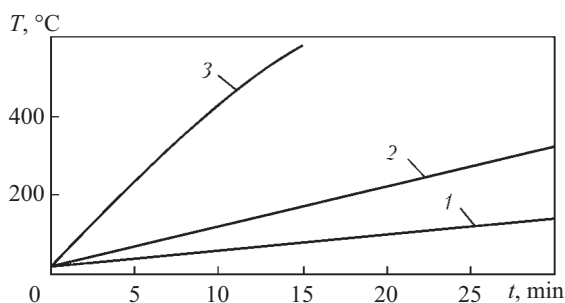


Fig. 5. The electrode temperature in relation to the heating time for different currents, A: 1) 1000; 2) 1500; 3) 2500.

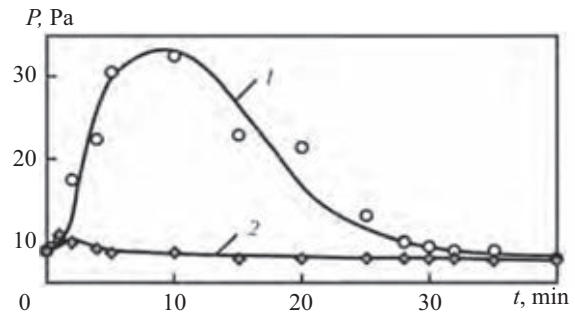


Fig. 6. Variation of pressure in the furnace chamber in the first (1) and repeated (2) heating of the electrode.

current and heating time was investigated. The experiments were used to develop the electrical conditions of heating the electrode during degassing (Fig. 5), taking into account the need for rapid heating of the electrodes to 450–500°C and maintaining the temperature at this level throughout the entire degassing period. The electrode temperature should not exceed 500°C because of the possible undesirable processes of dissolution by titanium of the residual atmospheric gases in the preliminary vacuum conditions.

The electrode heating conditions were based on supply of the voltage of 2.2–2.6 V to the ends of the electrode, ensuring the current intensity in the electron in the range 2250–2500 A, with a subsequent reduction to 1000 A in accordance with the specified program as a result of a small decrease of the voltage of the power source.

In the second experimental series, special attention was given to the variation of pressure in the furnace chamber in heating of the electrode. This characterises indirectly the processes of degassing of titanium sponge. The following experimental procedure was used. After assembling the electrode and sealing the furnace, the vacuum system was activated. After reaching the vacuum of 5.3 Pa (4×10^{-2} mm Hg), the electrode was heated to 400–450°C, with the recording of the variation of pressure in the melting space.

The experimental results show that in the first 5 min after applying the voltage and passing the electric current through

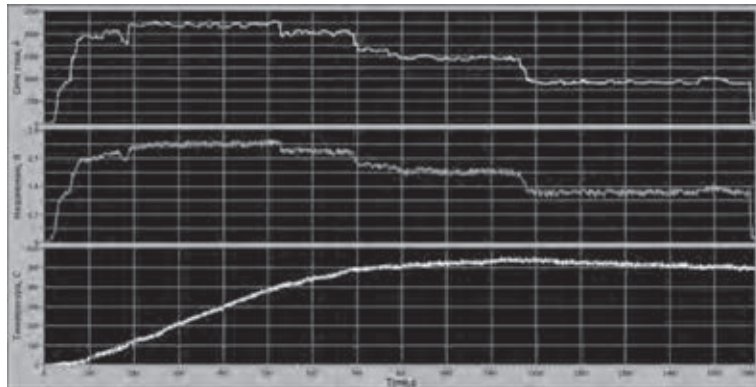


Fig. 7. Heating conditions of the electrode with passing current.

the electrode the pressure in the furnace starts to increase rapidly, indicating high-intensity degassing of the electrode (Fig. 6). Subsequently, after 10 min of operation of the vacuum pump, the pressure starts to decrease gradually and after 20–30 min the pressure is stabilised at the level slightly lower than the initial level.

In preheating the electrode after the small increase the pressure in the furnace is restored to the initial level already after five min (Fig. 6, position 2). This indicates the removal of the adsorbed moisture from the electrode and completion of the degassing process.

In the final series of the experiments, the variation of the hydrogen content in the furnace atmosphere during heating of the electrode was investigated. For this purpose, after sealing and evacuation of the furnace, the melting space was filled with argon. This was followed by heating the electrode and pe-

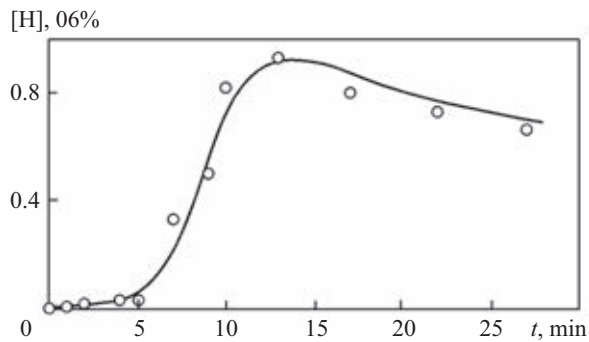


Fig. 8. The dynamics of the variation of the hydrogen content in the furnace atmosphere in heating of the electrode.



Fig. 9. Ingot of the VT1-0 alloy.

riodic removal of samples for chromatographic analysis to determine the hydrogen content of the furnace atmosphere. Subsequently, the experiment was repeated using the already ‘dried’ electrode.

The experimental results are presented in Fig. 7 and 8. The experiments show that 5 min after the start of the experiment was heating of the electrode by the

current above 200°C the hydrogen content of the atmosphere of the furnace are rapidly increased from 0.7–0.9 volume percent (Fig. 8). This indicates the evaporation of the adsorbed moisture from the electrode surface and also from the internal volume of the electrode as a result of the presence of discontinuities. In subsequent stages, the hydrogen content of the atmosphere slightly decreased which is associated evidently with the reversed processes of interaction of titanium with hydrogen. In the actual conditions of degassing of the electrodes, the evaporated moisture is removed from the melting space of the vacuum system.

In the repeated experiments, no hydrogen was found in the furnace atmosphere and this confirms the removal of the adsorbed moisture in the first heating cycle of the electrode.

After these experiments, some of the electrodes of remelted by magnetically controlled electroslag melting into titanium ingots with a diameter 100 mm (Fig. 9). Regardless of the fact that the ingots were melted using low-grade titanium sponge TG-130 and the storage time of the consumable electrode in the open air produced from the titanium sponge was very long (more than five years), the content of the atmospheric gases in the metal was as follows, % [O] 0.08–0.17; [N] 0.016–0.025; [H] 0.006–0.08, which corresponds to the standard requirements for the VT1-0 alloy.

Thus, the experiments confirm the efficient removal of the adsorbed moisture from the electrodes, compacted from titanium sponge by heating with electric current in evacuation of the chamber electroslag furnace. In the proposed method for degassing the electrode it is not required to use additional equipment and the duration of the technological cycle of melting the titanium ingots is not extended. This operation should be carried out efficiently with the electrodes produced from low-gradesponge, or the electrodes which have been stored for a long period of time in open air.

References

1. Garmata, V.A., et al., Titanium, Metallurgiya, Moscow, 1983.
2. Anoshkin, N.F., et al., Melting and casting of titanium alloys, Metallurgiya, Moscow, 1978.
3. Kompan, Ya.Yu. and Protokovilov, I.V., in: Proceedings of the international scientific and technical conference Special electrometallurgy: yesterday, today and tomorrow, Kiev 2002, 256–262.
4. Paton, B.E., et al., Probl. Spets. Elektrometall., 1992, No. 2, 7–11.
5. Trigub, N.P., et al., Sovremennaya Elektrometallurgiya, 2006, No. 4, 6–9.
6. Zaporozh'e Titanium-Magnesium Concern. Production technology; www.ztmc.zp.ua/ru/o-kombinate/tehnologiya-proizvodstva.
7. DSTU 3079-95 (GOST 17746-96). Titanium sponge. Committee for Standardisation, Metrology and Certification of Ukraine, 1995.

Submitted 16.1.2012

Electroslag melting of chromium bronze BrKh

A.V. Gnatushenko, F.K. Biktagirov and A.P. Ignatov

EO .P aton Electric Welding Institute, Kiev

It is shown possible to electroslag melt BrKh chromium bronze from non-compacted copper waste with alloying with chromium from the slag. The dependence of the chromium content of the metal on the amount of the chromium oxide in the slag is determined. The chemical composition and the main properties of the BrKh bronze produced by electroslag melting are determined.

Chromium bronze is one of the most widely used low-alloy dispersion-hardening copper alloys with the chromium content of 0.4–1.0%. Due to the combination of the high values of hardness, strengths and electrical and thermal conductivity, the alloy is used extensively in industry for the manufacture of various components, subjected in service to high mechanical and electric thermal loading, for example, electrodes in equipment for resistance welding, collectors of electric motors, solidification moulds of equipment for continuous casting of metals, etc (Table 1) [1, 2].

In most cases, the chromium bronze is melted in reflecting, induction and arc furnaces. General problems of the production

of this alloy in these melting systems are associated with the difficulties in alloy in copper with chromium. Chromium has limited solubility in copper in the solid state. At a eutectic temperature of 1345 K, the solubility of chromium is 0.65% [1]. This element is characterised by high affinity for oxygen and can be easily oxidised during melting. Therefore, to ensure more extensive dissolution of chromium in melting in the furnaces, it is important to maintain a higher temperature, and the oxidation of chromium should be prevented by using covering fluxes, shielding atmosphere, vacuum [2–4].

Copper is alloyed with chromium by two methods: either with pure chromium or with a copper–chromium master alloy

Table 1. Main areas of application of BrKh chromium bronze

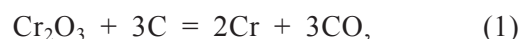
Metallurgy	Welding	Electrical engineering	Engineering	Other branches
Solidification moulds for continuous casting systems	Electrodes for resistance welding machines	Collector plates of powerful electric drives	Gears	Press moulds and dies in production of components from plastics and ceramics
Moulds for casting low-melting metals		Contact wheels	Braking blocks of aircraft and cars	
Drums – coolers for production of strips with amorphous structure		Electric current conductors	Components of internal combustion engines	

[2, 3]. In both cases, expensive pure chromium with the great not longer than Kh99 is used. In alloying by the first variant, it is recommended to use pieces with the size of 15–25 mm, and the metal temperature should not be lower than 1600 K. In addition to this, to ensure more extensive dissolution of the alloying components, it is necessary to increase the holding time of the melt in the superheated condition and refining of copper to remove oxygen. Long-term holding at a relatively high temperature increases the consumption of energy resources and results in rapid wear of the refractory (graphitised) lining of the furnaces. The degree of pickup of chromium is approximately 70–80%.

The application of the Cu–Cr master alloy makes it possible to reduce the melt temperature and shorten the melting time. However, this technology has a number of shortcomings. Firstly, melting of the master alloy requires the presence of additional technological operations and the appropriate melting equipment. The master alloy, produced by open melting, usually contains a large amount of oxygen resulting in the oxidation of chromium and its higher consumption. Therefore, to reduce the chromium losses, it is recommended to use vacuum melting furnaces. Secondly, since the chromium content of the standard master alloy is relatively low (6–7%), the fraction of chromium in the charges high (22–25%). In addition to this, the master alloy is often heterogeneous as regards the chemical composition, resulting in difficulties in obtaining the required chromium content in the melted bronze [2, 3].

Using the method of electroslag crucible melting with a nonconsumable electrode, the E.O. Paton Electric Welding Institute, Kiev propose a new method of melting chromium bronze BrKh from non-compacted copper waste (shavings, cut-offs, etc.). Copper is alloyed with chromium directly from the slag by reduction of chromium from the chromium oxide which is supplied in the required amount into the slag pool. The reduction agent is

represented by carbon-containing materials (milled coke or calcium carbide). The formation of metallic chromium, required for alloying copper, takes place as a result of the following reactions:



According to the thermodynamic data, the zero value of the variation of the Gibbs energy ($\Delta G^0 = 0$) of reaction (1) corresponds to a temperature of 1528 K, and for the reaction (2) to 1092 K. This shows that both the reduction reactions can take place in the conditions of electroslag melting of copper.

The production of chromium bronze has therefore a number of advantages in comparison with the traditional melting methods. Since the reduction of chromium takes place in the layer of the molten slag, its interaction with the atmosphere and possible oxidation are prevented.

Electroslag melting of the copper waste is accompanied by the refining of metal by the slag, including removal of oxygen, resulting in more extensive pickup of chromium by copper. In addition to this, as a result of the reduction of chromium oxide, fine particles of metallic chromium appear and this increases the copper–chromium interaction surface and the rate of dissolution of chromium in copper. This also creates an additional saving as a result of the application of copper waste which is cheaper than primary copper, and of chromium oxide Cr_2O_3 (the

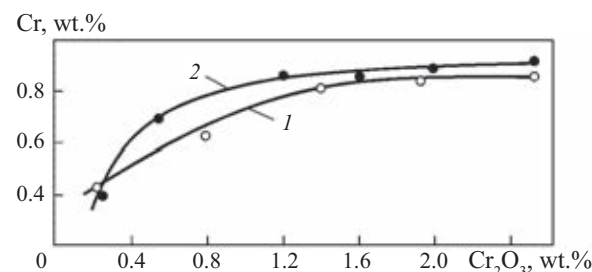


Fig. 1. Dependence of the mass fraction of chromium in the metal on the amount of the chromium oxide in the slag: 1) ANF-7 slag; 2) 50 CaF_2 -25 CaO -25 Al_2O_3 slag.

chromium content of the oxide is approximately 70%) instead of pure metallic chromium or Cu–Cr master alloy.

The experiments were carried out with electroslag melting of bronze BrKh

with alloying with chromium from the slag. 1 kg of copper shavings and fine sheet cut-offs were used. Slags (standard slag ANF-7 and 50 CaF₂–25 CaO–25 Al₂O₃) with no silicon oxide SiO₂ were used, to prevent saturation of the alloy with silicon and which is a harmful impurity in the given type of bronze. The chromium oxide was added to the slags in the amount required for the formation of chromium bronze of the regulated chemical composition, and part of Cr₂O₃ was added during formation of the slag pool, and the remaining amount during melting. In addition to this, in the course of melting Cr₂O₃ was also added to the slag since the reduced chromium on its own may be a reduction agent, for example, for copper oxides, present on the surface of the shavings.

According to the conditions of distribution of the elements between the contacting phases, part of chromium dissolves in the slag pool. To compensate the losses of chromium in the slag, chromium oxide was additionally added

Table 1. The chemical composition of bronze BrKh electricity smelting slag, wt. %

Melt No.	Cr	Ni	Si	Zn	Pb	Fe
1	0.63	0.01	0.04	0.012	0.025	0.04
2	0.7	0.01	0.04	0.010	0.030	0.05
3	0.6	0.01	0.06	0.020	0.020	0.05
BrKh	0.4-1.0	Total sum of impurities not greater than 0.3 wt.%				
GOST 18175-78						

Comment. The base is copper

Table 2. The chemical composition of bronze BrH electricity smelting slag, wt. %

BrKh bronze	σ_b , MPa	δ , %	HB	ρ , ohm mm ² /m
Electroslag melting after heat treatment	450-460	5-6	134-140	0.02
Requirement of TU 48-21-163-72	450-500	4-6	130-140	≤0.02

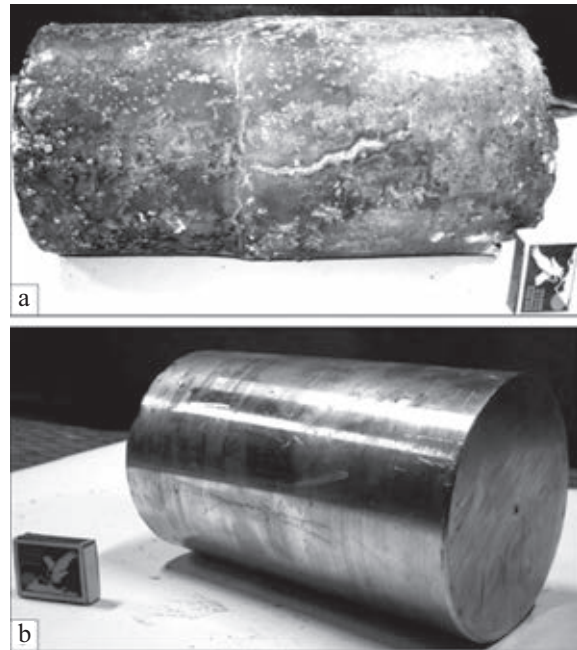


Fig. 2. Castings of BrKh bronze: a) after ???; b) after

to the slag melt on the basis of the calculation to obtain the content of 0.2–2.5 wt.% of Cr₂O₃. The reduction agent was milled coke which was added in the required amount together with the chromium oxide.

In the course of melting it was observed that the moment of formation of the slag melt is the start of rapid reduction of chromium as a result of the interaction of Cr₂O₃ with the carbon in the coke and, to some extent, graphitised electrode. This period is characterised by foaming of the slag, and the process is unstable. However, after melting all slag forming additions and short-term holding, the process is stabilised. Copper and permanence of the chromium oxide with the reduction agent are subsequently added gradually to the slag pool.

The experimental data were used to determine the dependence of the mass fraction of chromium in BrKh bronze on the amount of the chromium oxide in the slag (Fig. 1). To obtain the optimum chromium concentration of the alloy (0.5–0.9 wt.%), the Cr₂O₃ the content of the slag should be maintained in the range from 0.4 to 2.0 wt.%.

It is shown that it is feasible to use electroslag melting to produce chromium bronze from non-compacted copper waste with alloying with chromium by reduction of chromium from Cr_2O_3 in the slag pool.

Taking the experimental results into account, electroslag equipment A-550, modified for melting of copper alloys, with a 260 kW power source was used for verification of the possibilities of melting BrKh bronze and determination of the main technological parameters. Castings weighing approximately 50 kg were produced (Figure 2). The chemical composition of the metal of the castings is presented in Table 2 and shows that the concentration of the main alloying element (chromium) is in the recommended range (GOST 18175-78). The total content of the impurities does not exceed the permissible values. The properties of BrKh bronze, produced by electroslag melting, after heat treatment correspond to the requirements of the technical conditions (Table 3).

Thus, the experimental results were used to develop the technology of electroslag melting BrKh bronze from non-compacted copper waste by alloying with chromium with the reduction of chromium from Cr_2O_3 chromium oxide from the slag pool. Since the main production of chromium bronze is concentrated in the nonferrous metallurgy parts of the Russian Federation (??), this technology can be realised in engineering companies of Ukraine to satisfy the demand for these alloy.

References

1. Smiryagin, A.P. et al., Industrial non-ferrous metals and alloys, Metallurgiya, Moscow, 1974.
2. Mysik, R.K., et al., Metallurgiya Mashinostroeniya, 2010, No. 4, 37–42.
3. Mysik, R.K., et al., Protsessy Lit'ya, 2002, No. 1, 89–94.
4. Nikolaev, A.K. and Rozenberg, V.M., Alloys for electrodes for resistance welding, Metallurgiya, Moscow, 1978.

Submitted 16.01.2012

Distribution of non-metallic inclusions in the cast metal of 316 type steel after circumferential electroslag surfacing with liquid metal

**A.A. Polishko, L.B. Medovar, V.Ya. Saenko,
A.Yu. Tunik and S.N. Stepanyuk**

EO .P aton Electric Welding Institute, Kiev

The results are presented of the evaluation by the method A of the ASTM E45 international standard of the size, composition and nature of the distribution of non-metallic inclusions in the cast metal of the high-alloy type 316 (AISI) steel after consecutive circumferential electroslag surfacing with liquid metal in the cross-section of a modelling ingot.

One of the important criteria of the quality of cast metal, in addition to the microstructure, is the degree of contamination with non-metallic inclusions. With increasing mass of the ingot the size of the nonmetallic inclusions increases, the macro- and microstructure is impaired and this reduces the properties of cast metal. To ensure the guaranteed quality of cast metal in the large ingot which are used as the starting components for components for important applications, it is necessary to produce the homogeneous high-quality structure.

To produce large ingot with the guaranteed-quality structure, it is proposed to use the method of consecutive circumferential electroslag surfacing with liquid metal to increase the size of the ingots [1].

The nonmetallic inclusions of any composition, depending on their size in the conditions of high loading in service, may act as stress concentrators and areas of nucleation of cracks. This is unacceptable for important components, for example rotating sections of advanced steam and gas turbines.

At the present time, the inspection of non-

metallic inclusions in the Ukraine and CIS countries is carried out in accordance with GOST 801-72 standard [2] on the scale for three types of inclusions (oxides, sulphides, globules). The appropriate photographic reference specimens are attached to the standard. Quality is evaluated on the basis of the maximum scale number of the nonmetallic inclusions in six specimens, and the permissible value changes depending on the melting methods on the diameter of the product. However, this standard does not stipulate how many inclusions of the maximum scale number can be located on the inspected surface of the specimen.

Abroad, the degree of contamination with the nonmetallic inclusions is evaluated using the A method of the ASTM E45 standard [3] for four types of inclusions (oxides, sulphides, silicates and globules) of the fine antiques series (size) using the IR scale. The maximum and minimum scale number of the specific type of inclusion and the mean scale number are determined for each specimen.

In the present work, two methods were

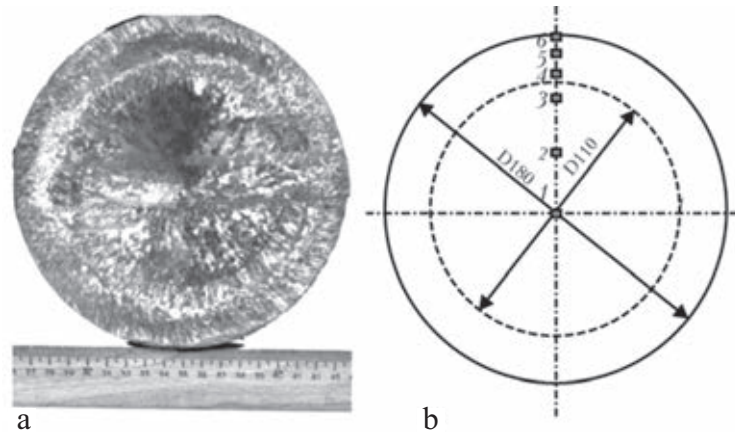


Fig. 1. Macrostructure of a transverse templated of the modelling two-layer ingot after electroslag surfacing with liquid metal (316+316) and the points of analysis of nonmetallic inclusions (b): 1) the axial part of the central ingot; 2) the middle of the radius of the central ingot; 3) the melting zone on the side of the central ingot; 4) the melting zone on the side of the deposited layer; 5) the middle of the deposited layer; 6) the edge of the deposited layer; the dashed line shows the line of fusion of the deposited layer with the central ingot.

used: qualitative (scale numbers) and quantitative inspection of the nonmetallic inclusions (method A according to ASTM E45 and method L2 according to GOST 1778[4] standard).

The aim of the present work is the evaluation of the size, composition and nature of distribution of the nonmetallic inclusions of

the cast metal of the type 316 alloy steel (AISI) after consecutive circumferential electroslag surfacing with liquid metal in the cross-section of the modelling ingot.

The initial material was the Cr-Ni-Mo type 316 high-alloy steel (AISI), with the following chemical composition, wt.%: < 0.08 C; 2.0 Mn; 2.0 Mo; 1.0 Si; 17.0 Cr; 12.0 Ni;

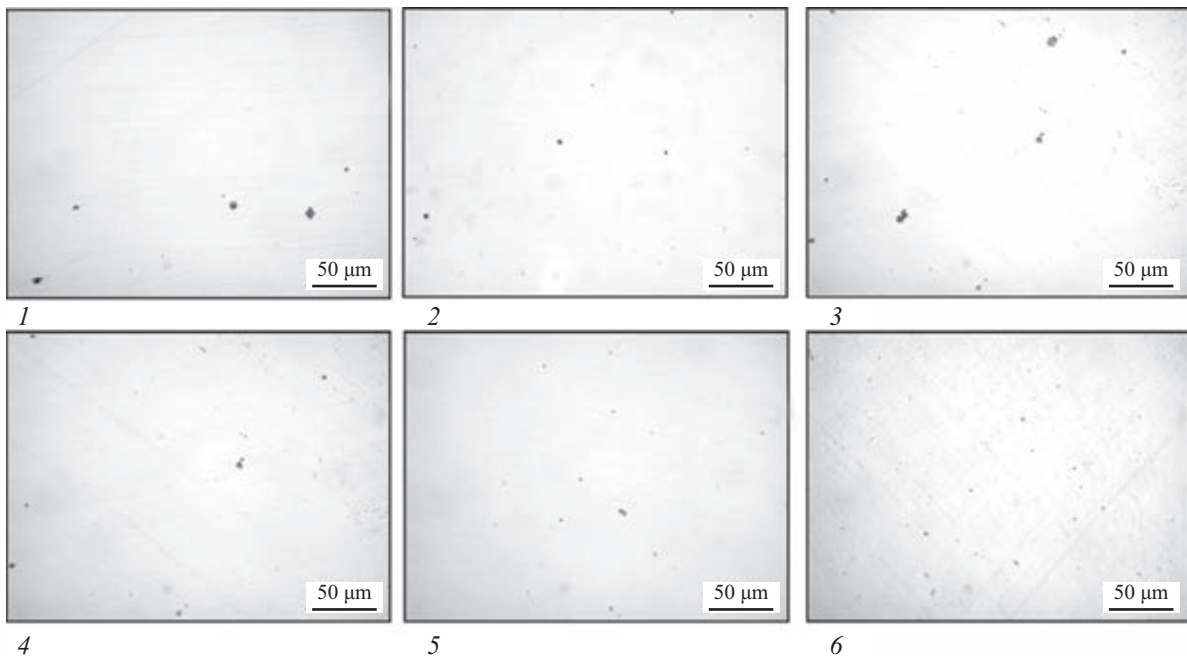


Fig. 2. The distribution of non-metallic inclusions in non-etched specimens (for the designation of the positions 1-6 see Fig. 1).

balance Fe; up to 0.03 S; P up to 0.045. The degree of contamination with nonmetallic inclusions was inspected using the method A of the ASTM E45 international standards and, for comparison, method L2, according to the GOST standard.

The size, composition and nature of distribution of the metallic inclusions were evaluated in the metal of the modelling two-layer ingot with a diameter of 110–180 mm, produced from the high-alloy Cr–Ni–Mo type 316 steel, produced in the course of the full-size experiments in the laboratory conditions by circumferential electroslag surfacing with liquid metal to increase the size of the ingot. The nonmetallic inclusions were analysed in the cross-section of the specimens taken from the characteristic zones of the modelling ingot according to Fig. 1, *B* at the points 1–6.

The nature of distribution of the non-

metallic inclusions was evaluated by optical microscopy in a Neophot-323 metallographic microscope, fitted with an attachment for digital photography of non-etched specimens. A small number of inclusions, from 1 to 6 (Fig. 2) was found in the field of the eyepiece. At the points 3–6 the deposited metal containing considerably smaller number of inclusions in the field of the eyepiece in comparison with the points 1–3 in the central ingot (Fig. 2).

To evaluate the dimensions and composition of the non-metallic inclusions in the cross-section of the modelling did, experiments were carried out using the method A of the ASTM E45 international standard which makes it possible, on the basis of the images of the non-etched surface of the specimens, to automatically classify the nonmetallic inclusions on the basis of the morphological types and also determine the series and scale number of the inclusions.

Table 1. Analysis of the non-metallic inclusions in the two-layer modelling ingot of 316 high-alloy steel

Examined area	Type	Size No.	Number (%)	Mean size, m	Group of inclusions acc. to GOST 1778 (method L2)
Ingot centre (point 1)	A	0.5	10 (59)	4.55	3
	AB		7 (41)	4.31	
Middle of ingot radius (point 2)	A	< 0.5	6 (29)	3.77	3
	AB	1.0	15 (71)	3.82	
Edge of ingot, fusion zone (point 3)	A	< 0.5	9 (45)	2.36	2
	AB	0.5	11 (55)	2.38	
Fusion zone in deposited layer (point 4)	A	< 0.5	8 (47)	2.95	2
	AB	0.5	9 (53)	2.46	
Middle of deposited layer (point 5)	A	< 0.5	10 (52)	2.56	2
	B		3 (16)	2.80	
	AB		6 (32)	2.46	
Edge of deposited layer (point 6)	A	< 0.5	17 (61)	1.67	1
	AB	0.5	11 (39)	1.88	
Comment. According to ASTM E45 the 'fine' series was determined for all types of inclusions					

The analysis procedure can be described as follows. Initially, the nonmetallic inclusions were classified on the basis of the brightness characteristics in the BEI regime (images in secondary electrons) using the analytical complex consisting of a scanning electron microscope JSM-35CF of the JEOL company (Japan) and x-ray spectrometer with energy dispersion of the X quanta (model INCA Energy-350, Oxford Instruments, Great Britain). The experiments were carried out at an acceleration voltage of 20 kV, magnifications 200–4000, elemental analysis was carried out in the range from B to U. The morphological features and the chemical composition determined by the energy dispersing spectral analysis were used for classification of the nonmetallic inclusions according to the type and dimensions.

The analysis results of the nonmetallic inclusions were processed using a special program for quantitative classification of the phases and inclusions (Feature).

The following types of non-metallic inclusions were analysed: sulphides A, aluminium oxide B, silicates C, globular oxides D and mixed type inclusions AB.

According to the ASTM E 45 international standard, the material contains the type A inclusions and a small amount (16%) of type B inclusions. In addition to this, the inclusions of the mixed type AB were found (Table 1).

The mean linear size of the nonmetallic inclusions for the central ingot was 2.36–3.82, and for the deposited metal 1.67–2.8 μm .

For comparison, the approximate groups of the inclusions were evaluated on determined in accordance with the method L2 according to the GOST 1778 standard. A small change (refining) of the size of the inclusions in the direction from the centre of the initial ingot to

the edge of the deposited layer was detected.

Thus, the results show almost the uniform distribution of the non-metallic inclusions in the cross-section of the modelling ingot of the 316 high alloy steel. All the types of nonmetallic inclusions are characterised by the 'fine' series. The experimental results show that the mean linear size of the non-metallic inclusions for the central ingot is 2.36–3.82 μm , and for the deposited layer 1.67–2.8 μm . A small scatter of the dimensions of the inclusions in the investigated zones was found: in the central zone of the initial ingot 4.31–4.55, in the melting zone 2.36–2.95, in the deposited layer 1.67–2.8 μm . On the whole, the maximum size of the nonmetallic inclusions in the cast metal of the modelling ingot after circumferential electroslag surfacing with liquid metal carried out to increase the size of the ingots of the 316 high-alloy steel with a diameter of 180 mm did not exceed 4.55 μm . For comparison, the ingots with a diameter of 120 mm of ShKh 15 steel were also investigated [5]. The maximum size of the non-metallic inclusions after electroslag remelting did not exceed 20 μm .

References

1. Paton, B.E., et al., *Sovremennaya Elektrometallurgiya*, 2007, No. 1, 3-7.
2. GOST 801-78. The ball bearing steel. Technical conditions, the Standards publishing house, Moscow, 1978.
3. ASTM E45-05. Standard test methods for determination of the content of inclusions in the steel, American Society for Testing and Materials, New York, 2005.
4. GOST 1778-70. Steel. Metallographic methods of determination of the nonmetallic inclusions, State Committee for Standards, Moscow, 1970.
5. Paton, B.E. and Medovar, B.I. (editors), *Electroslag metal*, Naukova Dumka, Kiev, 1981.

Submitted 29.11.2011



Development of new titanium biocompatible alloys for medical applications

V.F. Topol'skii, S.V. Akhonin, G.M. Grigorenko
and I.K. Petrichenko

EO .P aton Electric Welding Institute, Kiev

The mechanical characteristics of vanadium-free titanium alloys of different systems of alloying developed in Ukraine and designed for manufacture of different products for medical purposes are presented. The high level of biological compatibility and corrosion resistance of the developed titanium alloys is shown. Analyzed are the structural-phase composition of new titanium alloys after thermomechanical treatment, as metal of well as their welded joints. The feasibility of production of these alloys by the method of electron beam cold hearth melting was confirmed. The physical and chemical properties of the developed titanium alloys stipulate their wide application in orthopedy and stomatology.

Titanium alloys are used on an increasing scale in various branches of medicine, displacing the previously widely used stainless steels and cobalt–chromium alloys. The interest in titanium, characterised by the small specific weight, high corrosion resistance and high biological compatibility, has greatly increased and also as a result of the development of surgery in the area of replacement of joints by endoprosthesis and the result of the increase of the volume of application of implants in stomatology.

The materials used in the medicine (especially those used for the manufacture of endoprosthetic devices and implants) must ensure the long service life of components produced from them and, therefore, they should be alloyed only with biocompatible non-toxic elements, whereas the alloying

elements (vanadium, cobalt and nickel) may form toxic compounds in the human organism [1]. On the whole, the structural material for medical application should have the following characteristics:

- high strength and long-term efficiency in the conditions of a biological medium (corrosion resistance);
- absence of undesirable reactions of living tissue to the products of their wear; the capability of the implants and endoprosthesis to grow around the bone tissue (bio adhesion);
- absence of contraindications to autoclave or dry steam sterilisation;
- high plasticity and technological properties;
- low elasticity modulus;
- low cost.

However, these requirements are not satisfied by all titanium alloys. Until recently, the endoprosthesis and implants were produced widely using the materials such as unalloyed titanium and Ti-6Al-4V alloy. With high corrosion resistance, unalloyed titanium has a sufficiently high strength (400–500 MPa) which may cause undesirable complications not only in service of the component but also in its manufacture, and Ti-6Al-4V alloy contains toxic vanadium, and the dissolution of this element in the organism maybe the reason for inflammatory processes with toxicity features.

The titanium alloys for medical applications, developed in the EC countries, i.e., Ti-6Al-7Nb, Ti-5Al-2.5Fe-Ag, etc, are characterised by satisfactory combination of the mechanical characteristics and corrosion resistance [2, 3], and also do not contain toxic alloying elements. However, the composition of this alloy includes a large amount of expensive alloying components so that they are relatively expensive. These shortcomings are also typical of the recently developed titanium alloys based on the β -phase Ti-15Mo-5Zr-3Al, Ti-30Ta, β -21S (Ti-3Al-15Mo-2.6Nb-0.2Si) which also are characterised by the relatively low elasticity modulus, are in fact isoplastic [1].

Thus, it has become necessary to develop domestic medical titanium alloys without expensive alloying elements in large quantities and satisfying these requirements. Good weldability is an important parameter of the new alloys.

The E.O. Paton Electric Welding Institute, Kiev has developed to alloys for medical applications (TM1 of the Ti-Al-Nb-Zr [4] and TM2 of the Ti-Al-Nb-Fe-Zr system [5]), calculated for different strength levels.

These alloys were produced by the technology of electron beam melting with a cold hearth (intermediate container) (EBMCH). The EBMCH process is based on the horizontal feet of a consumable blank at the given rate into the melting zone with melting of the blank by the electron beams above the cold hearth when the cold hearth is filled, the liq-

Table 1. Mechanical characteristics of several titanium alloys.

Material	$\sigma_{0.2}$	σ_B	σ_{-1}	$E \times 10^{-4}$	δ	Ψ
	MPa			%		
BT1-0	320	400	170	11.1	25	–
Ti6Al 4V	795	860	400	11.5	10	25
Ti6Al 17N b (Switzerland)	900	1000	–	–	13	–
TiA 1N bZ r (TM1)	780	800	360	9.6	22	60
TiA 1N bZ rF e (TM2)	920	1000	–	–	16	40
Bone	250	–	200	2.5	0.5	–

uid metal is discharged into the solidification mould with the baseplate where the ingot is produced. In melting, the surface of liquid metal in the intermediate container and the solidification mould is heated with the electron beams guns. During melting of the ingot, the latter was withdrawn mechanically from the solidification mould. The process continued up to complete melting of the initial blank.

The consumable blank for the remelting process was produced from pure charge components in the form of titanium strips of VT1-00 grade and A95 aluminium, and also shavings of N6-1 niobium, E100 zirconium and commercial purity iron (Armco) grade 10895 (TM2 alloy) so that in any cross section the given content (in %) of the alloying elements and the base of the alloy was maintained.

Since the EBMCH processes carried out in a high vacuum (0.01–0.1 Pa), the alloying elements with the vapour tension exceeding that of titanium evaporate at a higher rate than the base and this results in changes in the composition of the alloy in comparison with the initial charge. This relates to aluminium in the investigated alloys. Therefore, to compensate the losses of aluminium through evaporation of this element in melting of the ingots an additional amount of aluminium was added to the initial charge calculated in accordance with the previously established relationships of the process of evaporation of the components of the alloy from titanium in EBMCH [6].

Table 2. The corrosion rate of titanium alloys, mm/year

Medium	TM2	TM2	VT1-0
1% HCl	–	0.0001	0.0035
5% HCl	0.0019	0.0002	0.0042
10% HCl	0.029	0.027	0.079
5% H ₂ SO ₄	–	0.0002	0.0039
10% H ₂ SO ₄	0.0005	0.0005	0.0063
20% H ₂ SO ₄	0.0005	0.0007	0.055
Concentrated H ₂ SO ₄	0.14	–	1.425

The blanks with the thickness of 6 mm were produced from the melted ingots by thermal mechanical deformation in a two-role reversing mill and subsequently subjected to relaxation annealing.

The mechanical properties of the alloy is developed and used in medicine are presented in Table 1.

In the development of stomatological, orthopaedic and cardiological prosthesis it is important to ensure that the material has not only the optimum ratio of the mechanical properties but is also characterised by the high level of the resistance of alternating loading and fatigue characteristics.

The fatigue characteristics of TM1 alloy and, for comparison, VT1-0 and Ti-6Al-4V alloys where carried out at the I.N. Frantsevich Institute of Powder Metallurgy using the procedure and equipment described in [7].

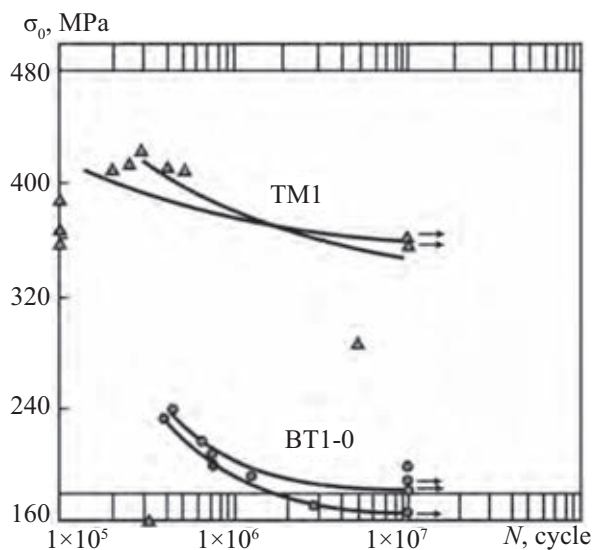


Fig. 1. Fatigue characteristics of titanium alloys.

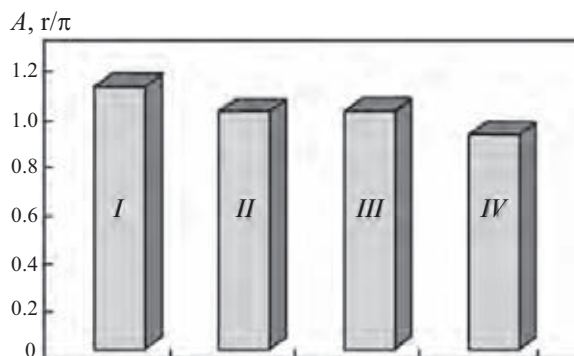


Fig. 2. Morphological characteristics of several metals: I) a chromium-cobalt alloys; II) gold; III) titanium; IV) TM1; A is the concentration of immunoglobulin.

The fatigue curves are presented in Figure 1. The comparison of the fatigue properties of the TM1 alloy, VT1, commercial titanium and VT6 alloy shows that the fatigue resistance of TM1 alloy is considerably lower than that of VT6 alloy but approximately twice as high as that of commercial titanium.

The TM1 and TM2 alloys are characterised by satisfactory weldability so that they can be used for producing welded structures in the manufacture of equipment and tools for medical purposes.

The TM1 and TM2 alloys were tested at the UkrNIIkhimmach for general corrosion in the solutions of sulphuric and hydrochloric acids at room temperature (Table 2).

Analysis of the results shows (Table 2) that the corrosion rate of the TM1 and TM2 alloys in the diluted hydrochloric and sulphuric acids is an order of magnitude lower than in the unalloyed titanium of grade VT1-0 in the same media. In the 10% HCl solution, the corrosion rate is lower than in the unalloyed titanium (at least twice as low), and in the 10 and 20% solutions of sulphuric acid the corrosion rate in the titanium alloys is lower than that of unalloyed titanium by one or two orders of magnitude, respectively.

In addition to the mechanical and corrosion properties, the TM1 and TM2 alloys where also investigated to ascertain the possibilities for use in medical practice.

The Ukrainian Scientific Research Institute of Traumatology and Orthopaedy investigated new alloys for corrosion, bioresistance and

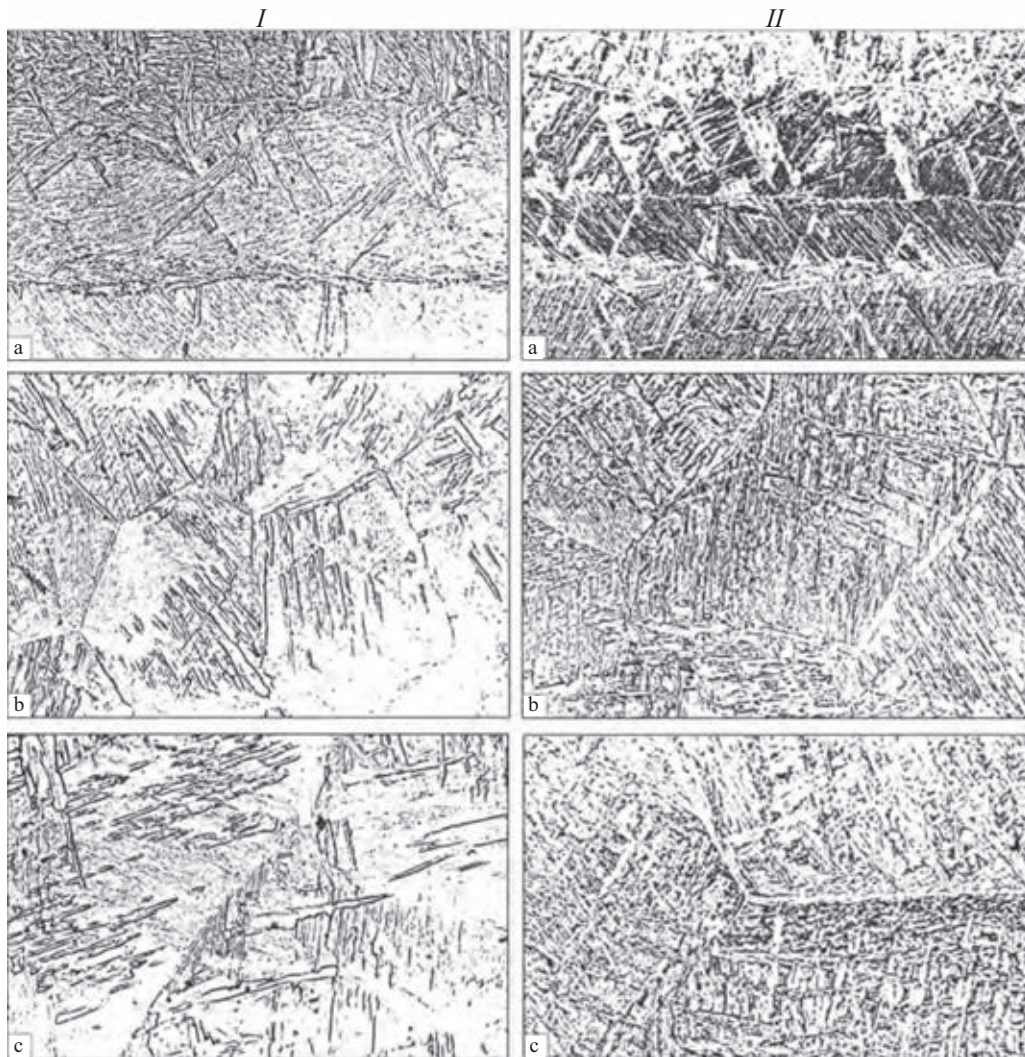


Fig. 3. Microstructures of the welded joints in TM1 (Ti–Al–Nb–Zr) I, $\times 250$ and TM2 (Ti–Al–Nb–Fe–Zr) II, $\times 300$ alloys: a) the parent metal; b) the heat affected zone; c) the weld metal.

biocompatibility in the organism of animals and the reaction of bone and paraossal tissue in implantation of specimens of these alloys. The experiments were carried out on 40 adult rats, the duration of observation of the experimental animals reached 180 days. As a result of the investigations, it was concluded that the new titanium alloys are characterised by satisfactory biological inertness and compatibility to that they can be used as the materials for the manufacture of prosthetic components.

The Institute of Ecohygiene and Toxicology has carried out labour hygiene investigations of the TM1 and TM2 alloys and con-

clusions were made regarding their suitability for reduction of medical semifinished products and components.

The Department of Orthopaedic Stomatology of the National Medical University Carried out morphological studies of the TM1 titanium alloys; special attention was given to the dynamics of the formation of immunoglobulin (the cells of immune protection) after adding a foreign body. The most efficient reaction of the immune system of the organisms in comparison with the chromium–cobalt alloy, gold and commercial titanium, used widely in stomatological, was recorded for the TM1 alloy (Figure 2).

On the basis of the investigations The National Sanitary Epidemiological Service of The Ministry of Health Protection of Ukraine issued a decision allowing the application of TM1 and TM2 alloys.

In addition to the determination of the mechanical, fatigue and corrosion characteristics, the structure of the new titanium alloys was also investigated. Since the manufacture of components for medical applications also include welding, the structure of both alloys and welded joints in these alloys was investigated.

The TM1 alloy (system Ti–Al–Nb–Zr) belongs in the group of titanium pseudo α -alloys and is thermally stable. In the condition after rolling, the alloy consists of the primary β -grains highly deformed and elongated in the rolling direction. The internal structure is represented by the colonies of the plate-shaped α -phase with different crystallographic orientation. In the metal of the heat affected zone and the welded joint at the boundaries of the primary β -grains examination shows the precipitation of the α' -phase with a 'coarser' morphology in comparison with the parent metal (Fig. 3).

The TM-2 alloy (system Ti–Al–Nb–Fe–Zr) alloy belongs in the group of the titanium ($\alpha+\beta$) martensitic alloys. In the rolled condition, the alloy has the structure formed by the plate shaped β -phase, but in the gaps between the α -phase there is the β -phase whose amount depends on the heat

treatment conditions. The structure of the heat affected zone metal is represented by equiaxed grains and that of the welded joint by the equiaxed primary β -grains elongated in the rolling direction with the martensitic internal α -phase (Fig. 1).

The TM1 and TM2 alloys and also their welded joints, have a structure characteristic of the alloys of the appropriate groups. No welding defects were found in the investigation of the macrostructure of the welded joints in these alloys.

Thus, the TM1 and TM2 alloys, developed at the E.O. Paton Electric Welding Institute, Kiev, are characterised by high mechanical properties are also satisfactory corrosion resistance and biological compatibility. Consequently, they can be used widely in various areas of medicine such as orthopaedy and stomatology.

References

1. Mutsuo, N., Proceedings of the 11th World Cup Congress on Titanium, The Japan Institute of Metals, Kyoto, 2007, 1417–1424.
2. Cao, P., et al., *ibid.*, 1509–1512.
3. Igoikin, A.I., *Titan*, 1993, No. 1, 7–10.
4. Paton, B.E., et al., Thermally strengthened and corrosion-resisting titanium alloys, Patent 7385, Ukraine, MPC S 22 S 14/00, 29.9.1995.
5. Paton, B.E., et al., Thermally stable high-erosion resistance titanium alloy, Patent 7386, Ukraine, MPC S 22 S 14/00, 29.9.1995.
6. Paton, B.E., et al., Electron beam melting of refractory and high-reactivity metals, *Naukova Dumka*, Kiev, 2008.
7. Lugovskoi, Yu.F., *Probl. Spets. Elektrometall.*, 1987, No. 4, 61–65.

Submitted 17.10.2011

Production by electron beam remelting of defect-free titanium ingots with controlled oxygen content

V.I. Kostenko, M.P. Kruglenko, A.N. Kalinyuk and P.A. Pap

Strategiya BM Company, Kiev

Experimental investigations were carried out on dissolution of titanium dioxide in melting of ingots by electron beam cold hearth remelting. The condition of melting was selected for installation TIKO-15, at which the complete dissolution of titanium dioxide, added to flux, occurs. This technology provides the producing of defect-free ingots with a preset interval of oxygen concentrations and value of oxygen equivalent.

One of the main tasks in the production of ingots of unalloyed titanium is the prevention of the formation in titanium of gas-saturated zones which, because of their high hardness, are regarded as stress concentration and sources of nucleation of fatigue cracks [1]. In electron beam remelting (EBR) of only titanium sponge, this problem is solved by using an intermediate container (cold hearth)[2].

However, at the present time, many companies require titanium with the specified range of the concentration of impurities because the restriction of the minimum and maximum content of the impurities ensures the required service properties (σ_B , σ_T , δ , Ψ) in a specific range for semi-finished and completed products so that it is necessary to alloy the initial charge with an additional amount of oxygen in the form of titanium dioxide. For example, according to the standards of the VSMPO-AVISMA Corporation, in some grades of unalloyed titanium Gr1-1, Gr1-2, Gr1-4 l, Gr1-5 tr, the distribution of oxygen in the ingots should not deviate by more than 0.01–0.02 wt.% from the specified distribution. According to the international standards ASTM B348-05, in addition to the specific

oxygen content, it is also necessary to ensure the required value of the oxygen equivalent O_E , calculated from the equation $O_E = \% O + 2.5\% N + 0.7\% C + 0.6\% Fe$ in the range 0.17–0.21%. Without alloying with oxygen it is almost impossible to solve these problems.

When adding an additional amount of titanium dioxide into the charge, it is important to investigate the processes of dissolution of the added titanium dioxide powder and homogenising of the melt in the cold hearth during electron beam remelting. Since the ranges of the concentration of oxygen and of its equivalent are very narrow, it is also important to take into account the macroliques of the elements, included in the calculation of the oxygen equivalent.

The company Strategiya BM have developed a technology of alloying titanium ingots with oxygen in equipment for electron beam welding with a cold hearth TIKO-15 (Fig. 1), which may be described as follows. The remelting starting material (consumable charge blank) is represented by the briquettes of titanium sponge, scrap metal. After loading the charge into the equipment and evacuating to the level of the residual pressure required

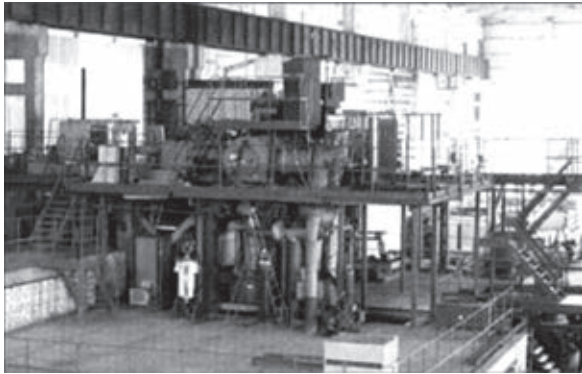


Fig. 1. TIKO-15 electron beam equipment.

for stable operation of the electron beam guns ($1 \times 10^{-1} \dots 1 \times 10^{-2}$ Pa), the blank is melted in the cold hearth until it is full and subsequently the liquid metal is periodically discharged into the solidification mould. The first portions after discharge result in the formation of the seed for the future ingot. Subsequently, in the given technological conditions, the ingot of the required height is melted. To produce the given concentration of oxygen in the ingot, the required amount of titanium is outside is added to the charge already taking into account the existing oxygen content. Titania is deposited on the surface of briquettes as a layer not thicker than 0.5 mm.

The melting point of titania (1870°C) is higher than the temperature of the melt which can be reached by superheating the metal (the melting point of titanium is 1670°C). Therefore, the titania does not melt and dissolves and the required time is longer with the increase of the thickness of the layer of titania.

Dissolution of titania in the melt is accompanied by the formation of oxygen-enriched zones [2]. According to the titanium–oxygen equilibrium diagram [3], titanium with the higher oxygen content is characterised by a higher melting point than that of pure titanium (Fig. 2). If the melt is not homogenised prior to discharge into the solidification mould, the oxygen-enriched metal may solidify ahead of the solidification front because the solidification temperature is higher and this may result in the formation of a zone with higher hardness in the ingots. This may be accompanied

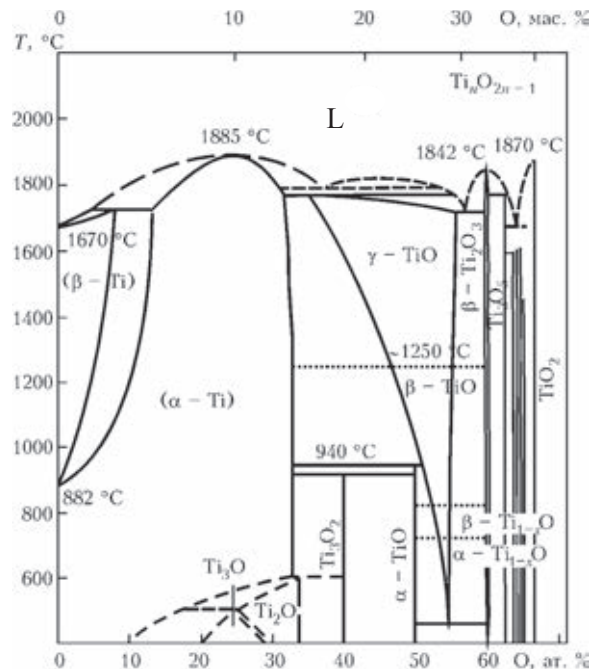


Fig. 2. The equilibrium diagram of the titanium–oxygen system.

by the formation of micropores.

It should also be mentioned that in solidification of the oxygen concentration of the solid phase increases even further because the distribution coefficient $k_0 = C_s/C_l$ is higher than unity: $k_0 \approx 1.5$ at mass fractions of oxygen smaller than 3.2%, and at higher fractions $k_0 \approx 2.5$ [4].

Thus, only the homogenised melt should be discharged into the solidification mould. Therefore, the dissolution τ_{calc} of the portion of titania and homogenisation time of the melt τ_{hom} should be shorter than the time during which the molten metal is held in the cold hearth. The time τ depends strongly on the geometry of the cold hearth and also the melting rate.

The required melting rate for this equipment was determined by experiments on the basis of the absence of oxygen-enriched zones in melted ingots. For example, at a melting rate of 11 kg/min, defects were not detected in the ingot by ultrasonic inspection because of small differences in the density and due to the absence of defects in the form of pores, cracks and also because of the large size of the ingot (630 mm). However, after rolling the metal, the oxygen-saturated areas showed the

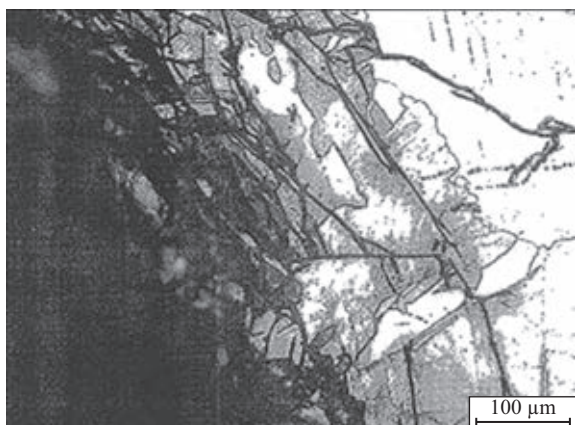


Fig. 3. The microstructure of a defect.

formation of microcracks and micropores as a result of considerably higher hardness [1].

Investigations of the defective zones of the rolled metal were carried out in the laboratory of VSMPO-AVISMA company. The microhardness of the parent metal was 1870–2160 MPa, whereas the microhardness in the defective zone was 5550–6450 MPa. The microanalysis of the oxygen content showed that the metal in the defective zone is characterised by a higher oxygen content (2.2–2.6 wt.%), whereas the mass fraction of oxygen in the parent metal was 0.13%. The microhardness of the metal of the oxygen-enriched defect in the titanium ingot is shown in Fig. 3.

After reducing the melting rate to 7.5 kg/min, no defects were detected in the cast metal or after rolling. Thus, by restricting the melting rate it is possible to produce the titanium ingots without defects and with the required level of oxygen as a result of adding the required amount of titania to the initial charge. By varying the content of nitrogen, carbon and iron in the initial charge, it is possible to produce titanium ingots with the required oxygen equivalent.

It should be mentioned that in electron beam melting of titanium the macroliqation of oxygen was observed only in the narrow transition zones at the start and end of melting and was not detected across the ingot [5]. Therefore, when adding TiO_2 to the charge, it should be taken into account that the oxygen in the transition zone at the

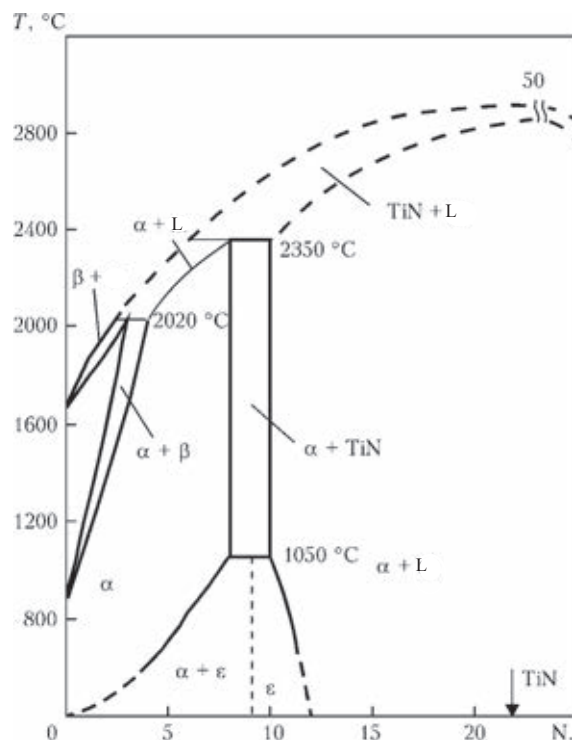


Fig. 4. The equilibrium diagram of the titanium-nitrogen system.

start of melting is characterised by a higher content, whereas at the end of melting the content is lower.

If it is required to produce ingots with the regulated oxygen equivalent, it is also important to take into account the macroliqation of other elements included in the calculation equation. If the program of the macro liqation of iron in electron beam welding was investigated in [6], no mention was made of nitrogen. This is associated mainly with the fact that the nitrogen is a very harmful impurities and its permissible concentration is very low, usually less than 0.015 wt.%. However, nitrogen is included in the equation for calculating the carbon equivalent with the highest coefficient, i.e., 2.5, since it is the strongest hardening element and its effect is very strong.

Examination of the equilibrium diagram of the titanium-nitrogen system shows (Figure 4) that at low concentrations the coefficient of distribution of nitrogen is higher than unity, as in the case of oxygen, and equals $k_0 \approx 1.9$. Therefore, the macro liqation in the case of nitrogen should be evident in electron beam

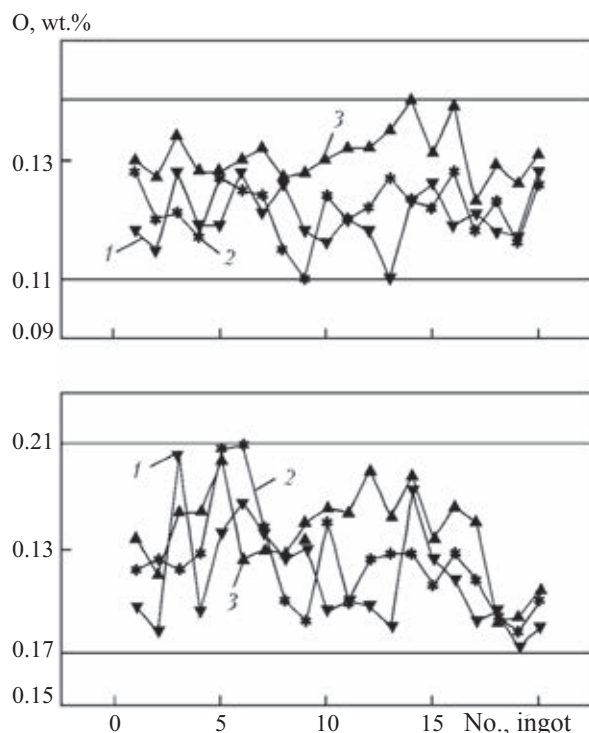


Fig. 5. The oxygen concentration in the ingots alloyed to 0.11–0.14% (a) and the oxygen equivalent in them (b): 1) riser; 2) the centre; 3) the bottom part.

remelting, similar to that of oxygen, i.e., the nitrogen concentration of the transition zone and the start of melting should be higher and the end lower [5]. For the experimental verification of this fact, melting of the ingot from a homogeneous charge was followed by detailed gas analysis in the laboratory of the E.O. Paton Electric Welding Institute, Kiev. Four samples were taken from the central part of the ingot and five samples from the bottom and top part of the ingot. The mean nitrogen concentration in the ingot was as follows, wt.%: 0.0098 in the central part, 0.0124 in the bottom part, 0.0081 in the top part of the ingot.

The mean mass fractions of oxygen in the ingots were as follows, %: 0.100 in the central part, 0.112 in the bottom part, 0.093 in the top part.

Thus, the macro liquation with respect to nitrogen was equal to only 0.004 wt.%. However, taking into account the multiplier of 2.5 in the calculation of the oxygen coefficient gives 0.01 wt.% which is quite high

at the background of the permissible value of 0.04 wt.%.

As an example, we consider the results of a series of pilot plant melts in TIKO-15 of titanium ingots with a diameter of 610 mm with the target oxygen content of 0.11–0.14 and the oxygen equivalent of 0.17–0.21 wt.%. The initial charge was in the form of briquetted TiO_2 sponge with the oxygen content of 0.05–0.08 wt.% and with additional alloying with TiO_2 powder in the amount required for obtaining the given oxygen content of the ingot. The charge was produced taking into account the presence in titanium sponge of impurities of carbon, iron, and nitrogen by selecting combinations of the content of these elements in order to obtain the required oxygen equivalent. The distribution of oxygen in the oxygen equivalent along the length of all melted ingots is shown in Fig. 5. As indicated by the graphs, the scatter of the values of the oxygen content and the oxygen equivalent is not outside the given range, indicating satisfactorily technological stability and predictability of the melting process.

Thus, a technology has been developed for producing defect-free titanium ingots with the regulated content of oxygen by the methods of electron beam melting with the cold hearth. The experiments were carried out to determine the melting rate for the given equipment at which the particles of titania are fully dissolves and the melt is homogenised in the cold hearth, and the ingots do not contain any oxygen-enriched defects. An industrial batch of the ingots with the required mass fraction of oxygen and also with the oxygen equivalent was produced.

References

1. Henry, J.L., et al., Metallurgical Transactions, 1973, No. 4, 1859–1864.
2. Paton, B.E., et al., Electron beam melting of titanium, Naukova Dumka, Kiev, 2006.
3. Hansen, M. and Anderko, K., The structure of the binary alloys, Metallurgizdat, Moscow, 1962.
4. Mitchell, A. and Kawakami, A., in: Ti-2007 Science and Technology, Kyoto, The Japan Institute of metals, 2007, 173–176.
5. Amelin, A.I., et al., Sovremennaya Elektrometallurgiya, 2009, No. 4, 29–32.
6. Amelin, A.I., et al., Titan, 2010, No. 1, 15–20.

Multilayer Ti/Al foils: methods of production, properties and application in pressure welding

A.I. Ustinov, Yu.V. Fal'chenko, T.V. Mel'nichenko, G.K. Kharchenko,
L.V. Petrushinets and E.A. Shishkin

EO .P aton Electric Welding Institute, Kiev
GV.K urd umov Institute of Physics of Metals

An electron beam method is presented for producing multi-layer foils on the base of intermetallide-forming base. Results of application of mentioned foils as intermediate interlayers in diffusion welding of titanium aluminides are considered.

The production of permanent joints in composites, intermetallic compounds and dissimilar materials by melting in the joining zone is usually accompanied by considerable degradation of their properties. The application of the method of diffusion pressure bonding (DB) in the solid-state makes it possible to avoid these changes in the structure of low-weldability materials in the weld zone. However, the application of this method in practice is complicated by the need to heat the metal of the weld zone to high temperatures (higher than $0.7 T_m$, where T_m is the melting point of the welded material), the application of high pressure, ensuring plastic deformation of the welded material, and long-term holding of the weld zone under these conditions [1]. Since the materials based on intermetallics and composite are difficult to the form, even in heating to high temperatures the application of the method of diffusion bonding is associated with a number of difficulties [2].

Considerable 'softening' of the conditions of formation of joints in low-deformability metals by the method of diffusion bonding (reduction of temperature in heating and of the level of applied pressure, and also holding

time) is achieved by introducing interlayers based on ductile metals between the welded surfaces [3–6].

It is assumed that in welding heating and application of pressure result in plastic flow of these interlayers which results in the deformation of the subsurface layers of the welded materials. This type of plastic deformation of the interlayer ensures, on the one hand, establishment of physical contact between the welded surfaces and, on the other hand, increases the density of defects in the subsurface layers thus accelerating the diffusion processes in the weld zone. Thus, the weld zone is characterised by the development of processes ensuring mutual inter-growth of the grains between the welded materials at lower temperatures and applied pressure, in comparison with diffusion bonding of the same materials without the interlayer.

At the same time, the use of ductile interlayers in diffusion bonding results in the formation in the weld zone of chemical heterogeneity and, consequently, the strengths and service properties of the welded joint are impaired [7]. The reduction of the degree of chemical heterogeneity in the weld zone by

reducing the thickness of ductile interlayers requires a large increase of welding pressure [8].

The chemical heterogeneity in the metal of the weld zone in diffusion bonding can be reduced, for example, by the application of interlayers consisting of layers based on components included in the composition of the welded material. For example, in welding intermetallic compounds the interlayer should consist of layers based on components forming the intermetallic compound, for example, the layers of aluminium and titanium. In welding, the laminated structure of the interlayer should transform into the structure of the intermetallic compound, for example, TiAl. The application of this approach using the laminate structures is complicated by the large thickness of the layers of the components and by the presence of an interface between them. These shortcomings should be eliminated using multilayer foils (MF) produced by consecutive deposition of components. By varying the thickness of the layers of the components and characteristics of their microstructure, it is possible to determine the path and kinetics of the synthesis reaction of the intermetallic compound in the foil during heating so that a structure, similar to that of the welded material, forms in the foil.

In this study, the Ti–Al system is used to generalise the results obtained in the development of the method of producing multilayer foils on the basis of intermetallic-forming components, and the possibilities of using them as the interlayer in diffusion bonding of titanium aluminides are investigated.

Methods of production and investigation of Ti/Al multilayer foils

The multilayer Ti/Al foils, consisting of the alternating layers of titanium and aluminium, were produced in equipment described in [9]. The principle diagram of deposition of the foils is shown in Fig. 1. For layer deposition of titanium and aluminium, the vacuum chamber was separated vertically by a continuous screen into two equal parts and

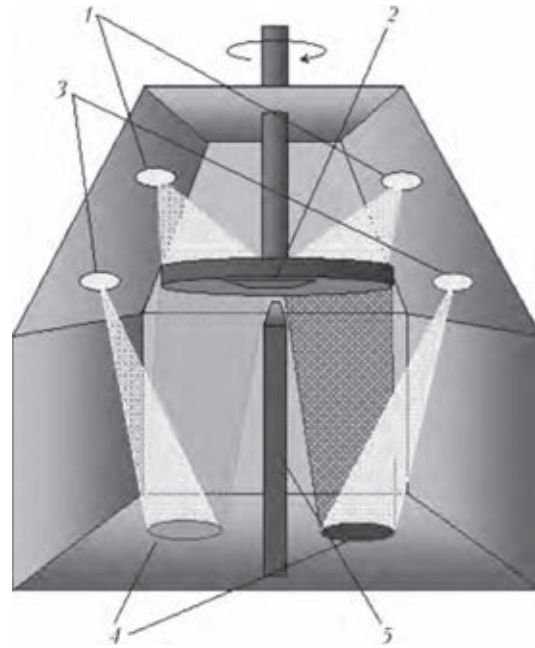


Fig. 1. Diagram of the process of electron beam deposition of multilayer foils: 1) heating electron beam guns; 2) substrate; 3) evaporating electron beam guns; 4) crucibleless for evaporation was ingots; 5) separating non-permeable screen.

copper watercooled crucibles were placed in each section. One of the crucibles contained a titanium ingots, the other one an aluminium ingot. Using the evaporating electron beam guns, a molten pool was produced on the surface of the ingots and elements were subsequently evaporated from the pools. The rate of evaporation was regulated using the electron beam current. The rotation of the substrate, fixed on the vertical shaft, and presence of the dividing screen made it possible to deposit successively layers of pure elements on the substrate whose temperature was maintained using the heating electron beam guns.

After completing the process of layer deposition of the components, the foil was separated from the substrate by depositing the thin layer of NaCl on the surface prior to deposition.

The ratio of the thickness of the components of the multilayer foils is determined by the ratio of the rates of evaporation of the ingots and their total thickness (the period of alternation of the layers) by the speed of

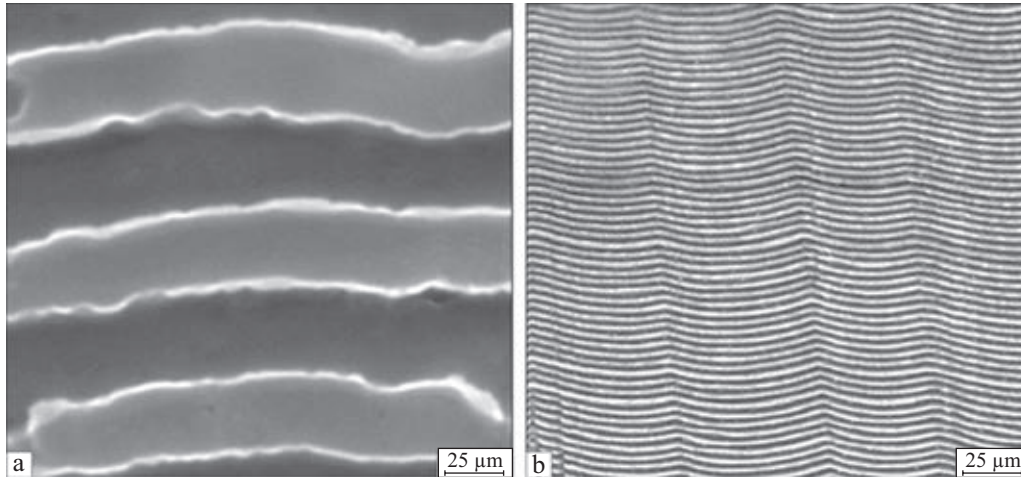


Fig. 2. Electron microscopy images of the microstructure of the cross-section of the specimens of the Ti/Al foil with the period of automation of the layers of 800 (a) and 50 (b) nm. The light layers correspond to titanium, the dark layers to aluminium.

rotation of the substrate. The total thickness of the foil at a specific evaporation rate of the components was defined by the duration of the cooling stage.

To determine the structure and chemical composition, the foils after deposition and he treatment were investigated by the methods of electron microscopy, and diffraction of x-rays and differential thermal analysis (DTA). The specimens for metallographic studies were produced by the standard procedure using a grinding–polishing machine Abramin (Struers). The structure of the foil was developed by the method of selective chemical etching.

The structure and chemical composition of the foil was analysed using a CamScan-4

scanning microscope, fitted with a Energy 200 energy-dispersing local analysis system and a Hitachi H-800 transmission electron microscope with the accelerating voltage of 200 kV. X-ray diffraction measurements were taken in the standard Q-2Q geometry in a DRON-4 for diffractometer in $\text{CuK}\alpha$ radiation. Measurements for DTA were taken in equipment VDTA-8 [9].

Structure of the Ti/Al multilayer foils

By varying the rate of electron beam evaporation of the components of the ingot and the speed of rotation of the substrate, thick (up to 200 μm) multilayer foils on the basis of intermetallic-forming components with different ratios were produced. The period of automation of the layers could be varied from 10 to 1000 nm.

Figure 2 shows the microstructure of the metal of the cross-section of the specimens of the Ti/Al foil with the submicron (more than 100 nm) and nanosized (less than 100 nm) periods of alternation of the layers. The foils consist of the continuous layers of titanium and aluminium and are characterised by the columnar structure, characteristic of the vacuum condensates, deposited at a substrate temperature of $< 0.5 T_m$.

The x-ray diffraction patterns of the specimens of the foils contain only the lines relat-

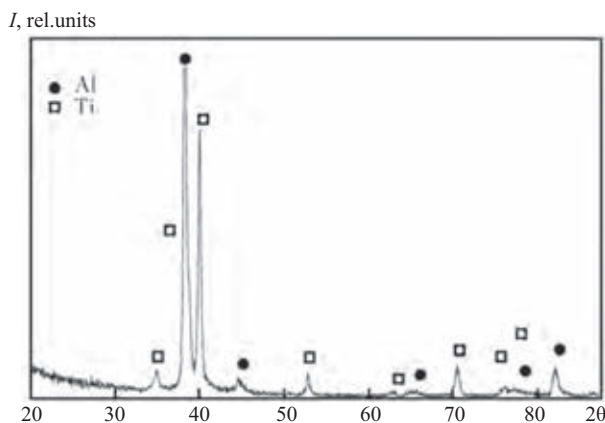


Fig. 3. X-ray diffraction pattern of the specimen of the Ti/Al foil after deposition ($\text{CuK}\alpha$ radiation).

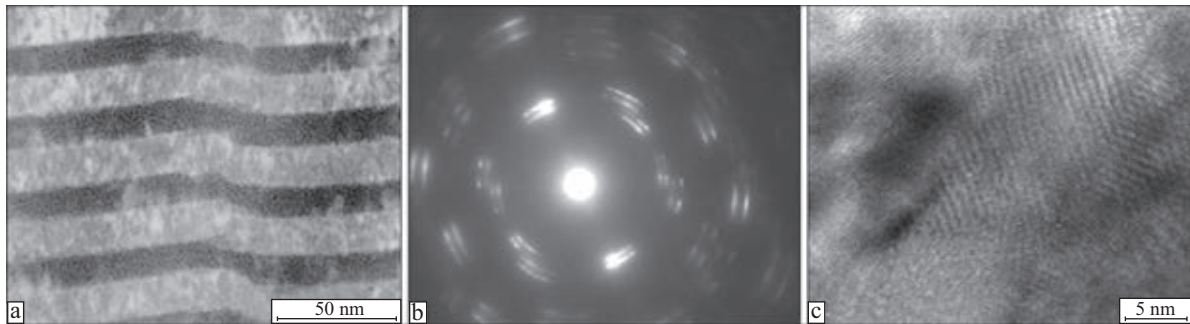


Fig. 4. Electron microscopic images of the microstructure of the cross-section (a), electron diffraction pattern (b) and electron microscopic image with high resolution (c) of the Al/Ti foil after deposition.

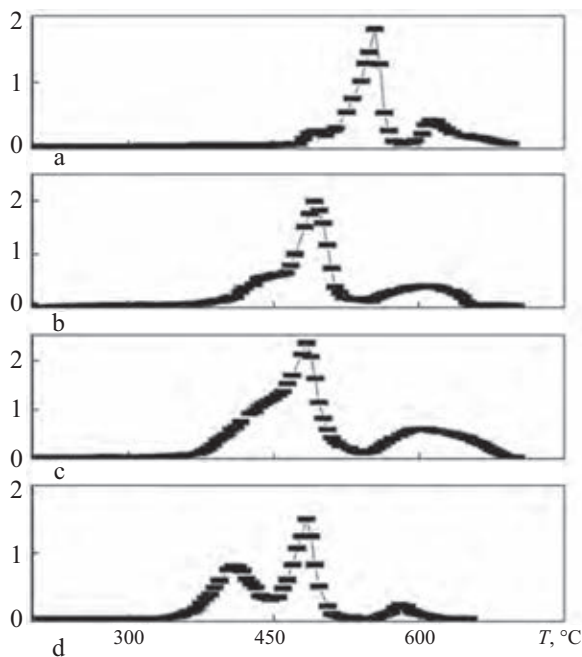


Fig. 5. The TA curves, obtained in heating at a rate of 50°C/min of Ti/Al multilayer foil with the equiatomic composition with the period of alternation of the layers of 700 (a), 500 (b), 300 (c) and 70 (d) nm.

ing to α -Ti and aluminium (Fig. 3), i.e., the process of deposition of the components as a result of diffusion processes is not accompanied by mixing of the components not only in the vapour phase but also in the solid state. No mixing takes place between the layers, as indicated by the distinctive boundaries of the layers in the absence of reflections from the intermetallic phases of the electron diffraction pattern of the foil (Fig. 4 a, b).

Analysis of the structure of the boundaries of the layers, produced by the method of

transmission electron microscopy with high-resolution shows at the boundaries of the layers there are no signs of precipitation of any phases, and the contact of the grains is coherent (Fig. 4 c). Thus, the conditions of their position of the multilayer foils prevent diffusion of titanium and aluminium at the boundary between the layers thus creating favourable conditions for the diffusion of components with increase of the foil temperature.

Reaction properties of the Ti/Al multilayer foils

With increase of the temperature of the multilayer foil, consisting of the intermetallic-forming components, the foil is characterised by the activation of diffusion processes with the formation of intermetallic phases and this is usually accompanied by intensive heat generation.

Figure 5 shows the thermal diagrams, produced in slow heating at a rate of 50°C/min of the specimens of the Ti/Al foil (chemical composition, similar to that of the TiAl intermetallic) which differ by the period of alternation of the layers. The DTA curves show that in heating the foil a cascade of phase transformations takes place in them. The temperature range and the rate of these processes greatly depend on the alternation period of the layers – with a reduction of the period the range of the phase transformations is displaced to lower temperatures and the intensity of the first stage of phase

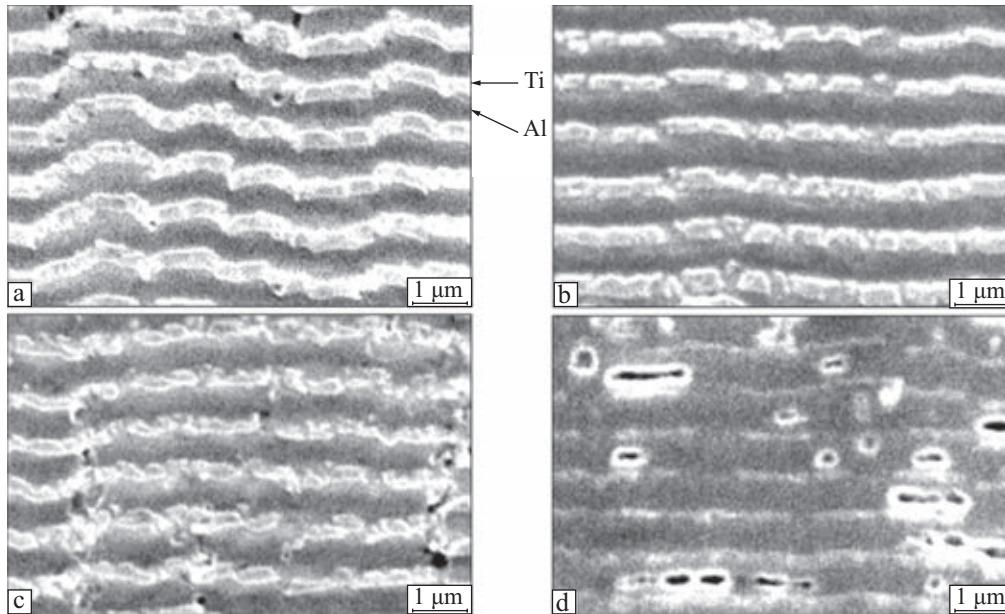


Fig. 6. Microstructure of the cross-section of the specimens of the foil with the period of automation of the layer of 800 nm in the initial condition (a) after heating to 350°C (b), 450 (c) and 550°C (d), and also after holding for 5 min at these temperatures.

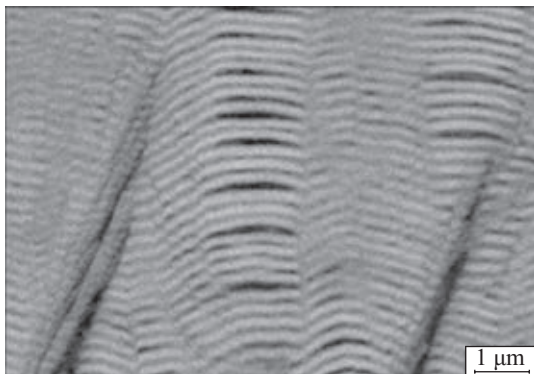


Fig. 7. Electron microscopic image of the cross-section of the Ti/Al multilayer foil after heating in vacuum to 600°C.

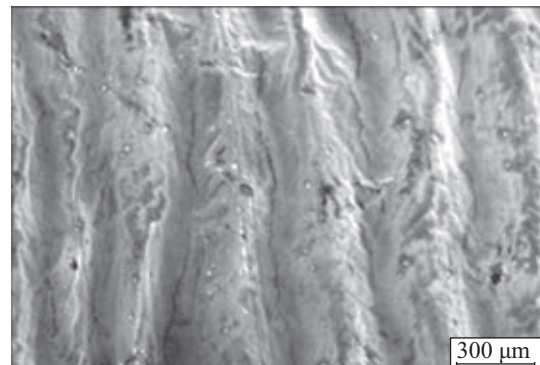


Fig. 8. Microstructure of the surface relief of the Ti/Al foil after the SHS reaction.

transformations greatly increases.

X-ray diffraction analysis of the specimens of the foils, heated to different temperatures in the range 250–700°C, has been described in detail in [9]. On the basis of the investigations it may be concluded that in heating the specimens of the Ti/Al multilayer foils with the chemical composition similar to the equiatomic composition in the temperature range 350–650°C, the sequence of the phase transformations can be expressed as follows: $\text{Al} + \text{Ti} \rightarrow \text{Al}_3\text{Ti} \rightarrow \text{Al}_5\text{Ti}_2 \rightarrow \text{Al}_2\text{Ti} \rightarrow \text{AlTi}$. In addition to this, in heating to temperatures

of approximately 550°C, the AlTi_3 intermetallic compound forms in the foil and in further heating of the foil the compound transforms to intermetallics with a lower aluminium content. The formation of the AlTi_3 phase together with the thermodynamically justified sequence $\text{Al}_3\text{Ti} \rightarrow \text{Al}_5\text{Ti}_2 \rightarrow \text{Al}_2\text{Ti} \rightarrow \text{AlTi}$ indicates the realisation of two channels of phase transformations, determined by two diffusion processes – bulk diffusion of the titanium atoms into aluminium and the grain boundary diffusion of the atoms of aluminium in titanium.

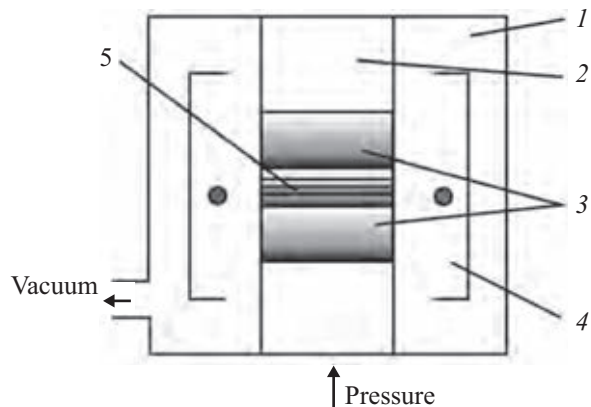


Fig. 9. Diagram of equipment for vacuum diffusion bonding: 1) vacuum chamber; 2) clamping bar; 3) welded specimens; 4) electron beam heater; 5) the Ti/Al foil.

It should be mentioned that in all stages of phase transformations, the Ti/Al multilayer foils retain the laminated structure (Fig. 6). Analysis of the microstructures of the cross-section of the Ti/Al multilayer foils indicates that in the initial stages of heating the diffusion processes in the distribution of the components resulting from these phase transformations lead to changes in the structure of the layers – thickness of the layer – with the fragmentation of the layers (Fig. 6, *b, c*). When the temperature to which the specimens are heated is increased to 550°C the thickness of the titanium layers decreases and a composite consisting of a mixture of intermetallic phases, enriched with titanium and aluminium, forms (Fig. 6, *d*).

The low values of the temperature of phase transformations, taking place in the Ti/Al foil during heating, and the multistage nature of these processes are determined to a higher degree by the structure of the vacuum condensates, deposited at temperatures lower than $0.3 T_m$. The deposition conditions support the formation of a higher concentration of the defects of the vacancy type both in the volume and at the grain boundaries. On the other hand, these defects caused the diffusion mobility of the components and the formation of intermetallic compounds at the relatively low temperatures of heating the foil, and on the other hand lead to the formation of pores (Fig. 7).

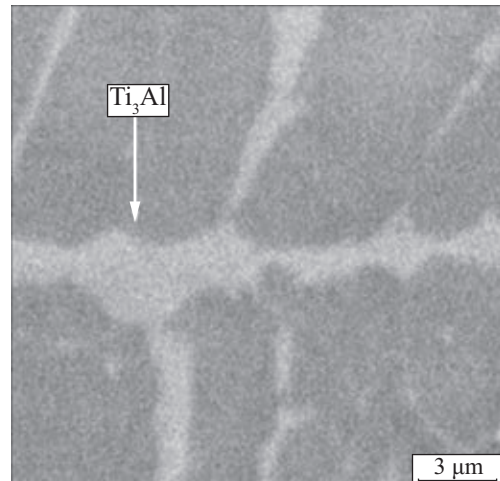


Fig. 10. Microstructure of the metal of the weld zone of the specimens of TiAl intermetallics, produced in vacuum diffusion bonding (without the interlayer).

Rapid heating of the multilayer foils results in the reaction of self-propagating high-temperature synthesis (SHS). Figure 8 shows the microstructure of the surface relief of the Ti/Al foil after the SHS reaction. It is evident that this structure of the surface of the foil leads to the establishment of a physical contact with the welded surfaces.

On the basis of the analysis of phase and structural transformations, taking place in the multilayer foil during heating, and also taking into account the special features of the microstructure of the foil produced in this process in different stages of the phase transformations and the generation of a large amount of heat, it may be assumed that the application of the foils as interlayers activates the diffusion processes in the bonding zone.

Example of application of multilayer foils in diffusion bonding of titanium aluminide

The Ti–Al aluminium intermetallics were welded in a vacuum chamber of U-394M equipment, fitted with systems for static loading of the specimens and electron beam heating (Fig. 9). The surfaces of the specimens prior to welding were ground in a Diamond wheel and subsequently degreased. The prepared specimens with the size of $10 \times 10 \times 4$ mm with an interlayer were placed

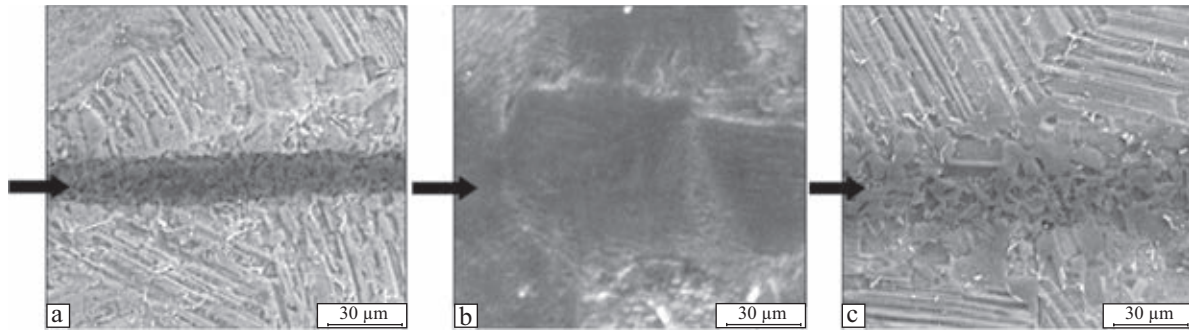


Fig. 11. Microstructure of the weld zone of the specimens of the TiAl intermetallic compound in vacuum diffusion bonding at a pressure of $P = 10$ MPa using the Ti/Al multilayer foil; the arrows indicate the areas of joining.

in the vacuum chamber. Uniform heating was ensured by using a ring-shaped electron beam heater placed on the level of the joint. The welding parameters were varied in the following ranges: $T = 900\text{--}1200^\circ\text{C}$, $t = 5\text{--}25$ min, $P = 10\text{--}70$ MPa. The vacuum in the working chamber was maintained on the level of 1.33×10^{-3} MPa.

The material for vacuum diffusion bonding was the Ti-48 at.% Al alloy with the additions of niobium and manganese with the two-phase state $\alpha_2 + \gamma$ ($\alpha_2\text{-Ti}_3\text{Al}$ and $\gamma\text{-TiAl}$, or even $\gamma\text{-TiAl}$), and characterised by high heat resistance. The joints in the $\gamma\text{-TiAl}$ intermetallic alloy without the intermediate foil were produced in the following conditions: $T = 1200^\circ\text{C}$, pressure $P = 70$ MPa, holding time $t = 20$ min.

The results of metallographic examination of the weld zone are shown in Fig. 10. The interface is clearly visible in the weld zone. Analysis of the structure of the weld zone in the phase contrast mode shows the formation of an intermetallic layer in the region of the joint. The composition of the interlayer, according to the results of local chemical analysis, is similar to that of the Ti_3Al intermetallic. The deformation of the intergranular boundary in the form of a brittle intermetallic interlayer reduces the strength of the welded joint and this results in the degradation of the service properties of the welded joint [10].

The interlayer in diffusion bonding of the specimens of the $\gamma\text{-TiAl}$ intermetallic alloy was in the form of a multilayer foil with the composition Ti-52 at.% aluminium with a thickness of $20 \mu\text{m}$ and the period of alternation of the layers (Ti/Al) 50 nm (Fig. 2, b). The selection of the multilayer foil as the interlayer is based on the results of investigations of the phase transformations during heating of the interlayer according to which the process of diffusion bonding of the specimens of titanium aluminide, the structure of the Ti/Al multilayer foil transforms to the structure similar to that of the welded material.

Optimisation of the technological parameters of the diffusion bonding process through the multilayer interlayer was described in detail in [11]. The microstructure of the welded joint, produced at the optimum parameters of diffusion bonding ($T = 1200^\circ\text{C}$, $t = 20$ min,

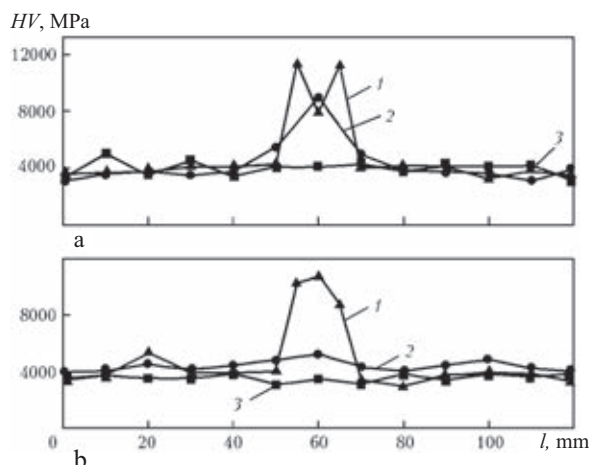


Fig. 12. The variation of the microhardness in the weld zone of the Ti-48Al-2Nb-2Mn (at.%) alloy in welding using Ni/Ti, Ni/Al and Ti/Al multilayer foils in the initial condition (a) and after annealing at 1200°C , 2h (b): 1) Ni/Al; 2) Ni/Ti; 3) Ti/Al.

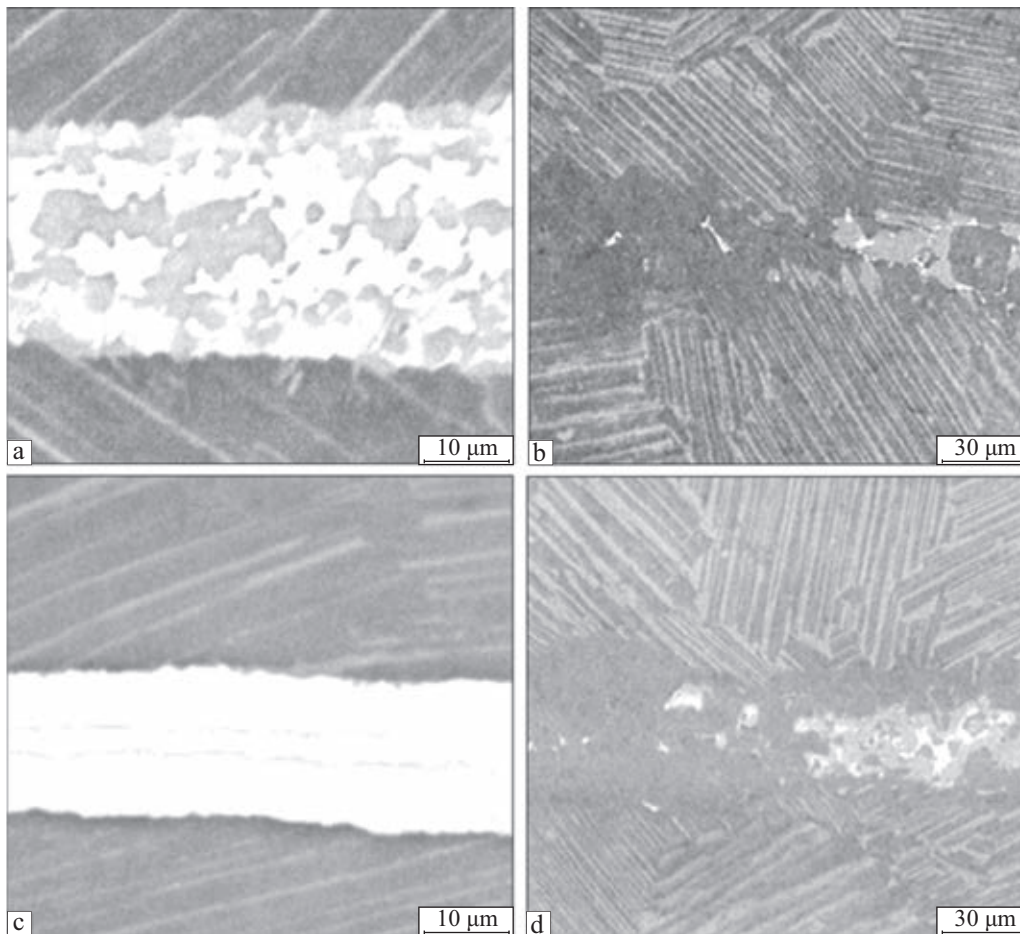


Fig. 13. Microstructure of the weld zone of γ -TiAl produced using the Ni/Ti Ni/Al multilayer foils after welding (a, c) and annealing (b, d) at 1200°C, 2h; the phase contrast mode.

$P = 10$ MPa) is shown in Fig. 11. The weld zone (in the area of position of the interlayer) is characterised by weak contrast indicating the differences in the chemical composition of the metal of this region in comparison with the adjacent areas, corresponding to the welded intermetallic alloys (Fig. 11, *a*). Comparison of the chemical composition of the metal of the weld zone (49.4Al, 49.8Ti, 0.8Mn at.%) and the welded titanium aluminide shows that the weld zone is depleted in niobium atoms. According to the results of metallographic and local chemical analysis, the niobium particles build at the interlayer/intermetallic boundary. The presence of manganese in the interlayer indicates the occurrence of diffusion processes in the weld zone during the reaction of solid-phase synthesis,

initiated in the multilayer foil during welding. The metal of the zone of the welded joint has a homogeneous structure (Fig. 11, *b*) and consists of equiaxed grains with the size of up to 10 μm with different lamellar structures, characteristic of the initial intermetallic compound.

Thus, analysis of the microstructure of the produced welded joint shows that the multilayer interlayer in the process of diffusion bonding results in the formation of intermetallic grains in the joint which grow into the welded material. The absence of pores and cracks in the weld zone and also the equal strength of the individual areas of the welded joint (Fig. 12) indicate the high quality of the welded joint.

Homogenising annealing of the welded

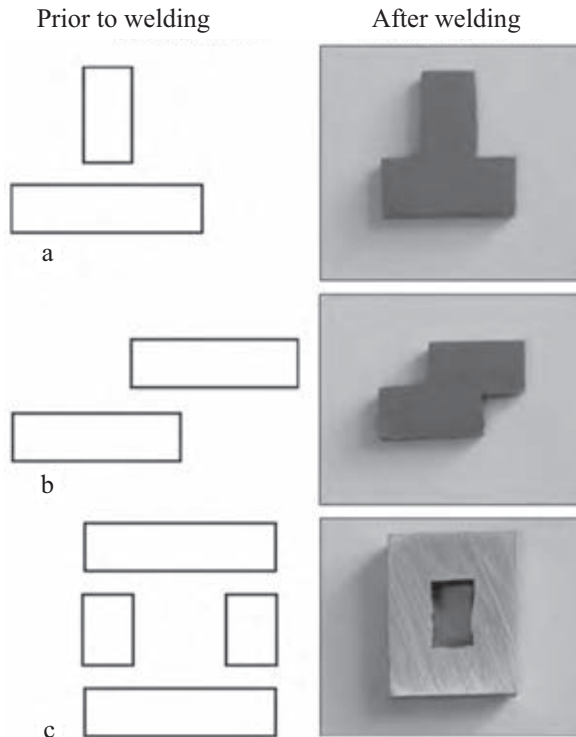


Fig. 14. General view of the assemblies of the T-shape (a), lap assembly (b) and box section type (c), produced from γ -TiAl alloy through the Ti/Al Nano layer foil.

joint at a temperature of 1200°C for 2h in vacuum increases its homogeneity as regards composition and structure (Fig. 11, *a*) but depletion in niobium of the metal of the weld zone remains unchanged which evidently can be removed using the multilayer foil containing niobium. The recorded changes in the microstructure of the metal in the weld zone indicate the high diffusion mobility of the components and may be determined by the processes of heat generation, accompanying solid-phase reactions, initiated in the multilayer foil.

Therefore, investigations were carried out into the effect of other reactive multilayer foils – Ni/Ti (Ti–44 at.% Ni) and Ni/Al (Al–46 at.% Ni) on the structure of the metal of the welded joints in the alloys based on γ -TiAl, produced by vacuum diffusion bonding [12].

The results of metallographic analysis of the weld zone are presented in Fig. 13. The application of the Ni/Ti and Ni/Al multilayer foils greatly activates the diffusion processes

in the joint. However, in both cases, welding is characterised by the formation of the transition zone of variable thickness with the non-uniform structure and composition, consisting of several phases. This leads to a large scatter of the microhardness values of the metal of individual regions of the welded joints (Fig. 12).

Additional annealing at 1200°C of the metal partially eliminates the non-uniformity of the chemical composition, structure and mechanical properties of the welded joints (Fig. 12 and 13). However, the presence of the (Ti, Ni)Al intermetallic in the joint results in the high microhardness of the individual areas of the welded joint, produced using the foil and Ni/Al. On the other hand, formation in the region of the foil of the composite structure whose phase components are characterised by high microhardness values can be utilised in welding identical composite materials based on titanium.

Thus, the occurrence in the weld zone of high-rate of diffusion processes method possible to produce high-quality welded joints and also used this approach for producing constructional elements of different types on the basis of the γ -Ti Al intermetallic alloys.

Figure 14 shows the design of T, lap and box section joints produced in a single welding cycle using the Ti/Al multilayer foil as an interlayer.

The results indicate the high efficiency of multilayer structures based on intermetallic forming components used as the interlayers in diffusion bonding. When using these foils, examination showed not only the ‘softening’ of the diffusion bonding conditions for producing permanent joints and also new possibilities of local alloying of the weld zone by introducing a foil with a modified composition. The high reactivity of these foils results in higher rate of diffusion processes without any additional increase of temperature and holding time of the weld zone.

The approaches developed in this study for using multilayer foils in vacuum diffusion bonding of the γ -TiAl intermetallic alloy can also be used in welding other low-weldability

materials, and particular, composite materials based on aluminium. We have developed, for example, technology of producing Al/Ni multilayer foils for use in welding AMg5 + 27% Al₂O₃ composite materials [13, 14]. The application of the Al/Cu multilayer for use in welding accelerates the diffusion processes, chemical activation of the welded surfaces and supports fine-dispersion hardening of the metal of the weld zone as a result of the SHS reaction of the intermetallics. The results of the tensile and shear tests indicate the improvement of the strength characteristics of the welded joints.

Conclusions

1. A high-speed method of producing thick (up to 200 μm) multilayer foils based on intermetallic-forming components by a layer electron beam deposition is proposed. The method method possible to vary the period of automation of the layers in the range from 10 to 1000 nm.

2. It is shown that the multilayer foils based on the intermetallic-forming components, produced by the method of successive electron beam deposition of the layers, characterised by the high reactivity which is linked with a high degree of perfection of the interface boundaries and the presence of vacuum condensates in the structure.

3. The experimental results show that the application of the nanolayer foils of the Al/Ti system as intermediate interlayers in dif-

fusion vacuum bonding produces the joints with the uniform distribution of the alloying elements in the joint included in the composition of the alloy, and the microstructure of mutually penetrating grains similar to the welded material at lower welding parameters. Consequently, the proposed technology, says can be useful joining low weldability materials.

4. It is shown that the application of the multilayer foils based on intermetallic-forming components, differing in the chemical composition from the welded material, makes it possible to modify the structure and chemical composition of the metal of the weld zone.

References

1. Kazakov, N.F., Diffusion bonding of materials, Mashinostroenie, Moscow, 1976.
2. Lee, C.S., et al., Journal of Materials Processing Technology, 1999, No. 89, 90, 344-349.
3. Duvall, D.S., et al., Welding Journal, 1972, volume 51, No. 2, 41-49.
4. Nesmikh, V.S., et al., Avt. Svarka, 1987, No. 5, 69-72.
5. Metelkin, I.I. and Doronina, A.A., Svar. Proiz., 1976, No. 5, 15-17.
6. Calvo, F.A., et al., Rev. Soldadura, 1987, volume 17, No. 2, 71-77.
7. Nami, H., et al., Journal of Materials Processing Technology, 2010, No. 210, 1282-1289.
8. Musin, R.A., et al., Diffusion bonding of creep resisting alloys, Metallurgiya, Moscow, 1979.
9. Karakozov, E.S., et al., Sovremennaya Elektrometallurgiya, 2008, No. 2, 19-26.
10. Karakozov, E.S., et al., Avt. Svarka 1982, No. 1, 7-10.
11. Ustinov, A.I., et al., Avt. Svarka, 2009, No. 1, 17-21.
12. Kharchenko, G.K., et al., Avt. Svarka, 2007, No. 7, 5-9.
13. Ishchenko, A.Ya., et al., Avt. Svarka., 2008, No. 12, 5-12.
14. Paton, B.E., et al., ibid, 2008, No. 12, 5-12.

Submitted 30.1.2012

Structure of molybdenum ingots modified with dispersed particles of a second phase

V.O. Mushegyan

Paton-Armeniya Scientific and Technical Centre, Kiev

Basing on numerous investigations of processes of evaporation and melting of metals in electron beam units, the ways of cold brittleness prevention in molybdenum ingots were defined. Methods of improvement of molybdenum ductility, such as refining from impurities, structure refining, adding modifiers, were experimentally found. The molybdenum modifying by zirconium carbide allowed refining significantly the structure of ingots and castings.

Molybdenum ingots are highly sensitive to the non-metallic impurities (especially oxygen) which cause the so-called cold shortness effect, i.e., a large reduction of plasticity, especially impact toughness of metal with a reduction of the ingot temperature to 400°C and lower [1]. In many cases, the ingots fracture spontaneously into individual crystals when taking out of the furnace under the effect of elastic stresses.

The structure of the ingots is influenced not only by the total amount of the impurities but also the grain size of the ingots [2]. Refining of the structure of the ingot increases the total area of the grain boundaries. Since the failure of the ingots is influenced by the impurities, distributed along the grain boundary, with an increase of the total area of the grain boundaries the specific number of impurities per unit area decreases and the plasticity of the ingots increases.

At the same time, some impurities, for example carbon in molybdenum, resulting in the phenomenon of high-temperature heterogenisation, i.e., the formation of carbide particles accompanied by the refining of the grains in the ingots and the improvement of the level of the mechanical properties. Thus, there is a certain non-monotonic dependence

of the properties of molybdenum ingots on the impurities were some impurities in specific amounts can improve or impair the properties of the ingots [3]. The extremum of the dependence, i.e., the optimum amount of the impurities resulting in the maximum increase of the point of the cold shortness threshold, can be determined (Fig. 1). These effects include the refinement of the structure of the ingots by the thermophysical methods as a result of intensification of solidification.

The task of optimisation of the content of impurities and the structure of the ingots for

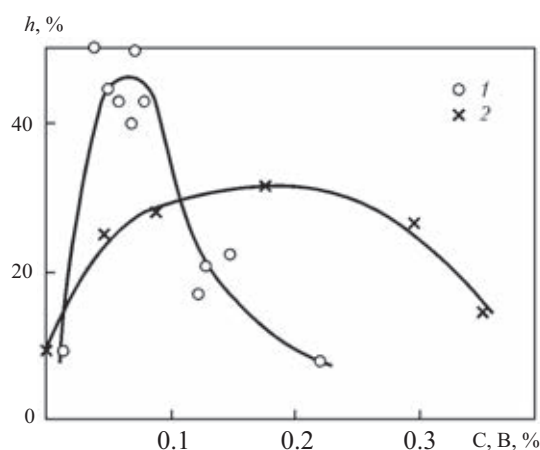


Fig. 1. Dependence of the relative upset h on the content of carbon (1) and boron (2) in Mo-C and Mo-B alloys [3].

improving the machinability of molybdenum alloys and temperature is obviously very urgent. The aim of the present work is the investigation of the possibilities of refining the grains of the primary structure of the ingot accompanied by improvement of the structure.

Electron beam melting increases the properties of the molybdenum ingots by refining the metal to remove the impurities; introduction of other elements during melting; regulation of the process of crystallisation of the ingots. The start of investigations of this type by the author of the article was represented by the experiments with the electron beam evaporation and deposition of heterogeneous condensates [4-8].

Investigations were carried out into the relationships governing the process of electron beam evaporation of molybdenum in the production of condensed materials of the Ni-Co-Cr-Al-Y-Mo type [4], the effect of the thermal conditions of crystallisation in electron beam heating of the structure of metallic materials, the mechanism of the effect of the concentration of the particles of the second phase in the metallic matrix and the structure and mechanical properties of dispersion-hardening materials [5]. As indicated by [5], at some volume fraction of the second phase when the mean free path between the particles is equal to the mean grain size D of the metallic matrix, the relative elongation of the two phase materials reaches the maximum value. The values of for the spherical particles were determined from the equation

$$\Lambda = \frac{2d}{3f}(1-f)$$

where d is the particle diameter; f is the volume fraction of the second phase. The peaks of the plasticity of the condensates, hardened with the oxide particles, were obtained at the condition $\Lambda = D$.

The determined dependences have been used in the present work in the electron beam cold hearth melting (EBCHM) of molybdenum in order to produce high-quality molybdenum ingots containing the optimum

Table 1. The chemical composition of the initial charge and molybdenum ingots in electron beam cold hearth melting

Type product	Mass fraction of elements, %					
	C	S	Fe	Cu	O	N
Metallic Mo in the form of sintered briquettes (TU RA28-54-529-61-661-2007)	0.1	0.01	0.5	0.01	1.0	–
EBCHM ingots, diameter 70 and 100 mm	0.002	<0.001	0.007	<0.001	0.0005	0.002

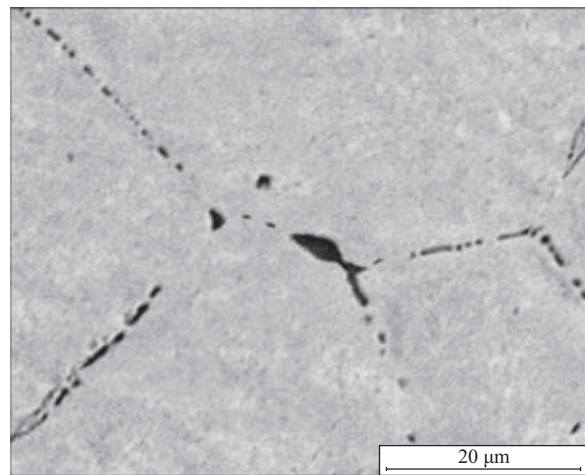


Fig. 2. Inclusions in molybdenum ingots produced by electron beam cold hearth melting.

amount of the impurities and characterised by reduced grain size [8]. Remelting with the cold hearth enabled purification of the initial molybdenum of the briquettes T URA28-54-529-61-661-2007 produced by Chistoe zhelezo company (Yerevan) to 97% of molybdenum: the oxygen content was reduced to 0.0005, the carbon content to 0.02 wt.% (Table 1). The application of peripheral heating [9] resulted in excess of refining of the macrostructure of the ingot in comparison with the molybdenum ingot, produced by traditional electron beam technology. The grain size decreased by approximately a factor of five, from 9 to 2 mm [8]. The size of the nonmetallic inclusions (molybdenum carbides and oxide)

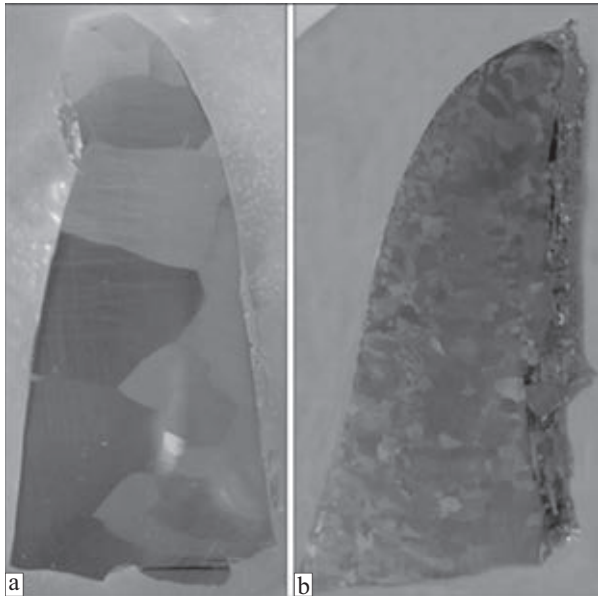


Fig. 3. Macrostructure of fragments of a casting 100 × 100 × 30 mm in size: a) pure molybdenum; b) molybdenum + 1% zirconium carbide (according to the charge).

Table 2. The results of measurements of the grain size in a casting of pure molybdenum, μm

Grain size No.	Grain length	Grain width	Grain size No.	Grain length	Grain width
1	600	1800	11	1700	1700
2	2200	3500	12	2000	2300
3	1800	2500	13	6000	7000
4	2500	4500	14	1000	1200
5	5000	6800	15	1200	1500
6	500	1000	16	2000	3000
7	6000	8000	17	2500	3000
8	1200	3000	18	5000	7000
9	7000	8000	19	3500	8000
10	1500	2100			
Intermediate mean value	2830	4120		2490	3470
Mean value				3200	

in the experimental ingots was 0.15–1.50 μm and the inclusions had a regular circular shape (Fig. 2).

Experiments were carried out to determine the effect of the carbide particles in the structure of the ingots (castings) of molybdenum in electron beam remelting. 1% of zirconium carbide was added to the initial molybdenum with the purity of 99.89 (+0.05) % in the process of formation of the charge. Castings

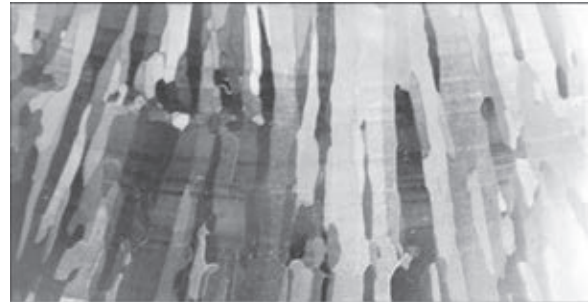


Fig. 4. The macrostructure of a molybdenum ingot produced by electron beam cold hearth melting, diameter 70 mm, modified with the zirconium carbide.

100 × 100 mm in size and 30 mm thick were produced from both initial molybdenum and its alloys with a zirconium carbide. The content of the picked up zirconium, as shown by the results of spectral analysis, was 0.28 (+0.02) percent. Thus, the extent of transfer of the zirconium carbide to the casting reached 30% of the preliminary charge. The fragment of the castings were investigated from the viewpoint of the structure and properties of the metal. Investigation of the structure (Fig. 3) showed a large reduction of the mean size of the crystals, more than a factor of 13 (3200:244 μm). The grain size was determined for the molybdenum specimen +1% of zirconium carbide by the secant method, and for the pure molybdenum specimens by the measurement of the linear dimensions of all the grains in mutually perpendicular directions (Table 2) in a Neophot-32 optical microscope using metallographic sections after etching. This large reduction of the grain size in the case of the modifying effect of zirconium carbide on molybdenum.

Molybdenum, modified with zirconium carbide was also used to produce ingots in a solidification mould with a diameter of 70 mm in the furnace for electron beam cold hearth melting. The macrostructure of the longitudinal section of the ingot is shown in Fig. 4. The ingots consisted of the grains with the cross-section of one-4 mm, elongated along the axis of the grains which is an order of magnitude smaller than in the molybdenum ingots produced by electron beam remelting (11-16 mm) [3].

The macrosection of the ingot was homoge-

neous, without cracks, the material was easy to grind. Cracking into individual crystals, as in the ingots of pure molybdenum produced by electron beam melting with large grains, was not detected. The determination of Brinell hardness in equipment TSh-2M (load 2943N, diameter of the steel sphere 10 mm, holding time 30 s) showed the value of 1430 MPa for the specimen of molybdenum + 1% of zirconium carbide, and the pure molybdenum specimen fracture during testing. The microhardness values, averaged out on the basis of the results of 12 tests (equipment PMT-3, load 50 g, loading 10 s) were almost identical, respectively 2280 and 2460 MPa.

The mean microhardness of the specimens of the metal of the ingot at a load of 100 g was 2160 MPa, which is slightly lower than for the 30 mm thick casting.

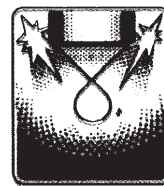
Thus, modification of the cast molybdenum with a small amount (up to 1%) of zirconium

carbide produce a large reduction of the grain size (by up to a factor of 30) in both the castings and the ingot.

References

1. Morgunova, N.N., et al., Molybdenum alloys, Metallurgiya, Moscow, 1975.
2. Podrezov, Yu.N., et al., Effect of the grain size on the hardening parameters, in: Electron microscopy and strength of materials, Trudy IPM, 2010, No. 17, 12–19.
3. Movchan, B.A. and Statkevich, V.N., Izv. AN SSSR, Metall., 1969, No. 2, 129–136.
4. Topal, V.I., et al., Spets. Elektrometall., 1987, No. 62, 62–66.
5. Movchan, B.A., et al., Probl. Spets. Elektrometall. 1988, No. 4, 47–50.
6. Mushegyan, V.O., et al., Spets. Elektrometall., 1985, No. 58, 62–68.
7. Lisikyan, A.S., et al., Probl. Spets. Elektrometall., 1990, No. 3, 65–68.
8. Mushegyan, V.O., Sovremennaya Elektrometallurgiya, 2010, No. 9, 28–31.
9. Zhuk, G.V., Metallurg. Gornorud. Promst'., 2003, No. 3, 36–38.

Submitted 10.01.2012



Plasma-arc melting on a dispersed substrate in a moving horizontal solidification mould

**V.N. Koleda, V.A. Shapovalov, F.K. Biktagirov,
V.R. Burnashev and V.V. Yakusha**

EO .P aton Electric Welding Institute, Kiev

Shown is the expediency of application of plasma melting in a horizontal mould on a dispersed substrate for compacting the sponge titanium into a slab ingot and melting of high-quality ferroalloys. Optimum values of the thickness of the dispersed layer and technological parameters of plasma melting, providing the reliable heat insulation of ingot being melted from walls and bottom of horizontal mould, are determined.

In addition to the vacuum-arc [1] and electron beam [2] technologies, plasma arc remelting can also be used efficiently for melting ingots of high-reactivity and refractory metals and their alloys, refining the surface layer of the ingots in producing high-quality ferroalloys and master alloys [3–5].

One of the varieties of plasma arc remelting of metallic materials is melting in a horizontal moving solidification mould [6]. The distinguishing feature of this method is the small depth of the metal pool. In comparison with melting in the vertical solidification mould, in this case the extent of development of liquation processes is considerably smaller and this is especially important in melting of alloys from the initial components characterised by large differences in the physical properties. In addition to this, the dimensions of the

melted ingots can be varied in a wide range, using different standard dimensions of the solidification mould and layer melting. The process makes it possible to remelt the charge of different grain size composition with the size from several to hundreds of millimetres and is greatly reduces the expenditure on the preparation of initial materials and also simplifies loading of the charge.

However, in this method, the developed surface of contact of the melted ingot with a copper baseplate and sidewalls of the solidification mould results in considerable heat losses which in turn results in a high specific consumption of electric energy and plasma forming gas.

The authors have proposed and developed a method of plasma-arc welding in a horizontal solidification mould which greatly reduces the extent of heat removal from the melted

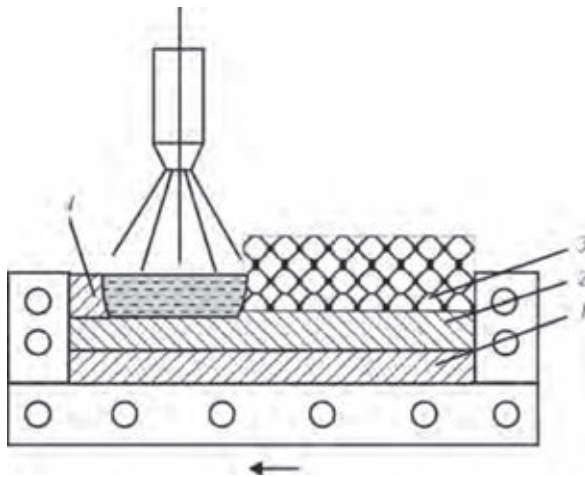


Fig. 1. Gradual layer melting of an ingot in the horizontal solidification mould: 1, 2, 4) the first, second and third layer, respectively; 3) the charge.

ingot to the watercooled elements of such a solidification mould. The method is based on the process carried out on the so-called dispersed substrate placed on the surface of the watercooled baseplate. The dispersed substrate has the form of a layer of particles of crushed metal of the same chemical composition as that of the melted ingot. The fraction of the particles and a thickness of the dispersed layer are selected to ensure that the liquid metal does not flow through the layer to the surface of the watercooled baseplate. In this case, the dispersed substrate partially melts.

In this study, investigations were carried out into the effect of the parameters of the dispersed substrate and the technological conditions of the process and the formation of the ingots, the quality and thermal energy parameters of plasma-arc melting in the horizontal mould.

Investigations were carried out in the OB1957 experimental plasma-Mac equipment at the E.O. Paton Electric Welding Institute, Kiev, with compacting of the titanium sponge into a flat billet with and without the dispersed substrate. Melting was conducted in a solidification mould with the internal size of $800 \times 300 \times 70$ mm. In melting, the solidification mould travelled at the given speed inside the melting chamber hour-long the longitudinal axis of the mould, and the plasma torch carried out regulated oscillatory

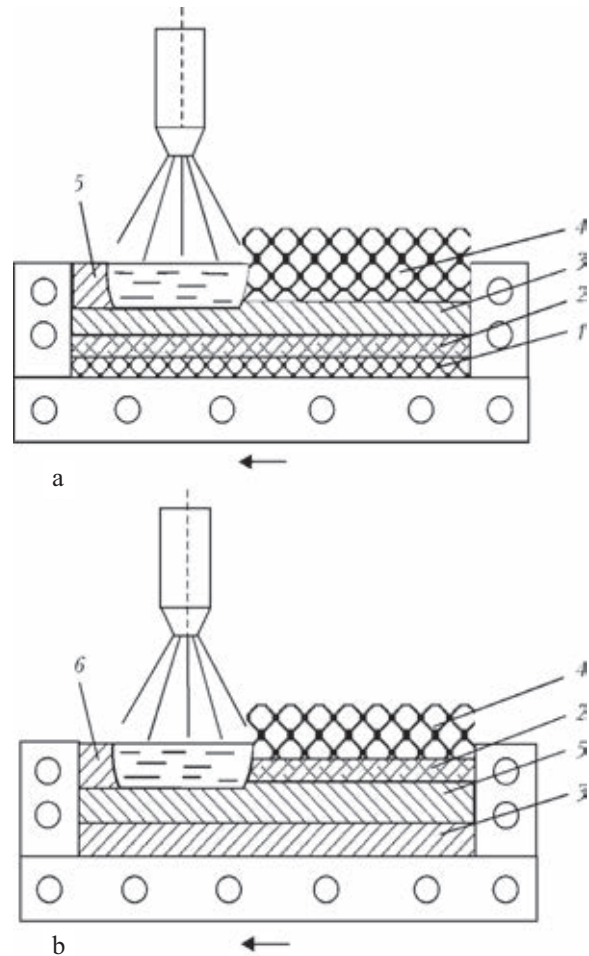


Fig. 2. Diagram of plasma-arc melting on a disperse substrate (a) with subsequent melting of the sintered layer (b): 1) a disperse substrate; 2) bloom; 3, 5, 6) the first, second and third layer, respectively; 4) the charge.

movement across the solidification mould. Melting of the charge, loaded into the solidification mould, started at one of the sides of the mould. A metal pool was produced along the entire width of the mould and travelled as a result of movement of the solidification mould in the direction of its opposite side. A gradual (along the length of the solidification mould) melting of the billets took place in this melting mechanism.

Figure 1 shows the diagram of the process of remelting the charge in the horizontal morning mould with the layer by layer melting of the flat billet. The first layer was melted with the guaranteed melting of the charge to the copper baseplate and the sidewalls of the solidification mould. Subsequent layers were

Table 1. Technological parameters of the process of compacting titanium sponge

Remelting method	Deposited layer	Mass of metal in a melt, k g	Ingot thickness, m m	Ingot deflection, mm	Consumption of electric power, kW	Argon flow rate, l /kg	Comment
Without dispersed substrate	1	20	21	–	5.7-5.9	120-130	–
	2	22	44	1-2	4.0-4.1	90-100	–
	3	20	65	3-4	4.4-4.5	80-90	–
With dispersed substrate	1	26	32	–	3.4-3.6	70-80	Ingot with bloom
	2	24	57	1-2	3.7-3.8	70-80	As above
	3	20	68	1-2	4.4-4.5	80-90	Remelting of bloom

melted to ensure melting of the underlying layer and defect-free formation of the billet.

In remelting the charge on the dispersed substrate, contact of the melted billets with the copper solidification mould took place only on its side planes. The lower part of the ingot was completely insulated from the copper baseplate by a dispersed substrate (Fig. 2, *a*). During melting the first layer, a sintered layer of the metal, the so-called bloom, formed in the lower part of the metal pool at partial melting of the dispersed substrate. After melting the required number of the metal layers, the billet was turned over and this was followed by the final stage of melting resulting incomplete melting of the bloom (Fig. 2, *b*).

The possibilities of melting on the dispersed substrate were verified in compacting into

a billet titanium sponge of TG-TV grade, fraction 30–50 mm. The dispersed substrate was produced from the titanium sponge with the size of 2–5 and 5–12 mm in different proportions. The melting conditions were as follows: the current in the plasma torch 850–1150 A, the frequency of transverse oscillations of the plasma torch 0.5–1.0 oscillations/minute, the speed of travel of the solidification mould 8–12 mm/min, arc length 110–150 mm. The amplitude of oscillations of the arc corresponded to the width of the solidification mould.

In the melting, the voltage in the arc and the stability of arcing were recorded. After completing melting, measurements were taken of the depth of penetration and the length of the pool and the quality of the produced ingots and distortions of the ingots (curvature

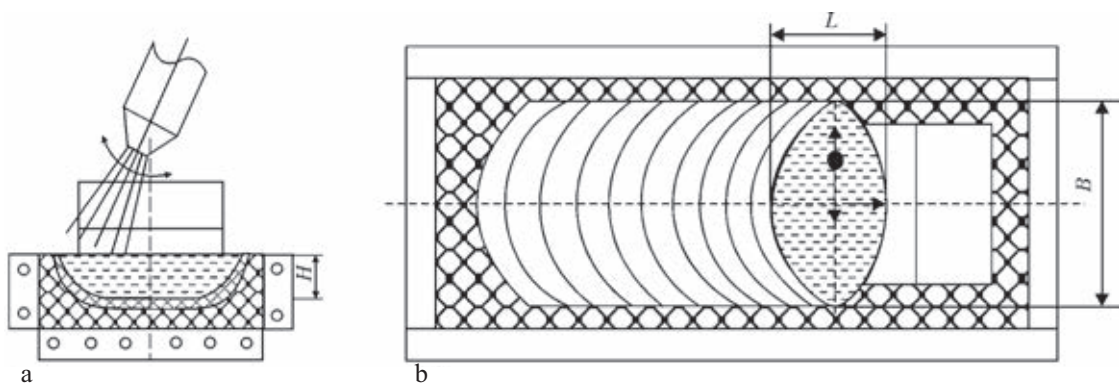


Fig. 3. Diagram of remelting the charge with the bottom and side insulation of the solidification mould with a dispersed substrate: *a*) the view from the side of the narrow phase of the mould; *b*) the top view; *H*, *L*, *B*) the depth, length and width of the metal pool, respectively.

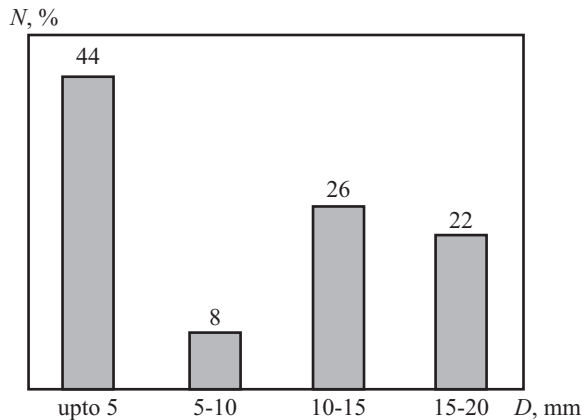


Fig. 4. Grain size composition of the dispersed layer; d) the size of the fraction; N the content of the fraction in the charge.

along the length and width). The investigations were used to select the optimum melting conditions ensuring melting of each layer to at least 20 mm. It was found that the increase of current above 1000 A results in splashing of metal. The main technological parameters of the compacting process are presented in Table 1.

As indicated by the table, the application of the dispersed substrate reduce the energy consumption and consumption of argon in melting the first and second layer of the ingot. In melting the third and further layers, these parameters were almost completely identical and because the heat losses from the metal tool take place mainly as a result of heating of the previously melted ingot.

Two melt charge consisting of scrap and waste of various ferroalloys if it is necessary to produce the ingot of the required size and ensure high quality of the surface, it is highly promising to use the technology of plasma arc melting on a dispersed substrate. In this case, the metal pool can be insulated not only from the baseplate but also the mould walls.

In subsequent stages, experiments were carried out with melting 70% ferrotitanium from titanium and steel scrap in a copper solidification mould on a dispersed substrate consisting of a crushed ferroalloy of the same grade. The solidification mould used for compacting the titanium sponge was also used for investigating the effect of the thickness of the layer of the display substrate and the

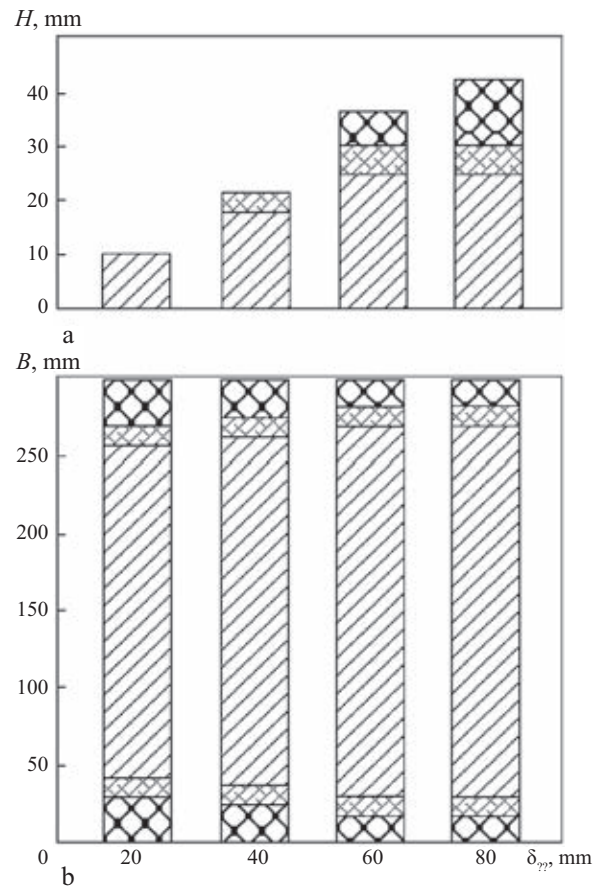


Fig. 5. The effect of the thickness of the disposal a) the formation of the ingot; a, b) the depth H and width B of melting and sintering of the dispersed layer, respectively.

formation of the metal pool.

The diagram of melting with the transverse oscillations of the plasma torch and longitudinal displacement of the solidification mould is shown in Fig. 3. The amplitude of the oscillations was 100 mm, the frequency 0.3 oscillations light min, the speed of travel of the mould 8 mm/min, plasma torch current 1000 A, arc voltage in a 70 mm long arc 40-45 V. The dispersed layer consisted of 70% ferrotitanium; its grain size composition is shown in Fig. 4. The bulk mass of the metal of the dispersed layer was approximately 3 kg/dm³.

After melting, the dimensions of the produced ingots, the sintered layer and the remaining dispersed substrate were investigated. Figure 5 shows the diagrams indicating the effect of the thickness of the disposal a) on the formation of the metal pool. At the

thickness of the dispersed a of 20 mm, the metal melts to the copper cooled bottom of the solidification mould. The increase of the thickness of the dispersed layer results in the formation of the sintered interlayer (not melted). The melting, the base of the ingot and the thickness of the sintered layer increased. A further increase of the thickness of the dispersed substrate Lisa the formation of an unmelted layer, ensuring heat insulation of the ingot in relation to the copper wall of the solidification mould during melting. Subsequently, the increase of the thickness of the dispersed substrate has almost no further effect on the variation of the depth and width of the melted metal layer.

Thus, it may be concluded that for the given design of the solidification mould and the current value of exceeding 1000 A, the optimum thickness of the dispersed layer in melting 70% ferrotitanium is 60 mm.

To determine the effect of the technological parameters of the process on the volume of the metal found at each moment of time in the liquid state, additional experiments were carried out with the substrate 60 mm thick. The results obtained in these experiments (Fig. 6) can be used to select the conditions of plasma-arc melting on the dispersed substrate ensuring the required dimensions of the metal pool for each specific case. These dimensions are important from the viewpoint of ensuring the uniform distribution of the elements in the volume of the ingot, melted from charges with different chemical and grain size composition, in this case, in melting 70% ferrotitanium from the titanium and steel scrap.

The data shown in Fig. 6 indicate that in the same technological conditions, the volume of the metal pool in melting under dispersed substrate is approximately twice as large as in remelting the charge in the copper solidification mould (presumably as a result of the depth of the pool) or in plasma-arc refining of the surface of flat billets [4, 6].

Thus, the experimental results show that the application of the dispersed substrate in plasma-arc melting in the horizontal morning

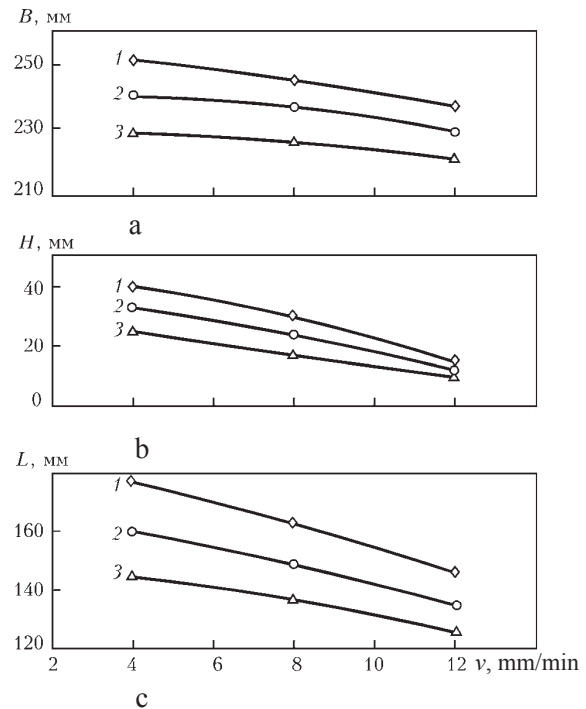


Fig. 6. Effect of melting current (1 – 1000; 2 – 900; 3 – 800 A) and the speed of travel of the mould on the width (a), depth (b) and length (c) of the liquid metal pool in remelting the dispersed layer with transverse oscillations of the plasma torch.

solidification mould as a result of reducing the heat losses into the watercooled solidification mould makes it possible to reduce greatly (by 15-20%) the specific consumption of electric energy and (almost halve) the specific consumption of plasma forming gas. This melting method is especially promising for compacting high-the activity and refractory metals, melting from scrap in waste of different ferroalloys and master alloys.

References

1. Musatov, M.I., et al., Tsvetn. Met., 1991, No. 12, 20–30.
2. Trigub, N.P., et al., Sovremennaya Elektrometallurgiya, 2006, No. 4, 6–9.
3. Klyuev, M.M., Plasma arc remelting, Metallurgiya, Moscow, 1980.
4. Latash, Yu.V., et al., In: Welding and special electrometallurgy, Naukova Dumka, Kiev, 1984, 265–276.
5. Latash, Yu.V., et al., Probl. Spets. Elektrometall., 1993, No. 2, 39–43.
6. Koleda, V.N., et al., Sovremennaya Elektrometallurgiya, 2006, No. 4, 20–23.

Submitted 25.11.2011



Dispersion-hardened titanium alloys of the Ti-Si-X system

G.M. Grigorenko, S.V. Akhonin, T.G. Taranova, S.G. Grigorenko
and O.M. Zadorozhnyuk

EO .P aton Electric Welding Institute, Kiev

Results of investigations of experimental alloys of Ti-Si-X system are presented, the interest to which was shown by the challenge of their application in aircraft industry and rocketry. Ingots of experimental titanium alloys were manufactured by the method of electron beam crucible melting with electromagnetic stirring, which allows producing the homogeneous melt and ingots, homogeneous in chemical composition, after cooling. Using the methods of light metallography, such as SEM, Auger-spectroscopy, the structure and properties of wrought titanium alloys of Ti-Si-X system with dispersion strengthening were examined. It was found that the presence of fine-dispersed strengthening particles of nanosizes, having non-homogeneous chemical composition in section, promotes the increase in strength.

The titanium alloys have a unique combination of the physical and mechanical characteristics (high values of specific strength, corrosion resistance, sufficiently high plasticity) and are therefore one of the most attractive structural materials, especially for aerospace applications, chemical engineering and medicine. In engine construction, the titanium-based creep-resisting alloys represent materials replacing the traditionally used creep-resisting alloys based on nickel, cobalt and iron.

Interest in the titanium alloys on the basis of the Ti-Si-X system is determined by the potential of using these alloys in aviation industry and rocket construction.

Silicon is an alloying element which may greatly increase the creep strength and heat

resistance of the titanium alloy. It should be mentioned that the investigations of the mechanical properties of the alloys of the Ti-Si-X system show that the addition of

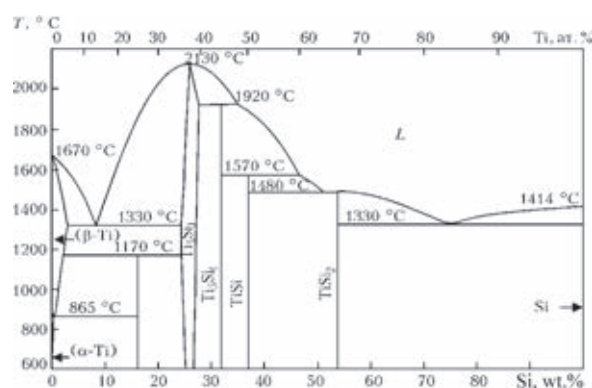


Fig. 1. Equilibrium diagram of the Ti-Si system [2].

Table 1. Chemical composition of experimental titanium alloys of the Ti-Si-X system

Alloy No.	Alloy grade	Al	Sn	Zr	Nb	Mo	V	Si	[O]	[N]
1	α	–	–	–	–	–	–	3.18	–	–
2	α	–	–	3.14	–	–	–	2.23	–	–
3	α	1.40	2.82	5.95	–	–	–	3.37	–	–
4	Pseudo- α	5.64	2.20	3.53	–	0.43	0.95	0.56	0.09	0.02
5	Pseudo- α	5.22	3.33	4.24	0.77	0.13	0.61	0.57	0.10	0.02
6	($\alpha + \beta$)	4.29	4.39	5.95	4.26	1.57	0.68	0.35	0.24	0.02

silicon in the amount exceeding the limiting solubility of silicon in α -titanium increases the strength and greatly reduces the plasticity [1]. For this reason, the silicon content of the industrial creep-resisting alloys is in the range of its solubility in α -titanium (up to 0.4 wt.%) (Fig. 1) [2].

The Ti-Si-X system is of special interest for investigations in which the additional improvement of the working temperature is achieved by adding alloys of silicides and other creep-resisting compounds into the structure of the alloys.

Recently, promising creep-resisting materials included alloys based on the Ti-Si-X system [3] but these alloys are characterised by very low plasticity at normal temperature which greatly reduces the technological properties and prevents these alloys from use in the sections and components of engines. Alloys of the Ti-Al-Si system with 2–3% of silicon have high creep strength and creep resistance but the plasticity of these alloys at room temperature is equal to almost 0 [4]. It should be mentioned that the various alloying elements, such as aluminium, tin, zirconium, niobium and molybdenum increased the strength and creep resistance. All the investigators, concerned with the development of titanium alloys, assume that the creep- and high-strength titanium alloys will be developed in this direction [5].

The aim of the present work is the examination of the structure and mechanical properties of the deformed experimental titanium alloys of the Ti-Si-X system with dispersion hardening.

Experimental materials, equipment and procedure

Ingots of experimental titanium alloys were melted by electron beam crucible melting with electromagnetic stirring [6] producing a homogeneous melt, and after cooling ingots with a homogeneous chemical composition. The diameter of the ingots was 70 mm, weight 5–10 kg. The produced ingots were subsequently subjected to thermomechanical treatment.

The first three layers were deformed by upsetting in a hydraulic press in a container. Treatment was carried out in the cycles: the first cycle – heating to 1165°C, 15–20% upsetting; second cycle heating to 1165°C, upsetting 10–15%; third cycle – heating to 1165°C, 7–10% upsetting.

The remaining alloys were rolled into 9–11 mm sheet in a two-roll reversing mill. When the required temperature in the furnace was reached, the components were held for 1 hour and subsequently deformed. To produce the fine-dispersion structure, in a rolling the specimens were deformed to 60–70% in the β -range (1050–1100°C), and the remaining specimens to 30–40% in the ($\alpha + \beta$) and α -ranges (980–900°C). After rolling, the metal was annealed at 800°C.

The deformed sheets were sectioned to produce specimens for examination of the microstructure and mechanical properties. The chemical composition of the experimental alloys was determined by spectral and chemical analysis, the gas content of the metal was determined in TN-114 and RO-316 gas analy-

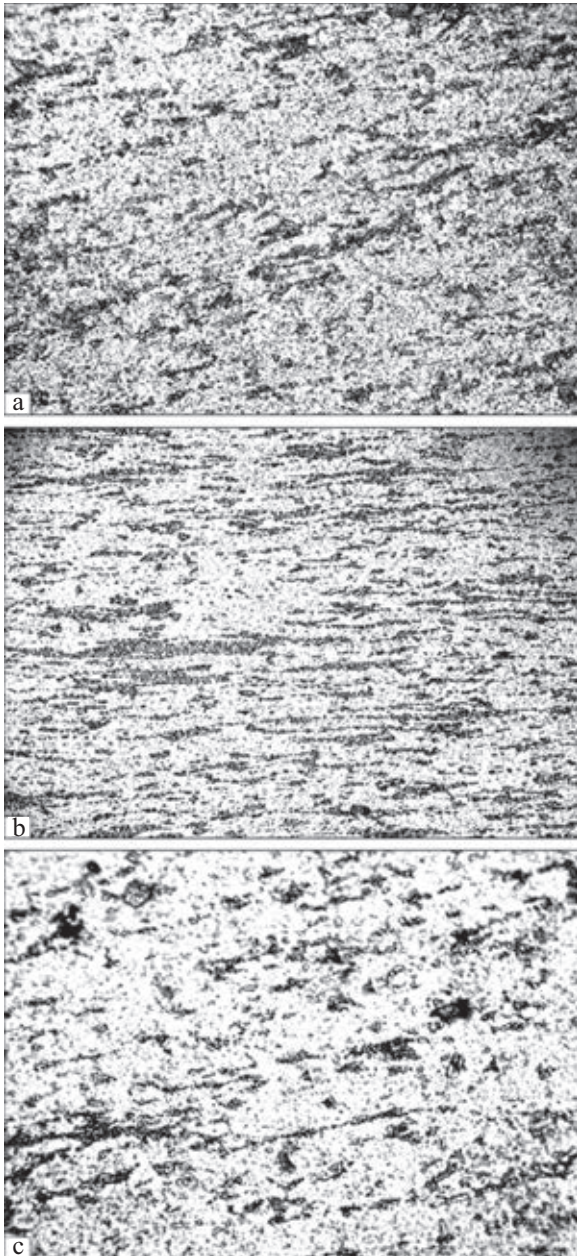


Fig. 2. Microstructure ($\times 200$) of the alloys: a) No. 1 (Ti-3.38Si); b) No. 2 (Ti-3.41Zr-2.23Si); c) No. 3 (Ti-4.01Al-2.28Sn-5.95Zr-3.37Si).

ser (LECO, USA). Metallographic studies and photographic the recording were carried out in a Neophot-32 microscope (Germany), fitted with a computer, an Olympus digital camera and an archive system. Microhardness was measured in a M-400 hardness metre (LECO, USA) at a load of 10 g. The macrostructure of the investigated specimens was examined by the chemical method of etching in a 4% alcohol solution of nitric acid.

X-ray studies of the specimens were carried out using a DRON-UM1 diffractometer in monochromatic $\text{CuK}\alpha$ -radiation by step scanning (35 kV, 25 mA, exposure time at a point 20 s, step 0.05°). The lattice parameters were calculated using a program for full-profile analysis of x-ray spectrum from a mixture of polycrystalline phase components Powder Cell 2.4.

The composition of the investigated alloys is presented in Table 1.

As regards the chemical composition, the alloys are characterised by some differences in comparison with the alloys already used in production and applied in actual structures.

Metallographic studies

The investigated titanium α -alloys No. 1 (Ti-3.4 Si), No. 2 (Ti-3.4 Zr-2.3 Si) and No. 3 (Ti-1.4Al-2.9Sn-6Zr-3.4Si) have similar structures consisting of the α -titanium matrix, with a large number of fine particles with the size of 1.5–2.0 μm , and clusters of large particles (up to 5 μm) distributed along the stretched grains (Fig. 2).

With increase of the content of the alloying elements the deformed structure becomes less evident but also microhardness increases. In the alloy No. 1 the microhardness of the matrix with the fine precipitate equalled 2900–3100 MPa, in the sections with clusters of large precipitates 3800–4100 MPa, in the alloy No. 2 it was respectively 3300–3500 and 4000–4200 MPa, and in the alloy No. 3 it was 3600–3800 4200–4800 MPa.

The specimens of the alloys No. 4 (Ti-5.6Al-2.2Sn-3.5Zr-0.4 Mo-1V-0.6 Si) and No. 5 (Ti-5.2Al-3.3Sn-4.2Zr-0.1Mo-0.6V-0.8Nb-0.6Si) belong in the group of pseudo- α -alloys. The microstructure of this alloy consists of α -plates with a small amount of the β -phase, precipitated at their boundaries. A large amount of the inclusions of different sizes, distributed both along the boundaries and inside the α -plates, was also found (Fig. 3).

The structures of the specimens No. 4 and 5 slightly differ in the dispersion of the α -phase,

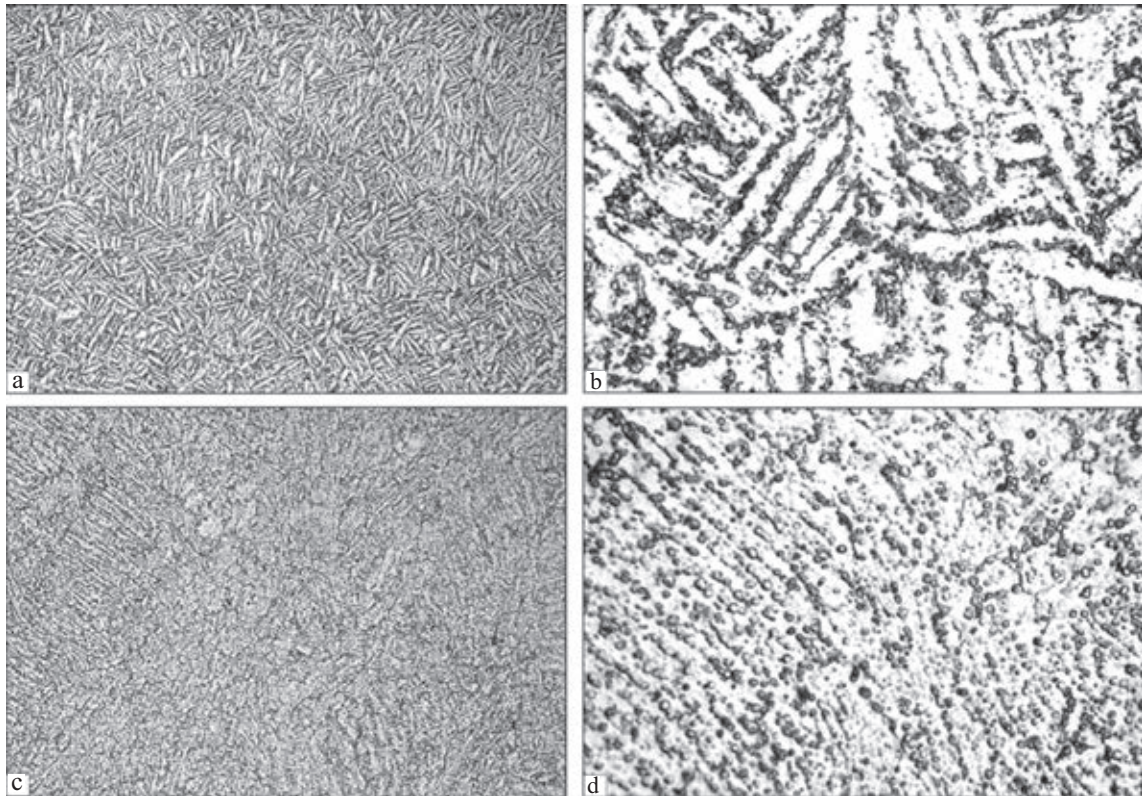


Fig. 3. Microstructure of the alloys: *a, b*) No. 4 (Ti–6Al–2Sn–4Zr–Mo–V–Si); *c, d*) No. 5 (Ti–5Al–3Sn–5Zr–Nb–Mo–V–Si); *a, c*) $\times 200$; *b, d*) $\times 1000$.

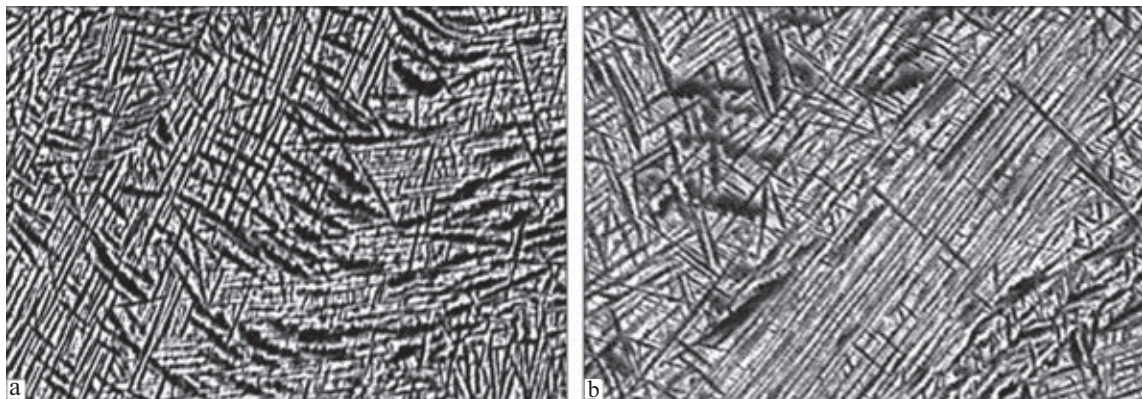


Fig. 4. Microstructure of the alloy No. 6 (Ti–4Al–4Sn–6Zr–4Nb–2Mo–V–Si); *a*) $\times 800$; *b*) $\times 1000$.

and also the distribution of inclusions and microhardness. In the specimen No. 4 the size of the α -plates is slightly larger, the inclusions are distributed mostly at the boundaries of the plate (Fig. 3, *a*), the microhardness equals 3600–3900 MPa. In the specimens No. 5, the α -plates are smaller, the inclusions are distributed more uniformly over the entire

surface (Fig. 3, *b*), the microhardness equals 4300–4500 MPa.

The alloy No. 6 (Ti–4.3Al–4.4Sn–6Zr–1.6Mo–0.7V–4.3Nb–0.4Si) belong in the group of the titanium ($\alpha+\beta$)-alloys of the martensitic. Martensite forms at the background of the two-phase structure and is the α' -phase of the needle structure, representing

Table 2. Mechanical properties of the experimental titanium alloys of the Ti–Si–X system

Alloy No.	Class	σ_B , MPa	$\sigma_{0.2}$, MPa	δ , %	KCV, J/cm ²
1	α	745.3	–	9.5	2.33
2	α	997.6	–	2.7	2.51
3	α	721.3	–	10.7	3.27
4	Pseudo- α	1209.8	1106.6	1.7	8.91
5	Pseudo- α	1273.6	1130.8	4.0	10.36
6	($\alpha + \beta$)	1422.4	1331.3	1.0	4.15

a supersaturated solid solution of the alloying elements in the α -titanium (Fig. 4) with the microhardness of 4000–4400 MPa.

Mechanical properties. The mechanical properties were determined by tensile loading of cylindrical specimens with a diameter of 3 mm. The results are presented in Table 2. Processing of the results of the mechanical tests showed the dependence of the tensile strength, yield limit and impact toughness of the investigated alloys on the content of the alloying elements.

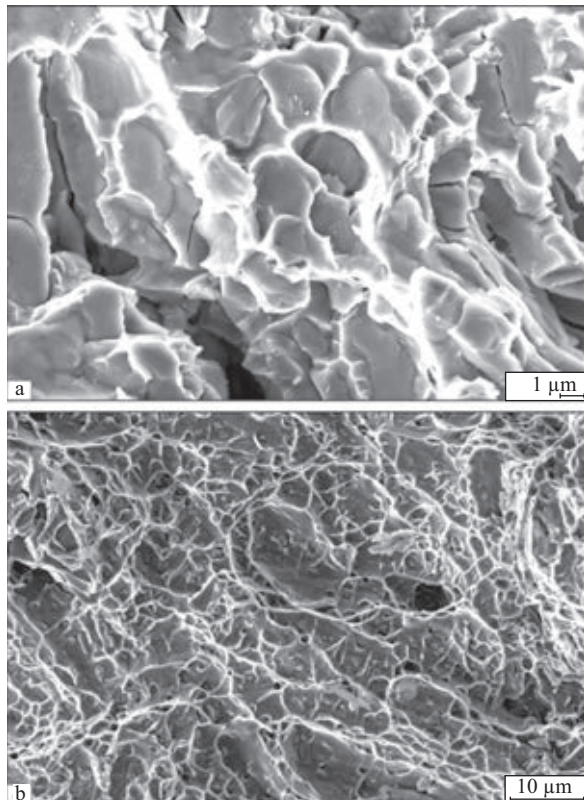


Fig. 5. Macrostructure of the fracture surface of alloy No. 1: a) brittle fracture area; b) single section of ductile failure.

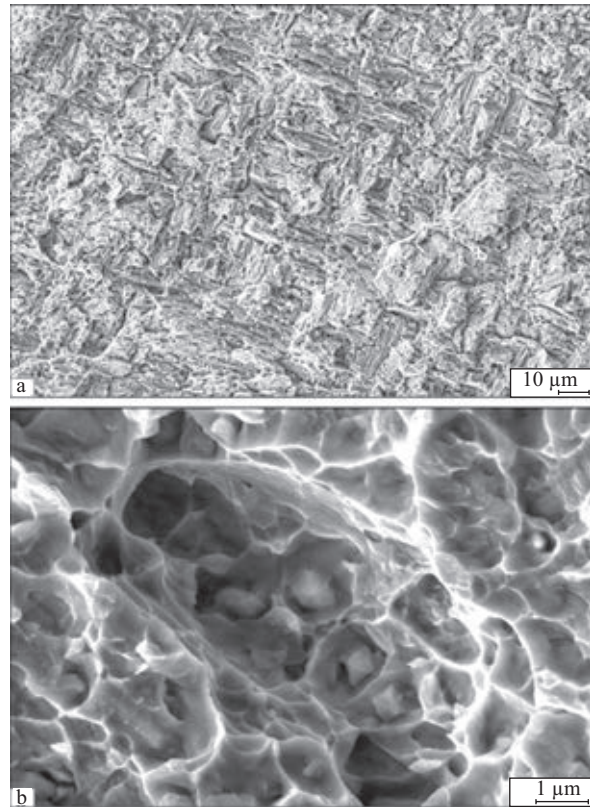


Fig. 6. Microstructure of the fracture surface of alloy No. 2: a) area with cleavage of facets; b) ductile area with fine-dispersion precipitates.

In the alloy No. 1, the strength and impact toughness were low. The alloy No. 2 which was alloyed with zirconium was characterised by higher strength with a low impact toughness. In the alloy No. 3, alloying with aluminium and tin resulted in the situation in which the strength and impact toughness were comparable with the binary alloy No. 1. In the pseudo- α -titanium alloys No. 4 and 5, a further increase of the amount of the alloying elements resulted in a large improvement of the strength characteristics and increased impact toughness. The alloy No. 6 ($\alpha + \beta$)-titanium is characterised by maximum strength, and its plasticity lower than that of the pseudo- α -titanium alloys.

Fractographic studies of the fracture surface of the specimen show that there are characterised by a well developed relief.

The fracture of the No. 1 alloy was brittle (Fig. 5). Fracture took place through the

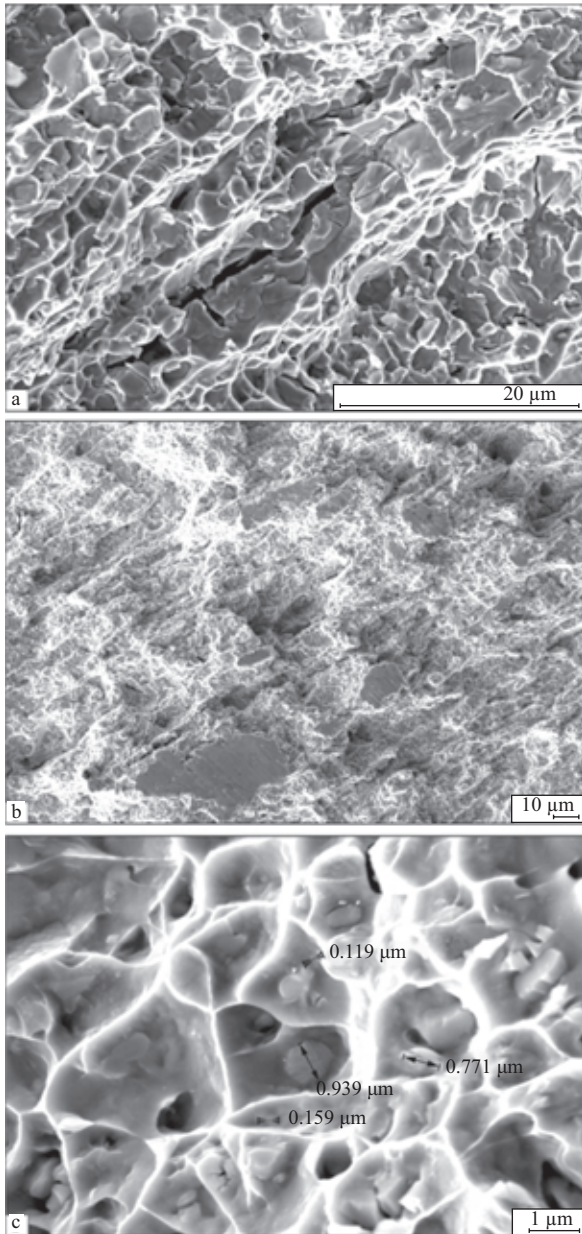


Fig. 7. Macrostructure of the fracture surface of the alloy No. 3: a) cleavage areas; b) secondary cracks; c) local ductile area with fine-dispersion particles.

phase precipitates of the titanium silicides Ti_5Si_3 , distributed along the grain boundaries. The larger particles (2–5 μm) are elongated and separate from the matrix. Fracture takes place through the brittle phases precipitate by cleavage of the particles up to 0.5 mm in size retain the coherent bond with the matrix. The nature of failure in these single sections is ductile and determined by the occurrence of the process of segregation of

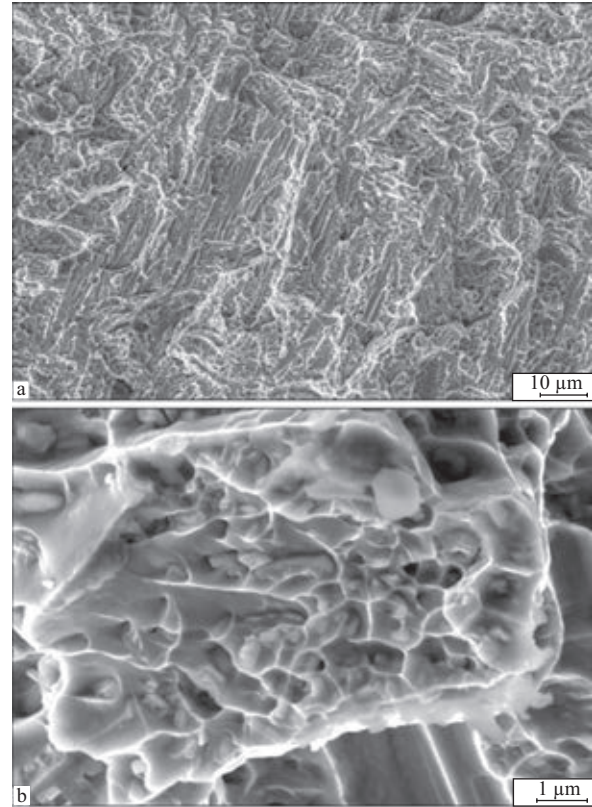


Fig. 8. Microstructure of the fracture surface of the alloy No. 4: a) the structure of old material in the brittle fracture area; b) ductile area with hardening nanoparticles.

the alloying and impurity elements at the grain boundaries.

The alloy No. 2 (Fig. 6) contains areas with cleavage facets in the α -titanium matrix which contain river-like patterns and are separated by separation ridges. The presence of a large number of quasi cleavage facets is explained by the effect of the separation mechanism of the contact planes of the structural components. Inside the facets there are ridges and between them – individual fragments of cleavage, formed as a result of plastic sheeting of the alloy in the conditions of tensile deformation. Shallow pits containing fine-dispersion particles with the size of 700 nm–1 μm indicate that the toughness is low.

In the alloy No.3 at a small magnification ($\times 300$) the fracture surface contain a large number of flat cleavage sections with the area $40 \times 70 \mu m$ (Fig. 7, a) determined by the formation of structural components distributed at the grain boundaries.

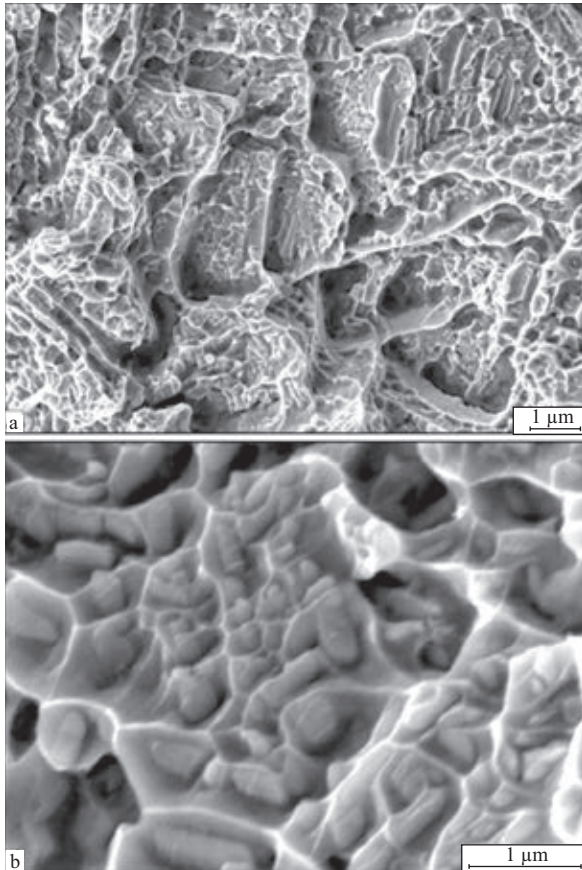


Fig. 9. Microstructure of the fracture surface of the alloy No. 5: a) transcrystalline fracture area; b) ductile fracture area with hardening nanoparticles (50-70 nm), formed by the dimpled mechanism.

The grains also contained secondary cracks passing through the body of the grain (Fig. 7, *b*). The stresses, formed in tensile loading result in the nonuniform microplastic deformation of the grains and stress concentration at the grain boundaries. At a high magnifications, the fracture surface showed deep pits, formed at the spherical inclusions which initiated local ductile failure formed directly around them (Fig.7, *c*). The size of the fine-dispersion hardening particles was 160–200 nm. They were circular and elongated in the rolling direction.

In the alloy No. 4, the failure was mixed, and the number of brittle fracture areas was considerably greater than that of ductile fracture areas (Fig. 8). Microcracks initiated preferentially at the grain boundaries. The grains are elongated, the size was $10 \times 30 \mu\text{m}$. The regions of the ductile failure

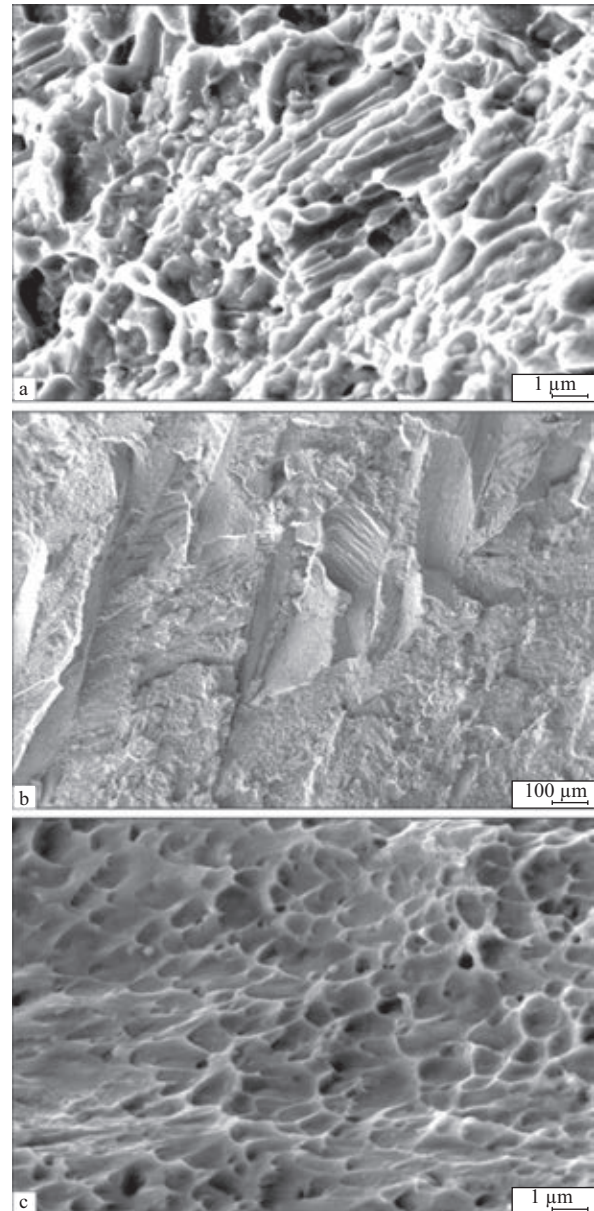
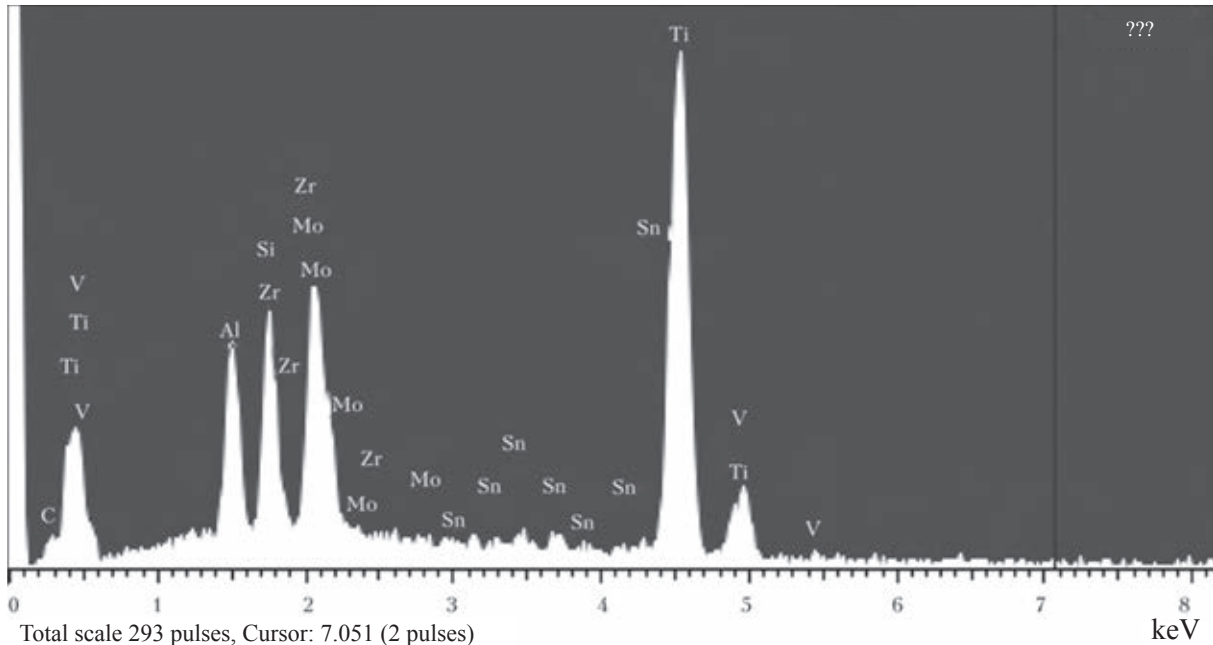


Fig.10. Microstructure of the fracture surface of the alloy No. 6: a) variation of the orientation of the fracture plane from grain to grain; b) fractured through the cleavage planes; c) the area of ductile local failure by the microvoid growth mechanism.

were determined by the presence of micro-dispersed hardening inclusions, distributed in the pits of the fracture surface. The composition of these particles was $(\text{Ti}, \text{Zr})_5 (\text{Si}, \text{Al})_3$, and the size did not exceed 150 nm. As regards stoichiometry, they were similar to the titanium silicides, alloyed with zirconium and aluminium (Fig. 1).

The grain size of the alloy No. 5 was 10-30 μm . Intergranular failure equalled 70%,



a

Element	Mass %	Atomic %
CK	1.75	6.93
AlK	3.55	6.28
SiK	4.55	7.73
TiK	67.37	67.05
VK	1.17	1.10
ZrL	18.10	9.46
MoL	0.44	0.22
SnL	3.07	1.23
Total	100.0	

b

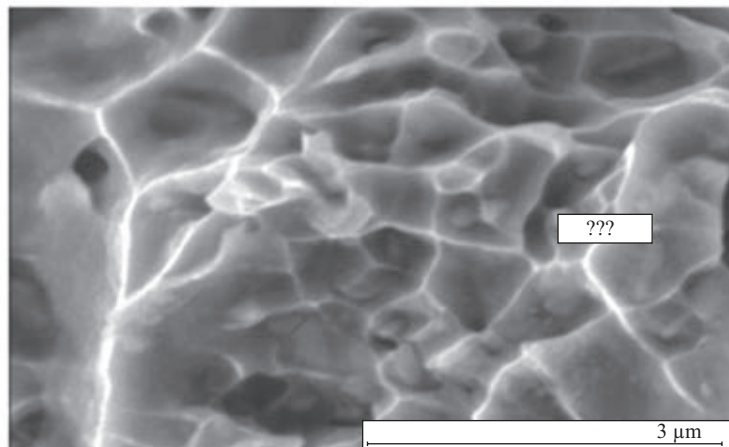


Fig. 11. Results of microanalysis of the hardening particles in the alloys of the Ti-Si-X system: a) analytical spectrum of the composition of particle; b) numerical values of the main alloying elements.

some of the grains were surrounded with secondary intergranular cracks, 30% – transcrystalline failure (Fig. 9, a). This failure is probably caused by the decohesion of the grain boundaries as a result of structural transformations and precipitation of inclusions in the intergranular space. Tensile stresses in tensile loading result in non-uniform microplastic deformation of the grains and stress concentration at the grain boundaries, and this is accompanied by the formation of microcavities which facilitate crack nucleation at the phase precipitates. The stress state forms

as a result of the high diffusion ability of the alloying elements from the volume of the grains to the grain boundaries during thermal mechanical treatment.

The increase of the stress concentration results in the formation of the suitable conditions for easy nucleation of the microcracks along the grain boundaries by the quasi-cleavage mechanism. This is indicated by the stone-like relief of the fracture surface which is usually found in the case of mixed failure, i.e., in cracking of brittle structural components and ductile failure of the matrix.

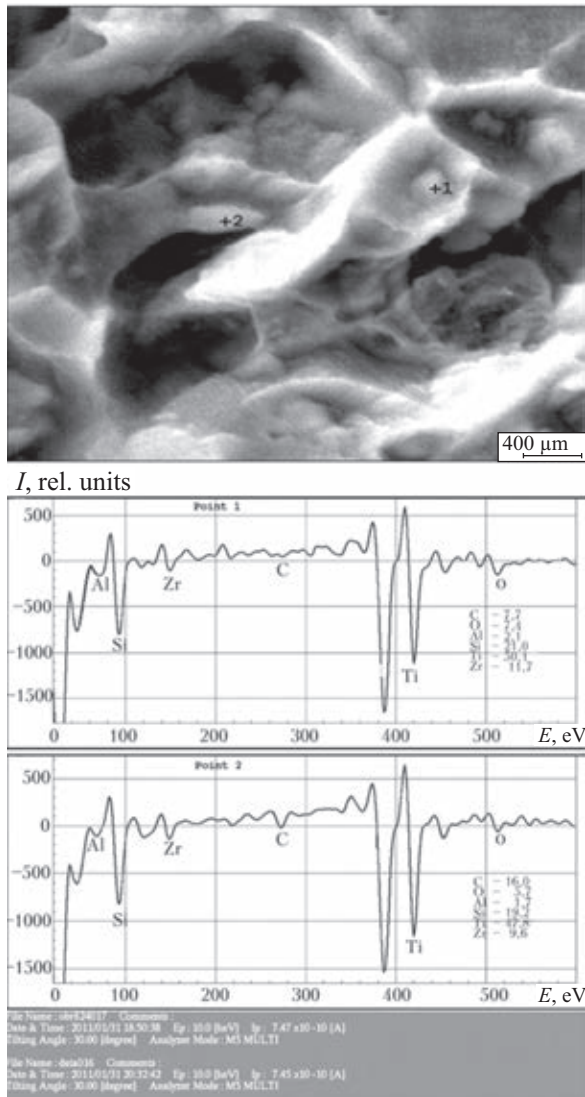


Fig. 12. The results of analysis (layer thickness approximately 20 nm) by the method of Auger spectrometry (at. %): point 1 (wt. %): C = 2.1; O = 2.7; Al = 1.3; Si = 13; Ti = 55.6; Zr = 24.6. Point 2 (wt. %): C = 4.6; O = 2.3; Al = 1.2; Si = 13.3; Ti = 56.9; Zr = 21.7).

The results showed that in the areas in which the aluminium is in the non-bonded condition, fracture takes place by the cleavage mechanism. In addition to failure by cleavage, there are also ductile areas formed by the dimpled mechanism of void coalescence (Fig. 9, *b*) containing hardening particles with the size of 50–70 nm.

The roughness of the surface relief of the alloy No. 6 is determined by the crystallographic nature of failure (Fig. 10). There are distinctive changes in the orientation of

the fracture plane from the grain to the grain with the size of 5–15 μm . Fracture takes place on the cleavage planes. The presence of inclusions results in local ductile failure by the micro-void growth mechanism. In this specimen, the hardening particles are fine-dispersed, the size is 130–160 nm.

More detailed studies of the composition of the fine-dispersion hardening particles, detected in the experimental titanium alloys of the Ti-Si-X system in equipment JAMP 9500F using two mutually supplementing methods: energy-dispersing spectrometric (EDS) and the Auger spectrometry.

The Auger microprobe with a field emission cathode JAMP-9500F (JEOL limited) is a multifunctional advanced system with high parameters of the technical characteristics. The combined and electron scanning microscope with the resulting capacity in secondary electrons (3 nm) and also a Auger spectrometer with the electron probe diameter of 8 nm and an energy-resolving capacity of $DE/E = 0.005\text{--}0.600$. The system is also fitted with an energy-dispersing spectrometer Oxford EDS INCA Energy 350 the analysis of elements (from beryllium to uranium) with the electron probe diameter 1 μm . The specimens examined in a superhigh vacuum of 5×10^{-8} Pa. Prior to investigations, the specimens were etched with argon ions.

Figure 11 shows the results of energy-dispersion spectrometry of the investigated specimens because of the small size of the inclusions, the energy dispersion spectrometry method makes it possible to determine only the integral chemical composition of the inclusions which is similar to that of titanium aluminide alloyed with zirconium and silicon. The methods of Auger spectrometry was used to determine the chemical composition on the surface of the Nano-inclusions (Fig. 12).

Comparison of the results of energy-dispersing spectrometry, Auger spectral and x-ray diffraction analysis shows that the inclusions regardless of the dependence on the nanosized have non-uniform composition. The internal part of the inclusions consists of

titanium aluminide alloyed with zirconium, and the surface is a silicide frame.

Conclusions

1. The relationship of the structure and mechanical properties of the titanium alloys with the dispersion hardening by intermetallics and silicides has been investigated.

2. The specimen results show that the technology of producing the alloys by electron beam melting with the electromagnetic stirring in a pool metal possible to ensure the uniform distribution of the hardening fine-dispersion particles in the ingots. The size of these particles in some alloys reaches the nanosize.

3. The results also show that these particles increase the strength but do not ensure the required plasticity of the alloys.

4. It has been shown that the hardening particles have a non-uniform chemical composition and are complicated chemical compounds of titanium, zirconium, aluminium and silicon. The silicon content of the surface

of the nanoparticles is considerably higher than in the middle part, and there is almost no aluminium.

5. It may be assumed that the dispersed particles are titanium aluminosilicides, alloyed with zirconium with a silicide frame.

6. The highest level of the mechanical properties was recorded by the complexly alloyed pseudo- α -titanium alloy No. 5.

7. The results indicate the promising nature of the development of these alloys and the need to continue studies in this direction.

References

1. Firstov, S.A., et al., *Metalloved. Term. Obrab. Met.*, 2009, No. 1, 14–20.
2. Kaufman, L., *Calphad*, www.himikatus.ru/art/phasediagr1/Si-Ti.php.
3. Khorev, A.I. and Khorev, M.A., *Titan*, 2005, No. 1, 40–53.
4. Firstov, S.A., *Fiz. Tekh. Vysokikh Davl.*, 2002, No. 3, 28–38.
5. Anoshkin, N.F. and Sigalov, Yu.M., *Tekhnol. Legkikh Splavov*, 2002, No. 1, 38–50.
6. Ladokhin, S.V., *Electron beam melting in casting production*, *Stal'*, Kiev, 2007.

Submitted 7.2.2012

Structural and phase transformations in the $Ti_{60}Cr_{32}Si_{18}$ phase, containing an approximant phase

A.L. Borisova, L.I. Adeeva, A.Yu. Tunik, M.V. Karpets,
S.N. Stepanyuk and L.K. Doroshenko

EO .P aton Electric Welding Institute, Kiev

Phase and structural transformations in mixture of powders, corresponding to composition of alloy $Ti_{60}Cr_{32}Si_{18}$, prone to the formation of quasi-crystalline phase, were investigated by the methods of differential thermal and X-ray phase analyses. It was established that an approximant of icosahedral phase (α -phase) in mixture with phase of Laves ξ - $TiCr_2$, alloyed by silicon, is formed in the alloy of the mentioned composition. Amount of α -phase can be increased up to 90 mass % as a result of heating up to 1700°C and up to 100% in adding of oxygen (in the form of SiO_2) into the mixture of powders in manufacture of ingot.

Quasi-crystalline phases or their approximants are characterised by a set of valuable properties, including high values of hardness, low friction coefficient, surface energy, heat conductivity, etc. Therefore, they are of considerable interest for many industrial applications [1, 2].

The Ti–Cr–Si system contains the $Ti_{60}Cr_{32}Si_{18}$ alloy which in rapid quenching in the presence of oxygen has the quasi-crystalline structure [3, 4]. Other phases, such as the β -phase of the Ti–Cr–Si and the Laves phases $TiCr_2$ form in the absence of oxygen.

In [5, 6] it was attempted to produce a coating with the quasi-crystalline structure by gas thermal spraying the $Ti_{60}Cr_{32}Si_{18}$ alloy in Air in the presence of oxygen. In addition to gas flame and atmospheric plasma spraying, the authors (for comparison) used vacuum plasma spraying. The main phases of the powder (β -Ti–Cr–Si and $TiCr_2$) remained in all the coatings, but in the gas flame and the plasma spraying in air a large amount of oxides was also formed. At the same time, the authors confirm the possibility of formation in the Ti–Cr–Si–O system of a quasi-crystalline

icosahedral structure (i -phase) at the specific parameters of plasma spraying in air.

Recently, the problem of the possibility of the formation of the icosahedral phase in the $Ti_{60}Cr_{32}Si_{18}$ alloy in the absence of oxygen and the role of oxygen in the formation has not as yet been solved. In this study, it is attempted to use the method of differential thermal analysis (DTA) to investigate the possibilities of producing a quasi-crystal in the alloy of the given composition in pure form or after adding oxygen.

The initial materials were represented by the powders of titanium, chromium and silicon of high purity (higher than 99.9 wt.%), and the source of oxygen was the silicon oxide powder which was added into the mixture, in accordance with the composition $Ti_{60}Cr_{32}Si_4(SiO_2)$, recommended in [7].

Differential thermal analysis was carried out in equipment VDTA-8M in helium at the heating/cooling rate of 80°C/min in ZrO_2 crucibles. The maximum temperature in heating was 1700°C. The specimens were studied by metallographic methods, x-ray diffraction phase analysis in equipment DRON UM-1

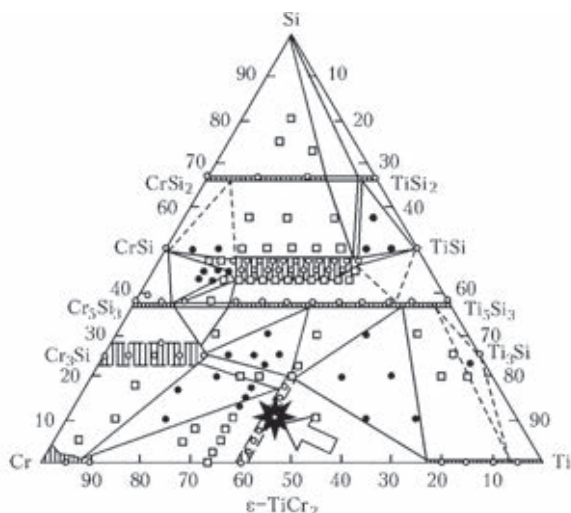


Fig. 1. Isothermal section through the equilibrium diagram of the Ti-Cr-Si system at 1000°C (wt.%): (○) single-phase; (■) two-phase; (●) three-phase region.

with monochromatised radiation $CuK\alpha$.

X-ray spectrum microanalysis (XSMA), investigation of the microstructure and determination of the quantitative elemental composition were carried out using an analytical system consisting of a JSM-35 CF scanning electron microscope (JEOL, Japan) and x-ray spectrometer with energy dispersion of X quanta (model INCA Energy-350, Oxford Instruments, Great Britain). The characteristic feature of this type of analysis is this localisation – the minimum region of excitation is only 1 μ m. One of the advantages of the energy-dispersing spectrometer is the possibility of simultaneous analysis of up to 50 elements and reflection of the entire detected spectrum. The images were produced in the regime of secondary electrons at $U = 20$ kV.

The investigations were carried out on specimens of ingots of the four following types:

1. Produced in an arc furnace with a non-consumable electrode in argon from a mixture of powders, at.%: Ti-60, Cr-32, Si-8;
2. From a mixture of powders of the same composition, produced by mixing in a planetary mill for 0.5 h;
3. From a powder produced by refining an ingot melted in an arc furnace (specimen No. 1);
4. From a powder of the refined ingot

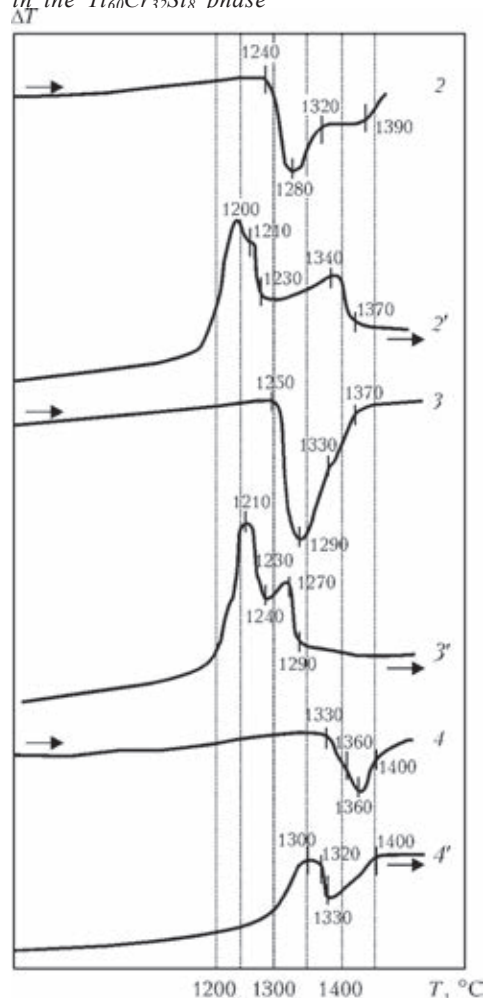


Fig. 2. DTA curves in heating (2–4) and cooling (2'–4') (the numbers of the curves correspond to the numbers of the specimens in Table 1).

with the calculated composition $Ti_{60}Cr_{32}Si_4$ (SiO_2)₄, melted in an arc furnace.

The specimens No. 1 was investigated in the initial condition, and the specimens No. 2–4 in the form of ingots, produced after DTA.

The diagram of the Ti-Cr-Si equilibrium systems investigated in the complete concentration range in [8]. The authors found a ternary compound of a variable composition with the homogenised range elongated along the iso-concentrate 45 at.% Si (15–39 at.% Ti); the width of the region of homogeneity was approximately 5 at.% (from 43 to 48 at.% Si). In addition, there are solid solutions with a large length based on the Ti_5Si_3 , Cr_5Si_3 and Cr_3Si binary compounds (Fig. 1). The region of homogeneity of the solid solution based on ξ - $TiCr_2$ is stretched

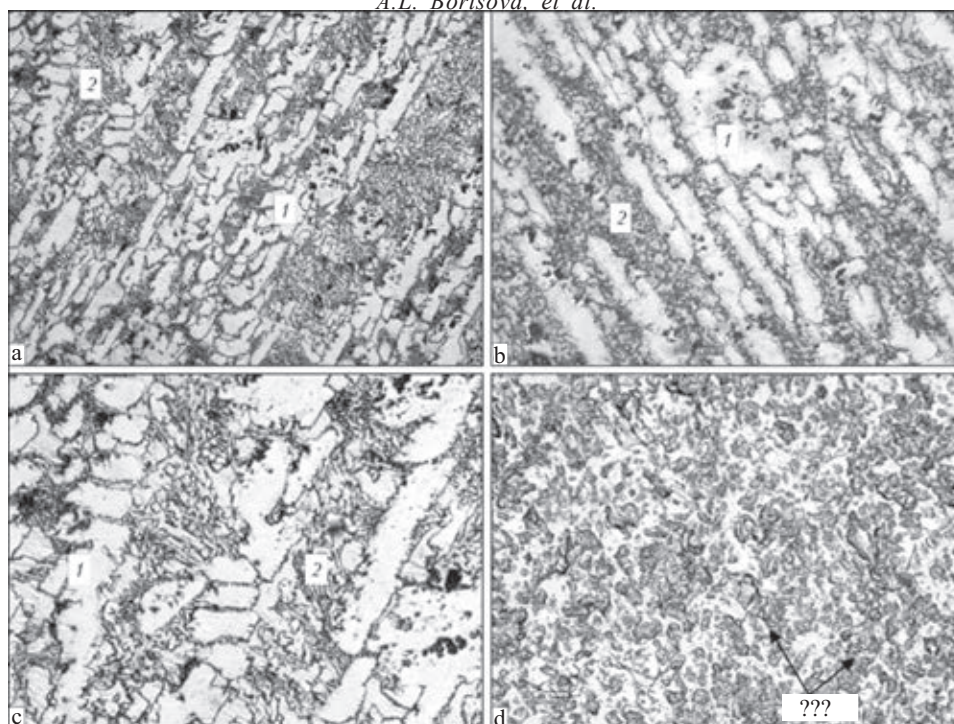


Fig. 3. Microstructure ($\times 400$) of an ingot of the $\text{Ti}_{60}\text{Cr}_{33}\text{Si}_8$ alloy – specimen No. 1 (a), DTA ingots of the specimens No. 2–4 (Table 1), etched.

Table 1. Results obtained in the investigations of the specimens

Specimen No.	DTA results (Fig. 2)	Microhardness of areas in Fig. 3, MPa	Phase analysis, %	XDA data (at.%, Fig. 4)
1	-	Dendrites 9450 ± 1250 (1)	62.2 % - $\xi\text{-TiCr}_2$ ($a = 0.494$ nm, $c = 0.805$ nm)	Ti-41.25 \pm 3.62; Cr-50.09 \pm 4.74; Si-7.94 \pm 1.05 (1)
		Interdendritic spaces 5390 ± 1050 (2)	37.8 % - Ti_5Si_3 ($a = 0.742$ nm, $c = 0.525$ nm)	Ti-64.33 \pm 1.71; Cr-24.51 \pm 1.41; Si-11.16 \pm 0.59 (2)
2	$T_s = 1240^\circ\text{C}$ $T_l = 1280^\circ\text{C}$ Two-stage crystallization	Dendrites 1070 ± 14 (1)	46.3 % - TiCrSi ($a = 1.308$ nm);	Ti-60.91 \pm 2.60; Cr-24.90 \pm 3.98; Si-12.91 \pm 1.70 (1)
		Interdendritic spaces 7420 ± 580 (2)	53.7 % - $\xi\text{-TiCr}_2$ ($a = 0.49$ nm, $c = 0.801$ nm)	Ti-43.84 \pm 3.70; Cr-45.58 \pm 4.40; Si-9.28 \pm 0.84 (2)
3	$T_s = 1250^\circ\text{C}$ $T_l = 1290^\circ\text{C}$ Two-stage crystallization	Dendrites 12080 ± 830 (1)	75.9 % - $\alpha\text{-TiCrSi}$ ($a = 1.313$ nm);	Ti-59.92 \pm 0.51; Cr-29.20 \pm 0.6; Si-10.87 \pm 1.16 (1)
		Interdendritic spaces 7380 ± 640 (2)	24.1 % - $\xi\text{-TiCr}_2$ ($a = 0.493$ nm; $c = 0.800$ nm)	Ti-44.36 \pm 3.5; Cr-51.00 \pm 3.9; Si-4.64 \pm 0.5 (2)
4	$T_s = 1330^\circ\text{C}$ $T_l = 1380^\circ\text{C}$ Single-stage crystallization	Single-phase fine-grained structure 13140 ± 1020	100 % - $\alpha\text{-TiCrSi}$ ($a = 1.313$ nm)	Ti-60.5 \pm 0.8; Cr-32.7 \pm 1.05; Si-7.84 \pm 1.6

Comment. 1. Here T_s is the solidus temperature; T_l the liquidus temperature; 2. The numbers in the brackets are the numbers of the investigated areas.

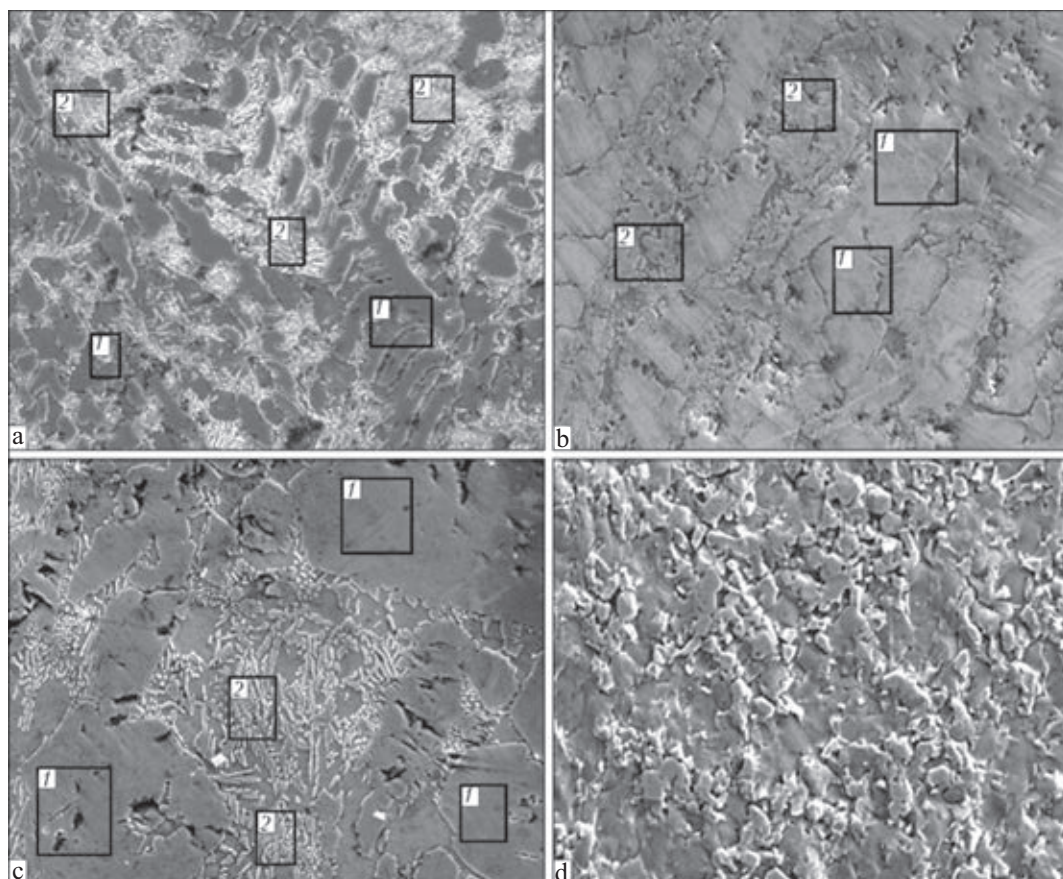


Fig. 4. Microstructure ($\times 500$) of the specimens recorded in the SET mode: a) No. 1; b) No. 2; c) No. 3; d) No. 4 (characteristics of the specimens and the results of x-ray diffraction analysis of the individual sections are presented in Table 1).

along the iso-concentrate from 33.5 at.% Ti to 20 at.% Si. The composition $Ti_{60}Cr_{32}Si_8$ is included in the two-phase range on the diagram of the phase equilibrium of the Ti–Cr–Si system, including the Laves phases ξ - $TiCr_2$ and Ti_5Si_3 (indicated by the asterisk in Fig. 1).

Examination of the DTA curves showed (Fig. 2) at the Nano large differences in the form of the service between the second and third specimens. They are characterised by very similar solidus and liquidus temperatures (difference is in the range $10^\circ C$). Solidification in both cases consists of two stages. The specimen No. 4 (composition with oxygen) is characterised by a large increase of the solidus liquidus temperature (approximately by $100^\circ C$), solidification consists of a single stage, and takes place in a smaller (in comparison with the previous specimens) temperature range.

Metallographic examination of the ingots

indicates that the structure of the specimens No. 1–3 contains light dendrites and a eutectic type structure, distributed in the inter-dendritic spaces (Fig. 3, a–c). In the specimens No. 1, the microhardness of the dendrites is approximately 1000 MPa and the microhardness of the interdendritic areas approximately 5000 MPa. In the specimens No. 2–3, the microhardness of similar regions was slightly higher (Table 1). The structure of the specimen No. 4 was almost completely single-phase, fine-grained with the microhardness higher than 13,000 MPa but as a result of the high brittleness of the structure a large number of spalling areas formed in the preparation of the section (Fig. 3, d).

The processing of the x-ray diffraction data by the methods of full profile analysis (Fig. 4) in the specimens No. 1 showed two phases based on crystalline lattices ξ - $TiCr_2$ and Ti_5Si_3 ,

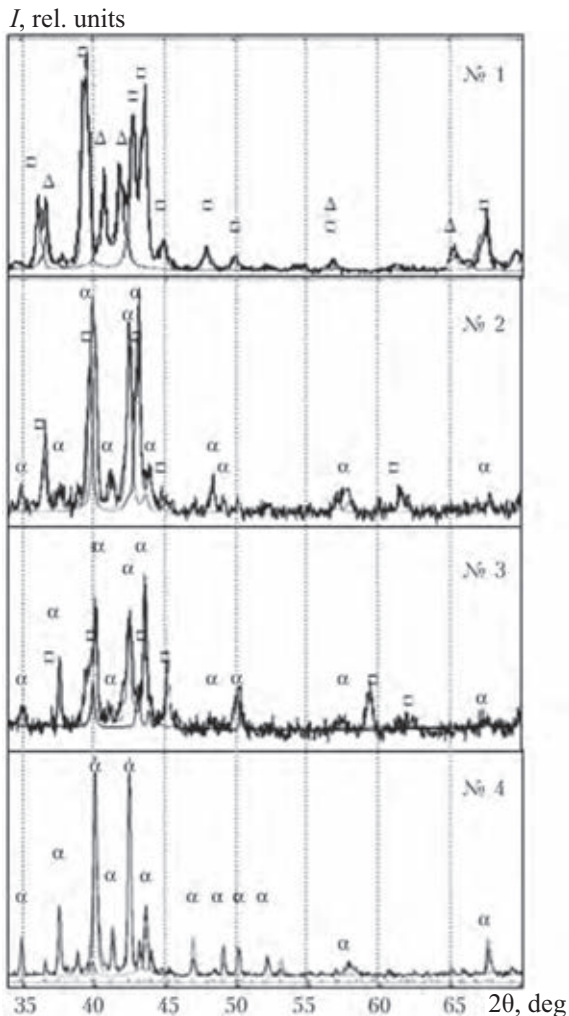


Fig. 5. The results of x-ray diffraction analysis of specimens No. 1–4 (Table 1); α) the approximatant phase; I) intensity; \blacksquare) Laves phase ξ -TiCr₂; Δ) Ti₅Si₃.

which corresponds to the two-phase region in the equilibrium diagram of the Ti–Cr–Si system for the given composition (Fig. 1).

In the specimens No. 2 and 3 two phases were also detected after DTA. One of these phases has a cubic lattice with the parameter of approximately 1.31 nm and the planar spacing is, corresponding to the values presented in [3, 4]. This structure is a cubic approximatant of the icosahedral phase of the alloy of the Ti–Cr–Si system (α -phase). The second phase has a hexagonal structure with a slightly different lattice parameter between the specimens 2 and 3 ($a = 0.4909$, $c = 0.8011$, and $a = 0.4934$, $c = 0.8001$ symbol nanometre, respectively). This phase can be regarded

as the Laves phases ξ -TiCr₂, alloyed with silicon. According to the isothermal section of the equilibrium diagram of the Ti–Cr–Si system, the region of the solid solution of silicon in ξ -TiCr₂ is enclosed in the following concentration range, at.%: 33.6–37.2 Ti, 66.6–46.6 Cr and 0–20 Si. Consequently, the formula of the Laves phases can change from TiCr₂ to Ti₃Cr₅Si₂. The specimen No. 4, in contrast to the previous ingots, consists of a single phase and mostly the α -phase.

Investigation of the ingots by the method of x-ray diffraction analysis (Fig. 4, Table 1) shows that in the specimens No. 1, the Laves phase is greatly enriched with silicon to 8 at.% (Table 1). In addition to the Ti₅Si₃ phase, the interdendritic areas with the eutectic-type structure obviously contain ξ -TiCr₂.

In accordance with the results obtained in x-ray phase analysis, in the DTA ingots 2–4, the sections 1, with a high hardness, are similar, as regards the content of titanium, chromium and silicon, to the initial formula Ti₆₀Cr₃₂Si₈ which, according to the time [3] corresponds to the icosahedral i -phase or the approximatant α -phase. The area of these sections on the metallographic sections increases in accordance with the increase of the content of the α -phase in the specimen, according to the x-ray diffraction analysis data. Sections 2 in the specimens No. 2 and 3 have approximately the same ratio of titanium and chromium, and the structure is of the eutectic type. These sections are evidently a mixture of phases – alloyed with silicon ξ -TiCr₂ and the α -phase, and their microhardness in comparison with the other ingots, is rather, and the areas of the sections in accordance with the x-ray diffraction analysis data, decreases with the increase of the amount of the approximatant phase (Table 1).

The experimental results show that the α -phase that not form in the ingot with the composition Ti₆₀Cr₃₃Si₈, melted by the arc methods without additional heating. The α -phase ingot consists of the Laves phase ξ -TiCr₂ and the titanium silicide Ti₅Si₃. However, the DTA ingot with the same composition is characterised by the crystalline approximatant

of the icosahedral phase in the mixture with the silicon-alloyed Laves phases ξ - $TiCr_2$. The amount of the α -phase in the melted ingot is 46.3 wt.%. The content of the α -phase can be increased to 75.9% in remelting of the ingot in the DTA system produced by the arc method in heating to a temperature of approximately 1700°C and cooling at a rate of 80°C/min. Additional alloying with oxygen makes it possible to produce 100% of the α -phase in the DTA ingot under the same heating and cooling conditions.

Thus, the experimental results show that in the $Ti_{60}Cr_{32}Si_8$ it is possible to produce the crystalline approximant of the icosahedral phase (α -phase) in a mixture with a silicon-alloyed Laves phases ξ - $TiCr_2$. The amount of the α -phase in the ingot is not large but it can

be increased to almost 90 wt.% as a result of heating to temperatures around 1700°C and up to 100 wt.% by adding oxygen to the alloy.

References

1. Adeeva, L.I. and Borisova, A.L., *Fiz. Khim. Tverd. Til*, 2002, No. 3, 454–465.
2. Borisov, Yu.S., et al., *ibid*, 2005, No. 1, 124–136.
3. Libbert, J.L., et al., *The American Physical Society*, 1994, volume 49, No. 17, 11675–11680.
4. Libbert, J.L., et al., *Journal of Non-Crystalline Solids*, 1983, volume 153–154, 53–57.
5. Bandyopadhyay, P.P., et al., *ITSC 2008, Maastricht*, 2008, 435–442.
6. Bandyopadhyay, P.P., *Surface Coatings Technology*, 2008, volume 203, 35–45.
7. Libbert, J.L., et al., *Philosophical Magazine*, 1999, volume A79, 2205.
8. Lysenko, L.A., et al., *Neorgan. Mater.*, 1971, No. 1, 175–177.

Submitted 28.10.2011



Aspects of using liquid cast iron in arc steel melting furnaces

R.V. Sinyakov

Donetsk National Technical University, Donetsk

Presented are the estimates of technological aspects of using the molten cast iron in arc steel-making furnace up to 80 % in the charge composition. Using the program complex «DesigningMelt», the modeling of melting with a different consumption of oxygen and electric power was made. The obtained results gave an opportunity to distinguish a criterion reflecting the optimum condition of application of the molten cast iron in the electric furnace. As such, it was suggested to use the ratio of supplied electric power to added oxygen for metal blowing per melting or ratio of mean power of supplied electric energy to mean rate of oxygen adding. Relation was obtained connecting the optimum share of cast iron in charge with a criterion of «optimality» of furnace operation.

The large increase in the price of energy resources, increasing demands on the flexibility of the process and its ecological parameters, and also the need to increase the proactivity force the metallurgical companies to close open hearth furnaces and transfer to alternative systems, including in particular arc steel melting furnaces (ASMF), releasing a large amount of liquid cast iron. In this case, it is necessary to use liquid cast iron is the charge component for the ASMF.

At the beginning of the century, approximately 30 ASMF operated in the world using liquid cast iron as a component of the charge [1]. Recently, the interest in this technology has increased appreciably [2]. This is associated with the reduction of the consumption of electric energy as a result of the physical

and chemical heat of cast iron [3-6], and the reduction of the content of residual elements in the final product [7].

However, as shown by industrial results with melting of the steel in the ASMF, the application of liquid cast iron are not always increase the productivity of the steel melting system. According to the investigations, carried out in [1, 8, 9], the dependence of the amount of liquid cast iron-productivity has an extremum, and the optimum is found in the range of 20-32% of cast iron of the mass of the charge. This is associated with the design special features of the system and the technology of melting steel in these furnaces. At the same time, data have been published on a high fraction of application of the cast iron in the ASMF, up to 50-60

[5] and even 80% [10].

Thus, to increase the productivity of the ASMF, it is important to determine the optimum fraction of liquid cast iron which, according to the data in [8], depends on the selected retail equipment for blowing oxygen and the removal of technological gases.

At the moment, there are no criteria which would make it possible to evaluate, without experiments in a real furnace, the optimum amount of liquid cast iron in the charge for the ASMF or the optimum parameters of operation of the ASMF for the given fraction of liquid cast iron.

It was required to determine the technological aspects of using liquid cast iron in the furnace up to 80% in the composition of the charge and try to specify a criterion linking the technical-technological possibilities of the ASMF and the optimum amount of liquid cast iron in the charge.

To solve the task, experiments were carried out with the DesigningMelt software [11] - the tool for developing new technological processes, and the evaluation of the application of new types of materials and equipment without using expensive and time-consuming experiments in a real furnace.

The process to be examined was melting of a steel in a 100 t arc steel melting furnace with window discharge of the semifinished product. The furnace operates with the liquid

residue of the metal of 10 t and slag off 5 t with the mean temperature of 1600°C. Furnace equipment consists of a 80 MV·A transformer, two oxygen injectors with the maximum consumption of oxygen of 2000 m³/h each, four gas-oxygen torch is with the power of 3.5 MW each, for injectors for blowing coal for slag foaming, to bottom samples for blowing the argon gas into the pool, bunkers for introducing the slack forming materials, etc. The metal scrap is loaded into the furnace in two boxes: top charge, bottom charge. Thus, the structure of the melt consists of six previous with the discharge of the metal taken into account [11]. In this case, the mass of the metal scrap in the baskets was assumed to be 65 and 60 t, respectively. According to the conditions of melting in the arc steel melting furnace, cast iron should be added to the charge and, if it is not available, it should be replaced with the carbon-containing materials (for example, coke). Usually, 15–20% of cast iron scrap is added to the charge and, therefore, the first basket contained 25 t of solid cast iron.

The conditions of introduction of electric energy, oxygen, coal, slag forming components, operation of the torches and also the moment of emptying the baskets were determined by the program software in accordance with the given technological and technical restrictions on the operation of equipment (Fig. 1).

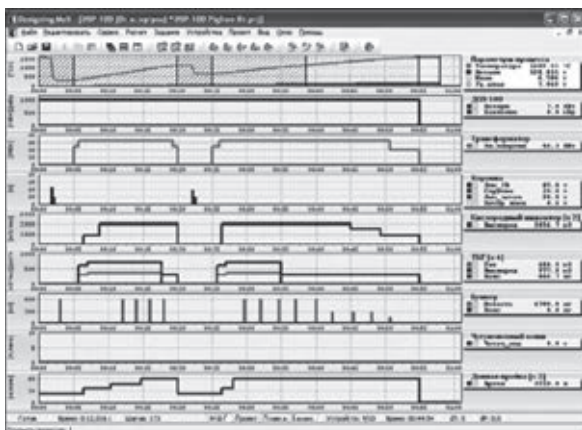


Fig. 1. Project of the process of melting steel in a 100 t arc steel melting furnace (basic melt).

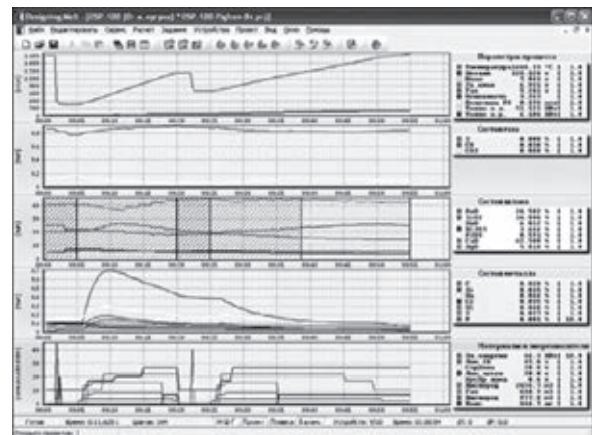


Fig. 2. The results of modelling the process of basic melting.

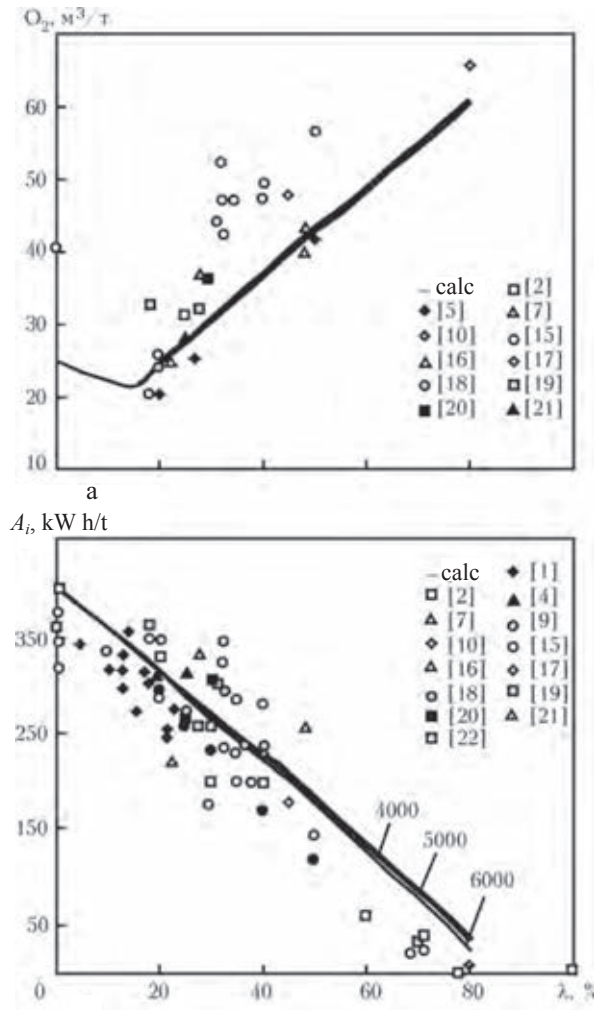


Fig. 3. Consumption of electric energy A and oxygen for 1 t of metal in relation to the fraction of liquid cast iron in the charge. The numbers of the curves (here and in Fig. 4, 6) denote the maximum total intensity of blowing the metal with oxygen.

After simulation (calculation of the project) we obtain the technological processes with the trajectory shown in Fig. 2 and the following parameters at the discharge stage: $[C]$ 0.06%, degree of oxidation of the slag (FeO) 24%; basicity of the slag 3.2; metal temperature $1640^\circ C$.

The calculated melt was regarded as the basic melt and the resultant parameters of the aim of simulation with the following restrictions: the carbon content at a discharge 0.059-0.061%; oxidation of the slag (content of iron oxide) no more than 25%; the slag basicity less than 2.9; metal temperature at discharge $1639-1641^\circ C$. The mass of metal at

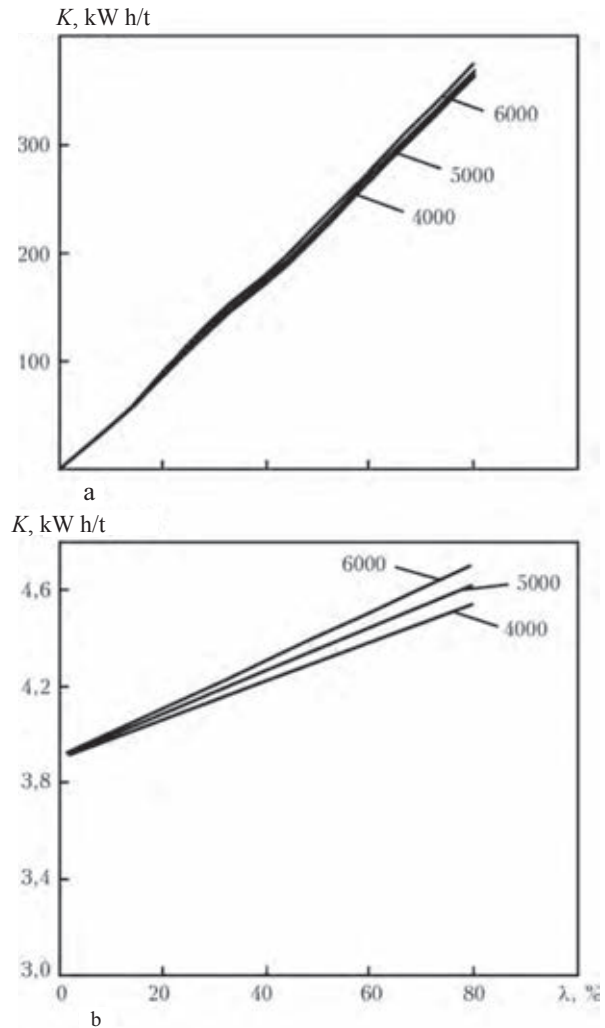


Fig. 4. Effect of the amount of liquid cast iron and the economic saving of electric energy K : a) absolute value; b) percent of cast iron.

discharge was assumed to be equal to 115 t.

Subsequently, the possibility of pouring in liquid cast iron was added to the melt project and the special design features of the arc steel melting furnaces [7, 12]: from the top with the open chute from the slag, through the working window of the furnace using a detachable chute and through a stationary chute, installed in the furnace. In this study, cast iron was poured through the stationary spout after partial melting of the first basket.

According to [3] this variant has shortcomings in the form of formation of conglomerates when using the next baskets with metal scrap. In these investigations, this shortcom-

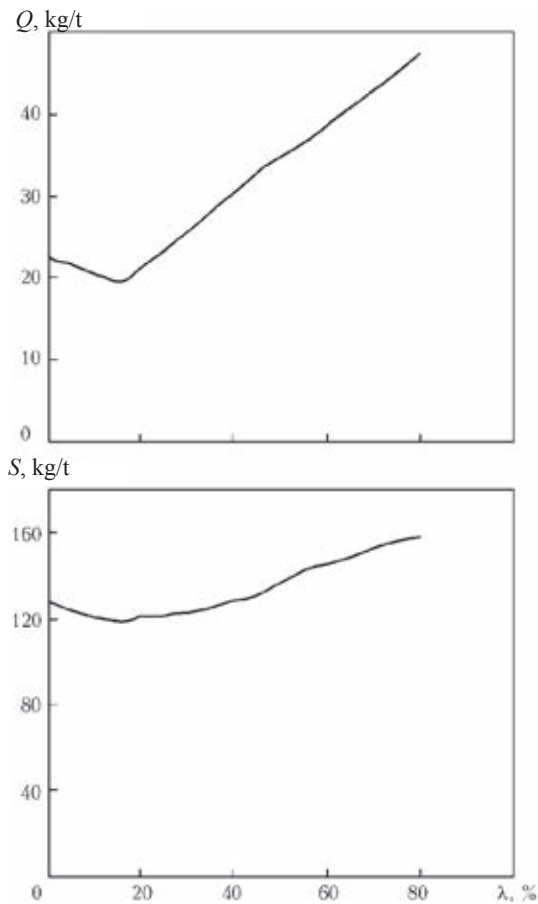


Fig. 5. Effect of the fraction of liquid cast iron on the amount of outgoing gases Q and the resultant slag S .

ing was partially balanced by earlier start of high rate blogging of the pool with oxygen. The mean pouring rate of the cast iron into the furnace varied in the range from 2[4] to 10[1] t/h, and in the actual process the pouring in rate of cast iron was assumed to be equal to 5t/h.

The cast irons, used in steel melting production, differ mainly in the chemical composition [13, 14]; in these investigations, the carbon content of liquid cast iron was 4.6, silicon content 0.5, manganese content of 0.7%, temperature 1300°C. In simulation, the solid part of the charge was replaced with liquid cast iron in the following sequence: initially the cast iron scrap from the charge; subsequently the metal scrap from the charge, and after melting of the bottom charge of the metal scrap from the charge.

The melting of the steel in the arc steel

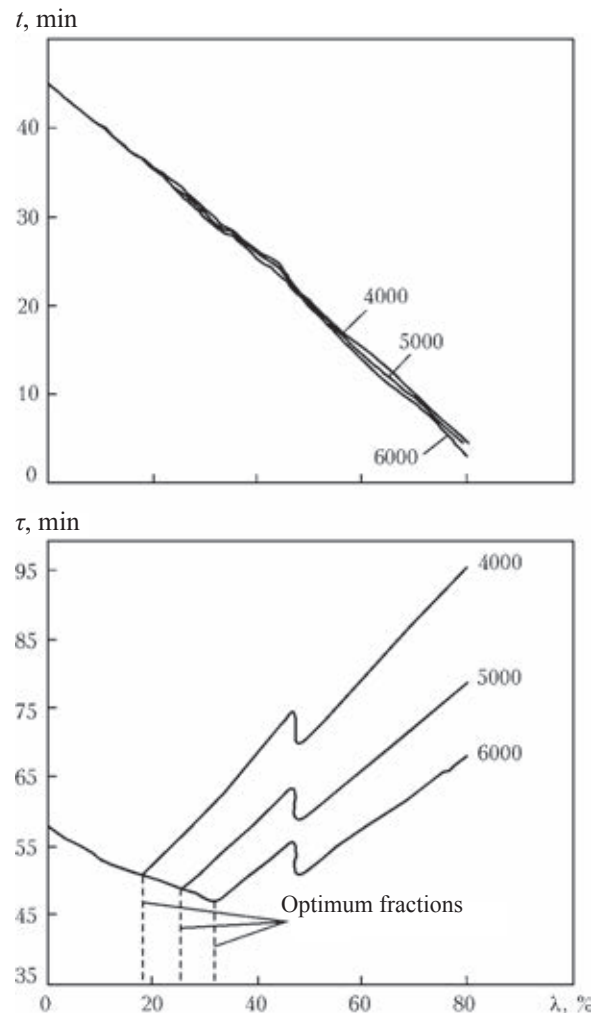


Fig. 6. Evaluation of the optimum fractional liquid cast iron per melt (calculated): t is the duration of operation of the furnace under current; τ is the productivity of melting.

melting furnace was simulated by three variants for different maximum consumption of oxygen (2000, 2500 and 3000 m³/h each) through oxygen injectors and using up to 80% liquid cast iron in the composition of the charge.

Comparative analysis of the results of simulation with the currently available industrial indicators of the operation of arc steel melting furnaces, we choose liquid cast iron as the charge show the adequacy of the models used in the DesigningMelt software. With increase of the amount of liquid cast iron in the charge, the consumption of electric energy decrease, and in the case of oxygen for blowing of metal it increased (Fig. 3).

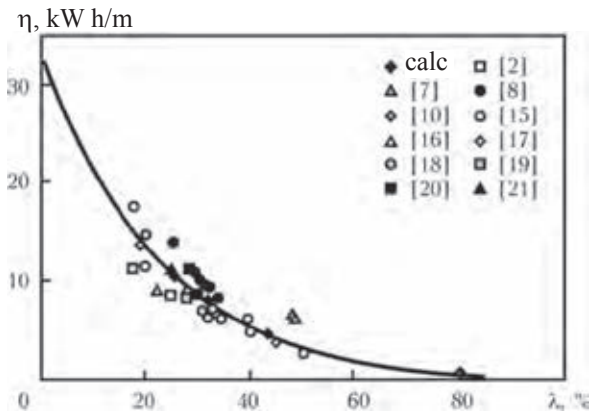


Fig. 7. Dependence of the ratio of the consumption of electric energy to the consumption of oxygen on the optimum fraction of liquid cast iron.

Consequently, the saving of electric energy already has 20% of liquid cast iron the composition of the charge was approximately 90 kW · h/t (Fig. 4a). Since in these investigations the solid cast iron was replaced, there was correspondingly no additional supply of energy with the chemical heat of cast iron. When replacing the metal scrap, the economic effect was even greater and, according to the calculations, carried out in [6], it was an 116 kW · h/t.

According to the data obtained by various authors, when supplying 1% of liquid cast iron into the charge, the saving of electric energy varies from 3.3 [8] and 3.5 [13] to 4.8 [5] kilowatt·h/t. As indicated by Fig. 4, *b*, this parameter is not constant and is linked by a direct proportional dependence with the amount of liquid cast iron and is also a function of the intensity of blowing the metal with oxygen.

The small reduction of the consumption of oxygen was recorded at the mass fraction of liquid cast iron in the composition of the charge up to 20% (Fig. 3). This is explained, firstly, by the presence of 20% of cast iron scrapping the charge, which was proportionately the replace with liquid cast iron, and this had no effect on the consumption of oxygen. Secondly, reduction of the consumption of electric energy reduce the consumption of the carbon-containing material for foaming of the slag and, correspondingly reducing the fraction of oxygen.

A shortcoming of the application of liquid cast iron in the charge for arc steel melting furnaces is the increase of the amount of slag and outgoing gases (Fig. 5) which must be taken into account when using this material in the composition of the charge.

As shown by Fig. 6, an increase of the fraction of liquid cast iron in the composition of the charge results initially in a reduction of the melting time (reaching the minimum value, and at a specific amount of cast iron the melting time starts to increase this confirms the extreme form of the dependence. The maximum productivity of the furnace is obtained at the minimum melting time which corresponds to the optimum fraction of liquid cast iron.

The inflection point on the curve at 48% for liquid cast iron in the charge of the arc steel melting furnace corresponds to the disappearance of the period of bottom charging of the simulation melt and as regards the density is approximately equal to the duration of the given period. The operating time of the furnace under current constantly decreases with increase of the amount of liquid cast iron in the charge, and the dependences non-linear (Fig. 6).

The optimum fraction of cast iron is not constant and depends on the power of gas blowing devices (Fig. 6). With increase of the intensity of blowing oxygen at the given how the transformer the optimum amount of liquid cast iron in the charge increases. Evidently, the reverse situation also applies - with increase of the power of the transformer the given blowing intensity of oxygen in the optimum fractional liquid cast iron in the charge decreases [8].

Thus, the optimum fraction of liquid cast iron in the charger depends mainly on the maximum productivity of equipment for introducing oxygen and the transformer power. The authors of the present article assumed that a possible criterion, which determine the optimum amount of cast iron in the charge for the arc steel melting furnaces maybe the ratio of the power of the transformer P_{tr} (kilowatt) to the intensity of supply of

oxygen P_{pr} (m^3/h):

$$\eta = \frac{P_{tr}}{P_{pr}} \quad (1)$$

Since the optimum welding process is the process in which the duration of operation of the transformer and equipment for introducing oxygen (at the maximum power) is almost identical and do not have any periods without current, equation (1) can be presented in the following form:

$$\eta = \frac{Q_{tr}}{Q_{pr}} \quad (2)$$

where Q_{tr} is the amount of the electric energy supplied per 1 t metal, kilowatt·h/t; Q_{pr} is the amount of oxygen for blowing of 1 t of metal, m^3/t .

For the optimum fractions of the liquid cast iron and simulation (Fig. 6) we determine the corresponding relationship (2) and constructed the curve (Fig. 7), describing the following expression

$$\eta = 34.4c^{-4.044\lambda} - 0.8 \quad (3)$$

where λ is the fraction of liquid cast iron in the composition of the charge for the arc steel melting furnace, %.

After carrying out transformations, we obtain the equations which makes it possible, using the technical and technological characteristics of the furnace, to determine the optimum fraction of liquid cast iron in the composition of the charge:

$$\lambda = 22.73 \ln \left(\frac{34.4}{\eta + 0.8} \right) \quad (4)$$

The points indicate the results of processing the industrial data on the operation of the arc steel melting furnace using equations (1) or (2). As shown in Fig. 7, the experimental data fit satisfactorily the resultant curve.

Conclusions

1. The estimates of the technological aspects of application of liquid cast iron in the arc steel melting furnace up to 80% in the composition of the charge are presented

in the advantages and shortcomings of using liquid cast iron are discussed.

2. Using the DesigningMelt software, the melting process was simulated using different consumption of oxygen and electric energy. The results have been used to determine a criterion reflecting the optimum conditions of application of liquid cast iron in the electric furnace, in the form of the ratio of the introduced electric energy to the added oxygen for blowing of metal in the melt.

3. The dependence, linking the criterion with the optimum fraction of liquid cast iron in the charge for the arc steel melting furnaces has been determined.

References

- Haissig M., Genter R. B., Villemin B. Hot Metal in EAFs AISE Steel Technology. – 2002. – № 3. – P. 41–48.
- Sampaio R. S., Jeremy J., Vieira J. B. Hot Metal Strategies for the EAF Industry // Iron & Steel Technology. – 2009. – № 2. – P. 31–37.
- Katunin, A.I., et al., Izv. VUZ, Chernaya Metallurgiya, – 2001. – № 4. – P. 24–26.
- The continuous charging of hot metal in the DC vessel of Cockerill-Sambre Marcinelle / B. Charue, M. Van Den Neste, C. Morettin et al. // 6th Eur. Elec. Steelmak. Conf. (Dusseldorf, June 13–15, 1999). – Dusseldorf, 1999. – P. 35–37.
- Production and use of pig iron and hot metal in the EAF steelmaking practice of Brazil and India / K. Scheidig, S. W. G. Scherer, T. B. Martins et al. // Ibid. – Dusseldorf, 1999. – P. 38–42.
- Luzgin, V.P., et al., Elektrometallurgiya, – 2010. – № 1. – P. 17–24.
- Godik, L.A., et al., Chern. Met., – 2009. – № 4. – P. 42–46.
- Won S.T. S., Jie F. The Development of Hot Metal Charging Process // SEAIISI Quarterly J. – 2010. – № 2. – P. 32–40.
- Fior A. A., Sellan R. EAF Hot Metal Processing at Integrated Steel Plants // AISE Steel Technology. – 2002. – № 3. – P. 20–25.
- Prokhorov, S.V., et al., Proc. 11th Steelmaking Congress, Chermetinformatiya, Nizhnii Tagil, 2011.
- Sinyakov, R.V., Sovremen. Elektrometall. – 2011. – № 2. – P. 34–37.
- Katunin, A.I., et al., Stal', - 2000. – № 5. – P. 33–35.
- Gudin, Yu.A., et al., Production of steel in electric furnaces, HGTU, Novosibirsk, 2010.
- Jian-Ping Duan, Yong-Liang Zhang, Xue-Min Yang. EAF steelmaking process with increasing hot metal charging ratio and improving slagging regime // Intern. J. of Minerals, Metallurgy and Materials. – 2009. – 16, № 4. – P. 375–382.
- Michael G. K. Grant, Kenneth C. Kaiser, Serban M. Cantacuzene. Optimization of Oxygen Steelmaking in Non-Conventional EAF Operations // AISTech 2005 Proceedings. – 2005. – V. 1. – P. 545–553.
- Abel M. The use of scrap substitutes like cold/hot DRI and Hot Metal in electric steelmaking // Archives

- of metallurgy and materials. – 2008. – 53, № 2. – P. 353–357.
17. High Efficiency Production Practice of a 100 t DC EBT EAF at Xing Cheng SteelWorks / Xiaohong Xu, Xiaojiang Ruan, Guowei Zhang et al. // AISTech Proceedings. – 2006. – V. 2. – P. 413–422.
18. Installation of praxair's coJet(r) gas injection system at sumikin steel and other EAFs with hot metal charges / Cates Larry, Fujimoto Kuniharu, Okada Yasukazu et al. // Ibid. – 2008. – V. 1. – P. 723–731.
19. Charging hot metal to the EAF using Consteel / T. Jiemin, W. Xuefeng, M. B. Ferri, P. Argenta // Millenium Steel International. – London, 2006. – P. 79–86.
20. Kiselev, A.D., et al., in: Current problems of electro-metallurgy of steel, Proc. 12th Int. Conf., Chelyabinsk, 2004 - P. 245–246.
21. Bigeev, V.A., et al., Current problems of electrometallurgy of steel, Proc. 12th Int. Conf., Chelyabinsk, 2007, P. 207–211.
22. Ivin, Yu.A., et al., Stal', – 2008. – № 7. – P. 49–50.

Submitted 28.9.2011